MATERIALS FOR ADAPTIVE STRUCTURAL ACOUSTIC CONTROL

Period February 1, 1995 to January 31, 1996

Annual Report

VOLUME VI

OFFICE OF NAVAL RESEARCH
Contract No.: N00014-92-J-1510

19960703 064

L. Eric Cross

PENNSTATE

THE MATERIALS RESEARCH LABORATORY
UNIVERSITY PARK, PA

DTIC QUALITY INSPECTED 1

DISCLAIMER NOTICE

UNCLASSIFIED

Technical Report
distributed by

DEFENSE
TECHNICAL
INFORMATION
CENTER

DTIC Acquiring Information
Imparting Knowledge

Cameron Station
Alexandria, Virginia 22304-6145

UNCLASSIFIED

THIS DOCUMENT IS BEST
QUALITY AVAILABLE. THE
COPY FURNISHED TO DTIC
CONTAINED A SIGNIFICANT
NUMBER OF PAGES WHICH DO
NOT REPRODUCE LEGIBLY.

REPORT DOCUMENTATION PAGE

Public reporting burden for this collection of information is estimated to average 1 hour per response, including the time for reviewing instructions, searching existing data sources, gathering and maintaining the data needed, and completing and reviewing the collection of information. Send comments regarding this burden estimate or any other aspect of this collection of information, including suggestions for reducing this burden, to Washington Headquarters Services, Directorate for Information Operations and Reports, 1215 Jefferson Davis Highway, Suite 1204, Arlington, VA 22202-4302, and to the Office of Management and Budget, Paperwork Reduction Project (0704-0188), Washington, DC 20503.

1. AGENCY USE ONLY (Leave blank)	2. REPORT DATE 3/13/96	3. REPORT TYPE AND DATES COVERED ANNUAL REPORT 02/01/95 TO 01/31/96

4. TITLE AND SUBTITLE

MATERIALS FOR ADAPTIVE STRUCTURAL ACOUSTIC CONTROL

5. FUNDING NUMBERS

6. AUTHOR(S)

L. ERIC CROSS

7. PERFORMING ORGANIZATION NAME(S) AND ADDRESS(ES)

MATERIALS RESEARCH LABORATORY
THE PENNSYLVANIA STATE UNIVERSITY
UNIVERSITY PARK, PA 16802

8. PERFORMING ORGANIZATION REPORT NUMBER

9. SPONSORING / MONITORING AGENCY NAME(S) AND ADDRESS(ES)

OFFICE OF NAVAL RESEARCH
CODE 1513:NRJ
800 NORTH QUINCY STREET
ARLINGTON, VA 22217-5660

GERALD T. SMITH
OFFICE OF NAVAL RESEARCH RES. REP.
536 SOUTH CLARK STREET, RM 286
CHICAGO, ILLINOIS 60606-1588

10. SPONSORING / MONITORING AGENCY REPORT NUMBER

11. SUPPLEMENTARY NOTES

12a. DISTRIBUTION / AVAILABILITY STATEMENT

DISTRIBUTION STATEMENT A
Approved for public release
Distribution Unlimited

12b. DISTRIBUTION CODE

13. ABSTRACT (Maximum 200 words)

SEE FOLLOWING THREE PAGES

14. SUBJECT TERMS

15. NUMBER OF PAGES

16. PRICE CODE

17. SECURITY CLASSIFICATION OF REPORT	18. SECURITY CLASSIFICATION OF THIS PAGE	19. SECURITY CLASSIFICATION OF ABSTRACT	20. LIMITATION OF ABSTRACT

GENERAL INSTRUCTIONS FOR COMPLETING SF 298

The Report Documentation Page (RDP) is used in announcing and cataloging reports. It is important that this information be consistent with the rest of the report, particularly the cover and title page. Instructions for filling in each block of the form follow. It is important to *stay within the lines* to meet *optical scanning requirements*.

Block 1. Agency Use Only *(Leave blank)*.

Block 2. Report Date. Full publication date including day, month, and year, if available (e.g. 1 Jan 88). Must cite at least the year.

Block 3. Type of Report and Dates Covered. State whether report is interim, final, etc. If applicable, enter inclusive report dates (e.g. 10 Jun 87 - 30 Jun 88).

Block 4. Title and Subtitle. A title is taken from the part of the report that provides the most meaningful and complete information. When a report is prepared in more than one volume, repeat the primary title, add volume number, and include subtitle for the specific volume. On classified documents enter the title classification in parentheses.

Block 5. Funding Numbers. To include contract and grant numbers; may include program element number(s), project number(s), task number(s), and work unit number(s). Use the following labels:

C	-	Contract	PR -	Project
G	-	Grant	TA -	Task
PE	-	Program Element	WU -	Work Unit Accession No.

Block 6. Author(s). Name(s) of person(s) responsible for writing the report, performing the research, or credited with the content of the report. If editor or compiler, this should follow the name(s).

Block 7. Performing Organization Name(s) and Address(es). Self-explanatory.

Block 8. Performing Organization Report Number. Enter the unique alphanumeric report number(s) assigned by the organization performing the report.

Block 9. Sponsoring/Monitoring Agency Name(s) and Address(es). Self-explanatory.

Block 10. Sponsoring/Monitoring Agency Report Number. *(If known)*

Block 11. Supplementary Notes. Enter information not included elsewhere such as: Prepared in cooperation with...; Trans. of...; To be published in.... When a report is revised, include a statement whether the new report supersedes or supplements the older report.

Block 12a. Distribution/Availability Statement. Denotes public availability or limitations. Cite any availability to the public. Enter additional limitations or special markings in all capitals (e.g. NOFORN, REL, ITAR).

- **DOD** - See DoDD 5230.24, "Distribution Statements on Technical Documents."
- **DOE** - See authorities.
- **NASA** - See Handbook NHB 2200.2.
- **NTIS** - Leave blank.

Block 12b. Distribution Code.

- **DOD** - Leave blank.
- **DOE** - Enter DOE distribution categories from the Standard Distribution for Unclassified Scientific and Technical Reports.
- **NASA** - Leave blank.
- **NTIS** - Leave blank.

Block 13. Abstract. Include a brief *(Maximum 200 words)* factual summary of the most significant information contained in the report.

Block 14. Subject Terms. Keywords or phrases identifying major subjects in the report.

Block 15. Number of Pages. Enter the total number of pages.

Block 16. Price Code. Enter appropriate price code *(NTIS only)*.

Blocks 17. - 19. Security Classifications. Self-explanatory. Enter U.S. Security Classification in accordance with U.S. Security Regulations (i.e., UNCLASSIFIED). If form contains classified information, stamp classification on the top and bottom of the page.

Block 20. Limitation of Abstract. This block must be completed to assign a limitation to the abstract. Enter either UL (unlimited) or SAR (same as report). An entry in this block is necessary if the abstract is to be limited. If blank, the abstract is assumed to be unlimited.

ABSTRACT

This report documents work carried forward over the fourth year of a five year ONR sponsored University Research Initiative (URI) entitled "Materials for Adaptive Structural Acoustic Control." The program has continued to underpin the development of new electro-ceramic, single crystal and composite materials combinations for both the sensing and actuation functions in adaptive structures.

For the lead based perovskite structure relaxor ferroelectric electrostrictors, new experimental and theoretical studies have underscored the critical role of nano-scale heterogeneity on either A or B sites of the ABO_3 in promoting dispersive dielectric response and the very strong opposing role of elastic stress and electrostrictive coupling in suppressing polarization fluctuations. Most important for practical application is the regimen where, under high electric field nano-polar regions begin to amalgamate into ferroelectric macro-domains with very mobile walls lead to unusually large extrinsic piezoelectric coefficients.

The program has explored a range of new relaxor:ferroelectric solid solutions which exhibit morphotropic phase boundaries between rhombohedral and tetragonal ferroelectric phases. Some of these compositions are much more tractable than PZT to grow in single crystal form. A major surprise is the very strong enhancement of the piezoelectric d_{33} and d_{31} in the crystal over that in the corresponding ceramic, and the massive anisotropy for different orientations and directions of poling. Optical studies suggest that the unusual effects reside largely in the extrinsic (domain controlled) response and we speculate about the mobility of walls in metastable phases, however further studies are required.

Antiferroelectric:ferroelectric phase switching studies in a wide range of compositions in the lead lanthanum zirconate stannate titanate system show that the first abrupt switchover to the rhombohedral ferroelectric phase only produces volume strain ~0.2% as checked both by dilatometry and by X-ray. There is a large enhancement under higher field to ~0.6% volume strain although the polarization does not change markedly. From thin film and single crystals studies there is mounting evidence of higher field ferroelectric:ferroelectric phase change, but again additional work is needed.

Size effect studies in perovskite ferroelectrics are continuing on this program and on the NSF/MRG in MRL. Scaling of the 90° stripe domains in thinned TEM samples of tetragonal composition begin to show departure from the accepted 1/2 power law at sub micron sizes. The structure of domains under the three dimensional constraints of grains inside the ceramic is still however almost completely unknown. Computer modeling appear to show promise and codes are being explored which permit the mutual interactions to be varied and the corresponding two dimensional structures visualized.

In composite sensors, the focus has continued upon the flextensional configurations with the new inexpensive cymbal shaped amplifier proving superior in every respect to the original "moonie." The flat section on the cymbal end cap permits very easy stacking of elements and work is now in progress to develop large area panels for low frequency testing at the Penn State ARL.

Work has continued on the thin sheet 2:2 piezoceramic polymer composites, where the transverse poling and low density lead to a desirable combination of low electrical and low acoustic impedance. An alternative fabrication procedure using extruded PZT honeycomb appears most attractive.

Two problems of major importance in actuation have been topics for study. First what are the "intrinsic" material limitations for high strain electrically driven actuation in polarization controlled systems, and secondly what are the practical limitations in multilayer actuators as they are currently fabricated and how may they be alleviated. Work on the first topic is now largely completed, showing that strains ~0.4% could be switched more than 10^9 cycles in suitable PLZT compositions. Such reliability however requires near theoretical density, homogeneity, grain size control, critical attention to electrodes and electric field uniformity, none of which are adequately controlled in current actuator systems.

For practical actuators fabricated by inexpensive tape casting and co-firing techniques electrode termination is a major problem. In the simple MLC like designs, cracks initiate at field concentrations associated with the tip of the buried conductor layer. A new floating electrode design has been found to reduce this problem. For cracking near the end surfaces, poling of the termination layers reduces their stiffness and markedly improves performance. In the conventional structures it is also found that the floating electrode may be used directly as an acoustic emission pickup, giving early warning of cracking problems.

Under resonant driving conditions, the problems in actuators are markedly different. Heat build up and temperature run-away are significant problems traceable to dielectric loss, and new hard compositions and anti-resonant driving methods have been explored to reduce these problems.

In integration work on the high activity 0-3 composites in nearing completion. A new type of zig-zag actuator is being explored for the capability to combine both longitudinal and transverse actuation. Under a new ONR sponsored program with Virginia Polytechnic Institute and University new double amplifiers combining bimorph and flextensional concepts are being examined.

Processing studies permit the fabrication of the wide range of compositions and forms required in these material researches. Rate controlled sintering is proving to be highly advantageous, particularly for reducing delamination in integrated structures. Electrophoretic and

dielectrophoretic forming are showing promise in green assembly of thick film components where high green density is critical.

Thin film papers have been selected from the very broad range of work in MRL because of their relevance to transduction in piezoelectric and in phase switching systems.

MATERIALS FOR ADAPTIVE STRUCTURAL ACOUSTIC CONTROL

Period February 1, 1995 to January 31, 1996

Annual Report

VOLUME VI

OFFICE OF NAVAL RESEARCH
Contract No.: N00014-92-J-1510

APPROVED FOR PUBLIC RELEASE — DISTRIBUTION UNLIMITED

L. Eric Cross

PENNSTATE

1855

THE MATERIALS RESEARCH LABORATORY
UNIVERSITY PARK, PA

TABLE OF CONTENTS

APPPENDICES

VOLUME I

General Summary Papers

1. Cross, L.E., "Ferroelectric Materials for Electromechanical Transducer Applications," *Jpn. J. Appl. Phys.* **34**, 2525-2532 (1995).

2. Fernandez, J.F., A. Dogan, Q.M. Zhang, J.F. Tressler, and R.E. Newnham, "Hollow Piezoelectric Composites," submitted to *Sensors and Actuators: A. Physical* (1995).

3. Uchino, K., "Recent Developments in Ceramic Actuators–Comparison among USA, Japan and Europe," Workshop on Microsystem Technologies in the USA and Canada, Dusseldorf (1995).

4. Trolier-McKinstry, S., J. Chen, K. Vedam, and R.E. Newnham, "In Situ Annealing Studies of Sol–Gel Ferroelectric Thin Films by Spectroscopic Ellipsometry," *J. Am. Ceram. Soc.* **78** [7], 1907-1913 (1995).

5. Nair, N., A. Bhalla, and R. Roy, "Inorganic Lead Compounds in Electroceramics and Glasses," *Am. Cer. Soc. Bull.* **75** [1], 77-82 (1996).

6. Gentile, A. and F.W. Ainger, "Single Crystals," Chapter 9, Materials Science and Technology, A Comprehensive Treatment, **17A** Processing of Ceramics, Part 1 (R.J. Brook, editor), VCH Verlagsgesellschaft mbH, Weinheim, Fed. Repl. of Germany (1996).

Materials Studies

7. Choi, S.W., J.M. Jung, and A.S. Bhalla, "Dielectric, Pyroelectric and Piezoelectric Properties of Calcium-Modified Lead Magnesium Tantalate-Lead Titanate Ceramics."

8. Kim, Y.J., S.W. Choi, and A.S. Bhalla, "Dielectric, Pyroelectric Properties, and Morphotropic Phase Boundary in La-Doped $(1-x)Pb(Mg_{1/3}Ta_{2/3})-xPbTiO_3$ Solid Solution Ceramics", *Ferroelectrics* **173**, 87-96 (1995).

9. Alberta, E. and A.S. Bhalla, "A Processing and Electrical Property Investigation of the Solid Solution: $(x) Pb(In_{1/2}Nb_{1/2})O_3-(1-x)Pb(Sc_{1/2}Ta_{1/2})O_3$," submitted to Ferroelectrics (1995).

10. Zhang, Q.M., H. You, M.L. Mulvihill, and S.J. Jang, "An X-ray Diffraction Study of Superlattice Ordering in Lead Magnesium Niobate," *Solid State Comm.* **97** [8], 693-698 (1996).

11. Zhang, Q.M., J. Zhao, and L.E. Cross, "Aging of the Dielectric and Piezoelectric Properties of Relaxor Ferroelectric Lead Magnesium Niobate–Lead Titanate in the Electric Field Biased State," *J. Appl. Phys.* **79** (6), 1-7 (1996).

2

VOLUME II

Materials Studies (*continued*)

12. Zhang, Q.M., J. Zhao, T.R. Shrout, and L.E. Cross, "The Effect of Ferroelastic Coupling in Controlling the Abnormal Aging Behavior in Lead Magnesium Niobate-Lead Titanate Relaxor Ferroelectrics," submitted *J. Mat. Res.*

13. Mulvihill, M.L., L.E. Cross, and K. Uchino, "Low-Temperature Observation of Relaxor Ferroelectric Domains in Lead Zinc Niobate," *J. Am. Ceram Soc.* **78** (12) 3345-3351 (1995).

14. Mulvihill, M.L., L.E. Cross, and K. Uchino, "Dynamic Motion of the Domain Configuration in Relaxor Ferroelectric Single Crystals as a Function of Temperature and Electric Field," 8th Euro. Mtg. Ferroelectricity, Nijmegen (1995).

15. Mulvihill, M.L., K. Uchino, Z. Li, and Wenwu Cao, "In-Situ Observation of the Domain Configurations During the Phase Transitions in Barium Titanate," accepted *Phil. Mag. B* (1995).

16. Oh, K.Y., K. Uchino, and L.E. Cross, "Electric Properties and Domain Structures in $Ba(Ti,Sn)O_3$ Ceramics."

17. Cao, W., "Elastic and Electric Constraints in the Formation of Ferroelectric Domains," *Ferroelectrics*, **172**, 31-37 (1995).

18. Cao, W. and C.A. Randall, "The Grain Size and Domain Size Relations in Bulk Ceramic Ferroelectric Materials," accepted *J. Phys. Chem. Solids* (1995).

19. Cao, W., "Defect Stabilized Periodic Amplitude Modulations in Ferroelectrics," accepted *Phase Transitions* (1995).

20. Sopko, J., A. Bhalla, and L.E. Cross, "An Improved Quantitative Method for Determining Dynamic Current Response of Ppyroelectric Materials,"*Ferroelectrics*, **173**, 139-152 (1995)

VOLUME III

Composite Sensors

21. Tressler, J.F., A. Dogan, J.F. Fernandez, J.T. Fielding, Jr., K. Uchino, and R.E. Newnham, "Capped Ceramic Hydrophones," submitted to Proc. IEEE Int'l Ultronics Symp., Seattle (1995).

22. Koc, B., A. Dogan, J.F. Fernandez, R.E. Newnham, and K. Uchino, "Accelerometer Application of the Modified Moonie (Cymbal) Transducer," submitted *Jpn. J. Appl. Phys.* (1995).

23. Zhao, J., Q.M. Zhang, and W. Cao, "Effects of Face Plates and Edge Strips on Hydrostatic Piezoelectric Response of 1-3 Composites," *Ferroelectrics* **173**, 243-256 (1995).

24. Wu, S.J., W. Qi, and W. Cao, "Numerical Study of Ultrasonic Beam Pattern of a 1-3 Piezocomposite Transducer," accepted *Proc. IEEE Trans. Ultrasonics, Ferroelectridcs and Frequency Control.* (1995).

Composite Sensors (continued)–Volume III

25. Wang, H., Q.M. Zhang, and L.E. Cross, "Tailoring Material Properties by Structure Design--Radially Poled Piezoelectric Cylindrical Tube," *Ferroelectrics Lett.* (in press).

26. Zhang, Q.M. and X. Geng, "Electric Field Forced Vibration of a Periodic Piezocomposite Plate with Laminated Structure and Reflection and Transmission of a Plane Wave at the Fluid-Composite Interface," submitted to IEEE Transactions on Ultrasonics, Ferroelectrics, and Frequency Control (1995).

27. Geng, X., and Q.M. Zhang, "Dynamic Behavior of Periodic Piezoceramic-Polymer Composite Plates," *Appl. Phys. Lett.* **67** (21) (1995).

28. Zhang, Q.M., "Transverse Piezoelectric Mode Piezoceramic Polymer Composites with High Hydrostatic Piezoelectric Responses," *Proc. Int. Conf. on Electronic Components and Materials Sensors and Actuators,* Xi'an, China, 159-162 (1995)

29. Zhang, Q.M., H. Wang, J. Zhao, J.T. Fielding, Jr., R.E. Newnham, and L.E. Cross, "A High Sensitivity Hydrostatic Piezoelectric Transducer Based on Transverse Piezoelectric Mode Honeycomb Ceramic Composites," IEEE Transactions on Ultrasonics, Ferroelectrics and Frequency Control **43** (1), 26-42 (1996).

30. Zhang, Q.M., J. Chen, H. Wang, J. Zhao, L.E. Cross, and M.C. Trottier, "A New Transverse Piezoelectric Mode 2-2 Piezocomposite for Underwater Transducer Applications," IEEE Transactions on Ultrasonics, Ferroelectrics, and Frequency Control **42** (4), 774-780 (1995).

31. Cao, W., Q.M. Zhang, J.Z. Zhao, and L.E. Cross, "Effects of Face Plates on Surface Displacement Profile in 2-2 Piezoelectric Composites," IEEE Transactions on Ultrasonics, Ferroelectrics, and Frequency Control **42** (1), 37-41 (1995).

32. Cao, W. and W. Qi, "Plane Wave Propagation in Finite 2-2 Composites," *J. Appl. Phys.* **78** (7), 4627-4632 (1995).

33. Qi, W. and W. Cao, "Finite Element Analysis and Experimental Studies on the Thickness Resonance of Piezocomposite Transducers," accepted *Ultrasonic Imaging* (1995).

34. Cao, W. and W. Qi, "Multisource Excitations in a Stratified Biphase Structure," *J. Appl. Phys.* **78** (7), 4640-4646 (1995).

VOLUME IV

Actuator Studies

35. Uchino, K., "Materials Update: Advances in ceramic actuator materials," *Materials Lett.* **22**, 1-4 (1995).

36. Uchino, K., "Novel Ceramic Actuator Materials."

37. Aburatani, H., K. Uchino, and A.F. Yoshiaki, "Destruction Mechanism and Destruction Detection Technique for Multilayer Ceramic Actuators," *Proc. of the 9th Annual International Symposium on the Applications of Ferroelectrics,* 750-752 (1995).

38. Uchino, K. "Manufacturing Technology of Multilayered Transducers," *Proc. Amer. Ceram. Soc.*, Manufacture of Ceramic Components, 81-93 (1995).

39. Uchino, K. "Piezoelectric Actuators/Ultrasonic Motors--Their Development and Markets," *Proc. 9th ISAF*, 319-324 (1995).

40. Dogan, A., J.F. Fernandez, K. Uchino, and R.E. Newnham, "New Piezoelectric Composite Actuator Designs for Displacement Amplification," in press *Proc. Euroceram 95* (1995).

41. Onitsuka, O., A. Dogan, J.F. Tressler, Q.Su, S. Yoshikawa, and R.E. Newnham, "Metal-Ceramic Composite Transducer, The 'Moonie' ," *J. Intelligent Materials Systems and Structures* **6**, 447-455 (1995).

42. Fernandez, J.F., A. Dogan, J.T. Fielding, K. Uchino, and R.E. Newnham, "Tailoring High Displacement Performance of Ceramic-Metal Piezocomposite Actuators 'Cymbals'," submitted to *IEEE Transactions on Ultrasonics, Ferroelectrics, and Frequency Control* (1995).

43. Hirose, S., S. Takahashi, K. Uchino, M. Aoyagi, and Y. Tomikawa, "Measuring Methods for High-Power Characteristics of Piezoelectric Materials," *Mat. Res. Soc. Symp. Proc.* **360**, 15-20 (1995).

44. Takahashi, S., S. Hirose, K. Uchino, and K.Y. Oh, "Electro-Mechanical Characteristics of Lead-Zirconate-Titanate Ceramics Under Vibration-Level Change," *Proc. 9th ISAF*, 377-382 (1995).

45. Takahashi, Sadayuki, Yasuhiro Sasaki, Seiji Hirose, and Kenji Uchino, "Electro-Mechanical Properties of $PbZrO_3$-$PbTiO_3$-$Pb(Mn_{1/3}Sb_{2/3})O_3$ Ceramics Under Vibration-Level Change," *Mat. Res. Soc. Symp. Proc.* **360**, 305-310 (1995).

VOLUME V

46. Zheng, Jiehui, Sadayuki Takahashi, Shoko Yoshikawa, Kenji Uchino, and J.W.C. de Vries, "Heat Generation in Multilayer Piezoelectric Actuators," submitted to *J. Am. Ceram. Soc.* (1995).

47. Uchino, Kenji, "Review: Photostriction and its Applications," in press *J. Innovations in Mater. Res.* (1995).

48. Chu, Sheng-Yuan, and Kenji Uchino, "Photo-Acoustic Devices Using $(Pb,La)(Zr,Ti)O_3$ Ceramics," *Proc. 9th ISAF*, 743-745 (1995).

Integration Issues

49. Matsko, M.G., Q.C. Xu, and R.E. Newnham, "Zig-Zag Piezoelectric Actuators: Geometrical Control of Displacement and Resonance," *J. Intell. Mat. Syst. and Struct.* **6** (6), 783-786 (1995).

50. Xu, Baomin, Qiming Zhang, V.D. Kugel, and L.E. Cross, "Piezoelectric Air Transducer for Active Noise Control," submitted *Proc. SPIE* (1996).

Integration Issues (continued)–Volume V

51.   Kumar, S., A.S. Bhalla, and L.E. Cross, "Underwater Acoustic Absorption by Collocated Smart Materials," accepted *Ferroelectric Letters* (1995).

52.   Elissalde, Catherine and Leslie Eric Cross, "Dynamic Characteristics of Rainbow Ceramics," *J. Am. Ceram. Soc.* **78** [8], 2233-2236 (1995).

Processing Studies

53.   Bowen, Christopher P., Thomas R. Shrout, Robert E. Newnham, and Clive A. Randall, "Tunable Electric Field Processing of Composite Materials," *J. of Intelligent Material Systems and Structures* **6** (2), 159-168 (1995).

54.   Zhang, Q.M., J. Zhao, T. Shrout, N. Kim, and L.E. Cross, "Characteristics of the Electromechanical Response and Polarization of Electric Field Biased Ferroelectrics," *J. Appl. Phys.* **77** (5), 2549-2555 (1995).

55.   Zhao, J., Q.M. Zhang, N. Kim, and T. Shrout, "Electromechanical Properties of Relaxor Ferroelectric Lead Magnesium Niobate-Lead Titanate Ceramics," *Jpn. J. Appl. Phys.* **34**, 5658-5663 (1995).

56.   Zipparo, M.J., K.K. Shung, and T.R. Shrout, "Piezoelectric Properties of Fine Grain PZT Materials," *Proc. IEEE Int'l Ultrasonics Symposium* (1995).

57.   Yoshikawa, Shoko, Ulagaraj Selvaraj, Paul Moses, John Witham, Richard Meyer, and Thomas Shrout, "Pb(Zr,Ti)O$_3$[PZT] Fibers–Fabrication and Measurement Methods," *J. Intell. Mat. Syst. and Struct.* **6** (2), 152-158 (1995).

58.   Hackenberger, W.S., T.R. Shrout, A. Nakano, and R.F. Speyer, "Rate Controlled Sintering of Low Temperature Cofired Ceramic Multilayers Used for Electronic Packaging."

59.   Randall, C.A., N. Kim, W. Cao, and T.R. Shrout, "Domain-Grain Size Relation in Morphotropic Phase Boundary, Pb(Zr$_{0.52}$,Ti$_{0.48}$)O$_3$," 7th US:Japan Mtg. on Dielectric and Piezoelecttric Ceramics, Tsukuba, 145-149 (1995).

60.   Cann, David P., Clive A. Randall, and Thomas R. Shrout, "Investigation of the Dielectric Properties of Bismuth Pyrochlores," accepted *Solid State Communication* (1995).

VOLUME VI

61.   Mulvihill, Maureen L., Seung Eek Park, George Risch, Zhuang Li, Kenji Uchino, and Thomas R. Shrout, "The Role of Processing Variables in the Flux Growth of PZN-PT Relaxor Ferroelectric Single Crystals."

Thin Films Ferroelectrics

62.   Chen, H.D., K.R. Udayakumar, L.E. Cross, J.J. Bernstein, and L.C. Niles, "Dielectric, Ferroelectric, and Piezoelectric Properties of Lead Zirconate Titanate Thick Films on Silicon Substrates," *J. Appl. Phys.* **77** (7), 3349-3353 (1995).

63. Udayakumar, K.R., P.J. Schuele, J. Chen, S.B. Krupanidhi, and L.E. Cross, "Thickness-Dependent Electrical Characteristics of Lead Zirconate Titanate Thin Films," *J. Appl. Phys.* **77** (8), 3981-3986 (1995).

64. Chen, H.D., K.R. Udayakumar, C.J. Gaskey, and L.E. Cross, "Electrical Properties' Maxima in Thin Films of the Lead Zirconate-Lead Titanate Solid Solution System," *Appl. Phys. Lett.* **67** (23), 3411-3413 (1995).

65. Gaskey, C.J., K.R. Udayakumar, H.D. Chen, and L.E. Cross, "'Square' Hysteresis Loops in Phase-Switching Nb-Doped Lead Zirconate Stannate Titanate Thin Films," *J. Mater. Res.* **10** (11), 2764-2769 (1995).

66. Yamakawa, K., S. Trolier-McKinstry, J.P. Dougherty, and S. Krupanidhi, "Reactive Magnetron Co-Sputtered Antiferroelectric Lead Zirconate Thin Films," *Appl. Phys. Lett.* **67** (14), 2014-2016 (1995).

67. Ravichandran, D., K. Yamakawa, A.S. Bhalla, and R. Roy, "Alkoxide Derived $SrBi_2Ta_2O_9$ Phase Pure Powder and Thin Films."

68. Thakoor, Sarita, A.P. Thakoor, and L. Eric Cross, "Optical Non-Invasive Evaluation of Ferroelectric Films/Memory Capacitors," *Mat. Res. Soc. Symp. Proc.* **360**, 157-167 (1995).

PROCESSING STUDIES

(continued)

APPENDIX 61

The Role of Processing Variables in the Flux Growth of PZN-PT Relaxor Ferroelectric Single Crystals

Maureen L. Mulvihill[1], Seung Eek Park[1], George Risch[1], Zhuang Li[2], Kenji Uchino[1] and Thomas R. Shrout[1]

[1]*Materials Research Laboratory, Pennsylvania State University, University Park, PA 16802, USA.*
[2]*Materials Science Division, Argonne National Laboratory, Argonne, IL 60439, USA.*

Relaxor ferroelectric single crystals of $Pb(Zn_{1/3}Nb_{2/3})O_3$-$PbTiO_3$ (PZN-PT) are of interest as high performance transducers due to their very large piezoelectric coupling and dielectric properties. A high temperature flux solution method was used to grow (1-x)PZN-(x)PT, where x = 0.0, 0.1 and 0.15 single crystals. Processing conditions were optimized to increase the size and yield of the perovskite crystals, including variation of the flux to composition ratio, cooling rate, soak time and soak temperature. The crystals varied in size from 0.01 cm to 1.5 cm on an edge, and in color from opaque to brown due to the changes in processing conditions. The crystals were characterized by XRD, dielectric constant and dielectric loss measurements. As the content of PT increased the transition from the paraelectric to the ferroelectric phase approached first order behavior and the crystal structure transformed from rhombohedral to tetragonal. This structure transition caused the lattice constant along the c-axis to elongate as the c/a ratio increased. At room temperature, the dielectric constants for the PZN-PT compositions along the [111] or [001] axes were as great as 5000 and the dielectric losses were as low as 0.01.

KEYWORDS: lead zinc niobate, lead titanate, relaxor ferroelectric, single crystal, transducers, piezoelectrics, flux growth

§1. Introduction

In contrast to a normal ferroelectric such as $PbTiO_3$ (PT), relaxor ferroelectrics exhibit a broad and frequency dispersive phase transition. $Pb(Zn_{1/3}Nb_{2/3})O_3$ (PZN) is an example of a relaxor ferroelectric material which has a disordered complex perovskite structure in which the Zn^{2+} and Nb^{5+} cations exhibit only short range order on the B-site. The maximum in the dielectric constant is obtained near 140°C. The transition temperature (T_{max}) and dielectric constant maximum (K_{max}) depend on the measurement frequency.[1,2,3] PZN has rhombohedral symmetry at room temperature[4,5] with space group R3m whereas the normal ferroelectric $PbTiO_3$ (PT) has tetragonal symmetry with space group P4mm and a transition temperature (T_C) at 490°C.

A complete solid solution is formed between $(1-x)Pb(Zn_{1/3}Nb_{2/3})O_3$ and $xPbTiO_3$ (PZN-PT). The morphotropic phase boundary (MPB) at x ~ 0.1 separates the rhombohedral and tetragonal phases at 25°C.[4,6,7] In contrast to the $PbZrO_3$ - $PbTiO_3$ (PZT) system,[8] the MPB for PZN-PT inclines as a function of temperature and composition, as shown in Fig. 1.[9]

Single crystal growth of PZN-PT by the flux technique is considerably easier than for PZT which makes PZN-PT a potential candidate material for high performance transducers. Several researchers have reported on the large piezoelectric ($d_{33}^* \sim 1500*10^{-12}$C/N), dielectric ($K_{RT} \sim 3000$), and electromechanical coupling parameters ($k_{33}^* \sim 92\%$) of PZN-PT based single crystals.[6,9,10] However, most of these studies failed to discuss processing conditions such as flux to composition ratio, soak temperature, soak time, and cooling rates. In this study, the variables which affect crystal growth of PZN and 90PZN-10PT are systematically controlled to determine the effect on size, color and morphology.

§2. Experimental Procedure

The PZN-PT single crystals were grown by the flux solution method.[11] The powders used were PbO, 99.9%, Pb_3O_4, 99.9%, and TiO_2, 99.99% from Aldrich Chemical Company. The ZnO and Nb_2O_5 powders were Grade 1 from Specialty Products-Johnson Matthey. PbO and Pb_3O_4 were used as the flux. Each batch was based on 450 grams of raw powder which was loaded into a 70 ml platinum crucible and charged several times at 900°C until the crucible was full.

The platinum crucible was covered with a platinum lid and placed in an alumina crucible. The alumina crucible was then sealed with an alumina lid using alumina cement to minimize PbO volatility and then placed in a bottom loading furnace.

Differential Thermal Analysis (DTA) was used to determine the initial processing conditions for the growth of PZN single crystals. One gram of 30:70 PZN:PbO ground crystals was heated in air at a rate of 3°C per minute to 1150°C then cooled at 10°C per minute. The processing conditions were varied in an attempt to achieve PZN-PT single crystals which were perovskite phase pure, greater than 1 cm in size, and high optical quality. The processing conditions which were analyzed are listed below:

1. Mole ratio of solute composition to flux (C:F)

2. Soaking time (t_{soak})

3. Soaking temperature (T_{soak})

4. Slow Cooling rate (C_S)

5. Transition temperature (T_{S-F}) between the slow (C_S) and fast (C_F) cooling rates.

The effect of compositional variation was studied by varying the mole ratio of solute composition to flux (C:F) from 26:74 to 40:60. Figure 2 illustrates the furnace profile for crystal growth. The furnace controller was programmed to reach the maximum temperature (T_{soak}) between 1150° and 1200°C. The samples were held at a constant soak temperature (T_{soak}) for 2 to 10 hours. The crucibles were then cooled at a slow rate (C_S) between 0.5 to 5°C per hour. The changes in soak temperature, time and slow cooling rate enabled the effect of these variables on the crystal color, morphology and size to be studied. After the furnace temperature cooled to a temperature between 800° and 900°, the furnace was cooled at the faster rate (C_F) to room temperature. The transition temperature between the slow cooling rate (C_S) and the fast cooling rate (C_F) determined the amount of pyrochlore phase formation. The fast heating (H_F) rate remained constant at 100°C per hour for every crystal run. The fast cooling (C_F) rate was held constant at -50°C per hour which will be discussed in section 3.6. The single crystals were removed from the flux with the aid of a warm 25 volume percent nitric acid solution.

Crystals from each batch were ground into a fine powder and examined by powder x-ray diffraction (XRD) for phase identification and lattice parameters. Single crystals were oriented along the [111] or [001] crystallographic axes using the Laué x-ray technique. The dielectric constants and losses were measured along the respective crystal structure polarization axes. The crystals were cut into thin sections and polished to a 3 μm surface finish. Circular gold electrodes were deposited with diameters ranging from 1 to 2 mm. The capacitance and loss of the crystal plates were measured as functions of temperature and frequency using a Hewlett Packard Programmable 4275A Multi-frequency LCR meter in a computer controlled furnace system.

§3. Results and Discussion

The DTA data for a 30:70 PZN:PbO sample is shown in Fig. 3. On heating, an endothermic peak occurred at 850°C which signified the melting of the PbO flux. On cooling, the crystallization of the PZN resulted in an exothermic peak at 1000°C. The crystallization temperature increased as the solute content increased. The cooling curve also showed a second exothermic peak near 850°C which is assumed to be pyrochlore crystallization which will be discussed later. A third exothermic peak occurred at 700°C which was associated with the flux solidification temperature.

3.1 Mole Ratio of Solute Composition to Flux, (C:F)

The composition to flux ratios, C:F, were varied from 26:74 to 40:60. PbO and Pb_3O_4 were used as the PbO source to determine the best source of raw material for the flux. Pb_3O_4 was considered a better flux than PbO since the decomposition of Pb_3O_4 to PbO released O_2 which would assist in the thermal mixing of the raw powders.[12] The three crystals runs used to examine the effect of the C:F are represented in Table I. With each of the crystal runs all the growth parameters were held constant except the C:F ratio. The ratio of 35:65 produced perovskite crystals with minimal pyrochlore phase. The 30:70 ratio produced yellow perovskite single crystals with approximately 15 percent pyrochlore phase. The 26:74 ratio produced 100% pyrochlore crystals. The stability of perovskite with respect to pyrochlore was found to be very sensitive to the C:F ratio and it was assumed that no perovskite crystals could be formed with a

4

ratio lower that 26:74. It has been found that PZN can be formed under an excess molten PbO environment.[13] Therefore, the temperature range where PZN phase can be formed using a PbO flux depends on the C:F ratio. This temperature range is associated with both crystallization temperature and decomposition temperature of the perovskite phase into the pyrochlore phase; therefore, decreasing the C:F ratio causes the decomposition temperature and crystallization temperature to increase and decrease, respectively. In other words, decreasing the C:F ratio caused the perovskite crystallization temperature range to decrease. Most of all, the increase of the decomposition temperature would be critical if the T_{S-F} in Table I were fixed since all of the perovskite phase would decompose into the pyrochlore phase. This decomposition in to the pyrochlore phase is expected to be the case for the 26:74 ratio batch, and will be further discussed in section 3.5.

3.2 Soak Time, (t_{soak})

The soak time, t_{soak}, was changed from 2 to 10 hours, as reported in Table II, to determine the effect on crystal growth. The effect of the soak times was compared using the MPB composition, 90PZN-10PT. The single crystals for the two soak times were similar in color (yellow) and size (0.6 cm). From this, it can be assumed that soaking time does not appear to have a significant effect on the crystal quality or size; therefore, a shorter soak time is recommended to reduce volatilization of PbO and ZnO.

3.3 Soak Temperature, (T_{soak})

While the DTA data indicated a soak temperature, T_{soak}, of ~1000°C would be sufficient to grow perovskite crystals, actual crystal runs demonstrated that higher temperatures were needed to produce crystals larger than a few 100 μm. Crystals grown using soak temperatures of 1150°C and 1200°C varied in size and color as represented in Table III. The higher soak temperature produced larger crystals (~1.5 cm) with a brown color and the lower soak temperature produced smaller crystals (~0.6 cm) with a yellow color. The growth rate at 1150°C was ~0.0024 cm/hr, compared to ~0.0047 cm/hr at 1200°C. The origin and effect of the color differences on measured dielectric properties are the subject of future investigation.

5

3.4   Slow Cooling Rate, (C_S)

PZN single crystals slow cooled at different rates varied in structure and color. The cooling rate, C_S, was altered from 0.5°C/hr to 5°C/hr as compared in Table IV. The crystals which were formed at the slowest rate, 0.5°C/hr, had only pyrochlore phase present which can be attributed to the decomposition of the perovskite phase. The crystals cooled at 2°C/hr had a perovskite structure with a yellow color. The crystals cooled using the fastest rate were perovskite and opaque. The opaque perovskite crystals contained many cracks; therefore, they were more brittle than the yellow perovskite crystals. The faster cooling rate supersaturated the solution and resulted in unstable growth conditions. An intermediate cooling rate ~1 to 2°C/hr was optimal to produce low defect perovskite PZN single crystals.

3.5   Lower Temperature Limit of Slow Cooling, (T_{S-F})

The crucibles were slow cooled down to the transition temperature between slow and fast cooling, T_{S-F}, which was varied between 900°C to 800°C. From the DTA data in Fig. 3, it was expected that the exothermic peak at 850°C was due to pyrochlore formation. From the experiments represented in Table V, it was confirmed that the second peak in Fig. 3 was the pyrochlore crystallization temperature. The percentage of pyrochlore phase formed can be reduced by setting T_{S-F} above 850°C.

3.6   Fast Cooling Rate, (C_F)

It must also be noted that it is very important to cool quickly through the pyrochlore phase region to avoid pyrochlore crystal formation. The fast cooling rate, C_F, was found to be associated with the decomposition of perovskite crystals into pyrochlore crystals. The size and yield of perovskite crystals decreased and pyrochlore crystals increased as the cooling rate decreased. At a C_F of -50°C/hr, the crystals maintained a high quality perovskite structure without cracking.

3.7   Crystal Morphology

In each crystal growth run, a fraction of pyrochlore phase formed on the top layer of the crucible which depended on processing conditions. The pyrochlore phase was very easy to

identify and remove since it had an orange-red color and octahedral morphology with the symmetry m3m, as illustrated in Fig. 4(a).

Perovskite PZN crystals showed an arrow-head shape, as illustrated in Fig. 4(b), as found by previous researchers.[1,3,7] The typical crystal morphologies for PZN-PT are presented in Fig. 5. Although the rhombohedral perovskite crystals did not exhibit a fully faceted well developed morphology, the {111} faces which indicates the rhombohedral morphology could be indexed. It was expected that the morphology of the crystals would have been cubic since according to Fig. 1 the crystals should have had a cubic symmetry when they were grown. This means that if perovskite crystals were grown under stable growth condition a cubic morphology should have occurred. Even though it is not obvious why PZN perovskite crystals have a rhombohedral morphology with an arrow-head shape, it can be assumed that the PZN perovskite crystals were not grown under stable conditions, but under metastable conditions in a PbO excess environment. From the as-grown morphology, it can be expected that the formation for the perovskite crystals under metastable conditions can be followed by the decomposition of the crystal into another phase (the other phase being pyrochlore) if appropriate growth conditions are not maintained which was supported by this work.

3.8 Dielectric Constant and Loss Measurements

All single crystals characterized by dielectric measurement were confirmed as perovskite by XRD. The dielectric constant and dielectric losses were measured along the [111] and [001] directions of the psuedocubic unit cell. All of the dielectric loss values measured at high (>225°C) and low (<25°C) temperatures were low which suggested that the crystals had minimal number of defects.

Dielectric constant and loss variations of PZN with temperature is shown in Fig. 6. This [111] oriented crystal showed typical relaxor-type ferroelectric phase transition behaviors in which the dielectric constant maximum lowered from ~53000 to ~43000 and shifted to higher temperatures from 140°C to 150°C with increasing frequency from 100 Hz to 100 kHz.

According to previously reported work,[4-7] the 90PZN-10PT single crystal composition should lie along the morphotropic phase boundary at room temperature. In the case of PZN-PT, the MPB varies as a function of temperature and composition. Thus, the MPB is not a particular composition but a range of compositions, and therefore a mixed phase was expected for this crystal. The XRD data for the 90PZN-10PT composition is shown in Fig. 7. All peaks could be indexed as mixed rhombohedral and tetragonal phases. The lattice parameters of the rhombohedral and tetragonal phases are a = 4.051Å, α = 89.93° and a = 4.033Å, c = 4.080Å, respectively. Near room temperature a dramatic change in the dielectric loss occurred accompanied by a slight change in the dielectric constant. These changes signified the rhombohedral to tetragonal transition which coincides with a previous report.[10] Although the 90PZN-10PT composition showed more of a first-order phase transition than the PZN crystal, it still had some relaxor behavior with the onset temperature of 148°C below T_{max} as shown in Fig. 8. The T_{max} occurred near 160°C with a dielectric constant near 45000 for 100 Hz.

Single crystal XRD analysis for the 85PZN-15PT revealed that this composition had a single phase tetragonal structure. This crystal showed the first-order, Curie-Weiss behavior as expected for the tetragonal structure. Figure 9 shows the dielectric constant and loss variations on temperature for [001] oriented crystal. Sharp first order transitions were found at a temperature of 205°C with a maximum dielectric constant near 34000.

In Table VI, the dielectric constant, dielectric loss and transition behavior of the as-grown crystals are summarized. As expected, the morphotropic phase boundary crystal (90PZN-10PT) showed the highest dielectric constant at room temperature. The maximum dielectric constant (K_{max}) at the transition temperature decreased with increasing PT content.

§4. Conclusions

The growth of PZN-PT single crystals using the flux method produced high quality, low defect, perovskite crystals. However, it was found that the perovskite crystals were grown under metastable conditions which could easily decompose into pyrochlore crystals with changes in processing conditions. The PZN-based crystals varied in size and color depending on the

8

processing conditions. A solute composition to flux ratio of 30:70 to 40:60, Pb_3O_4 as the flux, and a soak time of 2 hours produced perovskite crystals. Larger crystals were grown by increasing the soak temperature to 1200°C. A cooling rate between 1°C/hr and 2°C/hr produced perovskite crystals which were near defect-free and mechanically strong. The crystals which were slow cooled down to 900°C were nearly 100% perovskite phase since the pyrochlore crystallization which began at 850°C was avoided.

The dielectric constant and loss calculations determined by capacitance measured as a function of temperature showed a trend towards more first order behavior as the concentration of PT was increased. The increase in PT caused the dielectric constant at room temperature to peak at 10%PT. In all three crystal compositions measured, the dielectric loss was less than 0.05 at room temperature which signified high quality, low defect, single crystals.

Acknowledgments

References

1) V.A. Bokov and I.E. Myl'nikova: Sov. Phys.-Solid State **2** (1961) 2428.

2) N.P. Khuchua, V.F. Bova, and I.E. Myl'nikova: Sov. Phys.-Solid State **10** (1968) 194.

3) J. Kuwata, K. Uchino, S. Nomura: Ferroelectrics **22** (1979) 863.

4) S. Nomura, T. Takahashi and Y. Yokomizo: J. Phys. Soc. Jap. **27** (1969) 262.

5) Y. Yokomizo, T. Takahashi, and S. Nomura: J. Phy. Soc. Jap. **28** (1970) 1278.

6) J. Kuwata, K. Uchino, and S. Nomura: Jpn. J. Appl. Phys. **21** (1982) 1298.

7) Z.P. Chang, A.S. Bhalla and L.E. Cross: IEEE Transactions (1986) 482.

8) B. Jaffe, W.R. Cook and H. Jaffe: Piezoelectric Ceramics, eds. J.P. Roberts and P. Popper, (Academic Press. London and New York. 1971) Chap. 7, p. 136.

9) J. Kuwata, K. Uchino and S. Nomura: Ferroelectrics **37** (1981) 579.

10) Y. Yamashita: Jpn. J. Appl. Phys. **33** (1994) 5328.

11) W. Tolksdorf: Handbook of Crystal Growth-Bulk Crystal Growth, eds. D.T.J. Hurle, (Elsevier Science B.V. North-Holland, 1994) Vol. 2, Chap. 10, p. 563.

12) Y. Yamashita, Personal Communication, Toshiba Corporation, Kawasaki Japan.

13) H.M. Jang, S.H. Oh, and J.H. Moon: J. Am. Ceram. Soc. **75** (1992) 82.

List of Figures

Fig. 1

Maureen Mulvihill, Seung Eek Park, George Risch, Zhuang Li, Kenji Uchino and Thomas Shrout
Desired breadth undetermined, shrink so it fits and is clear to read.
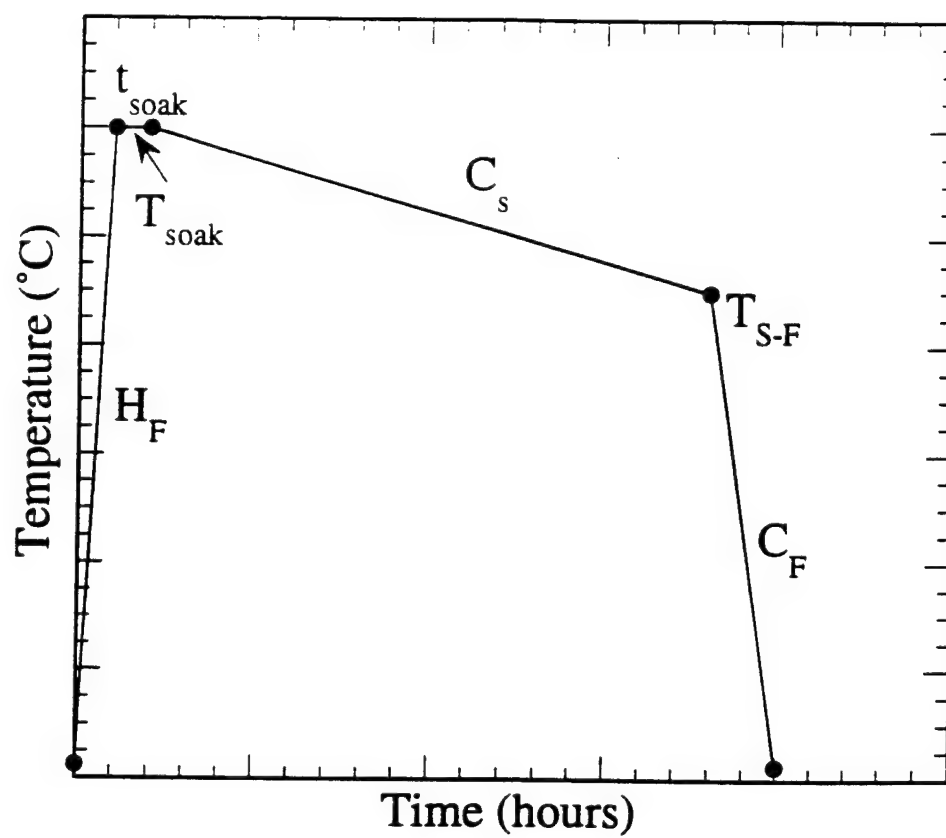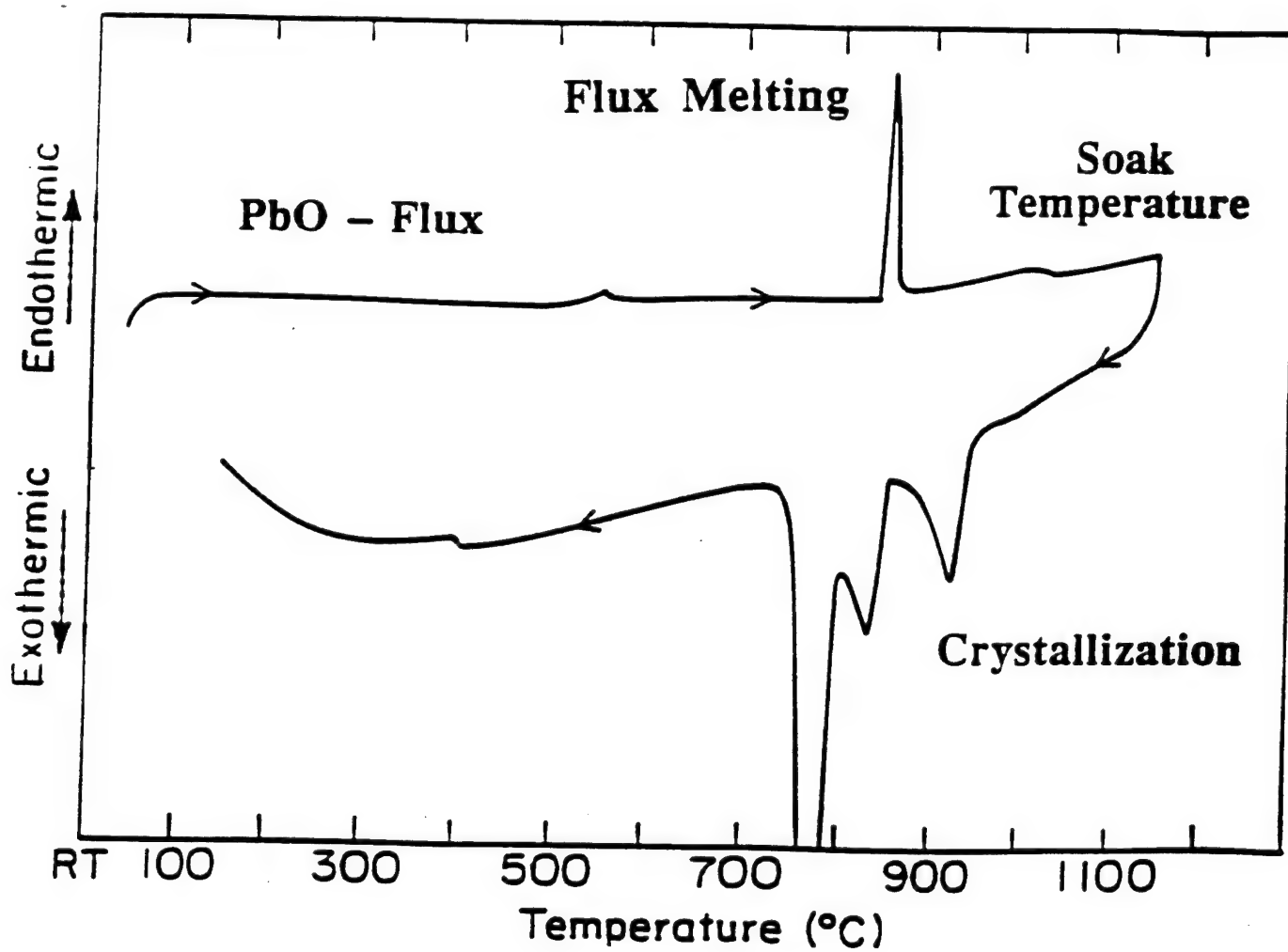
Fig. 2:

Maureen Mulvihill, Seung Eek Park, George Risch, Zhuang Li, Kenji Uchino and Thomas Shrout
Desired breadth undetermined, shrink so it fits and is clear to read.

Fig. 3:

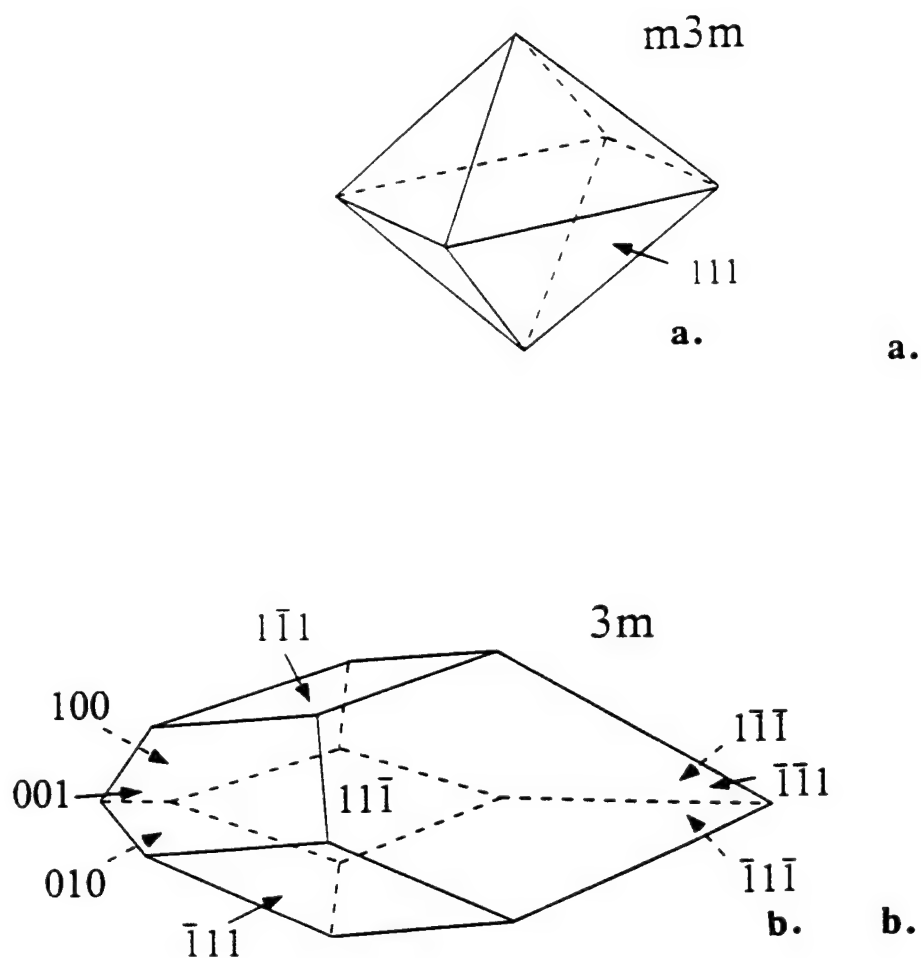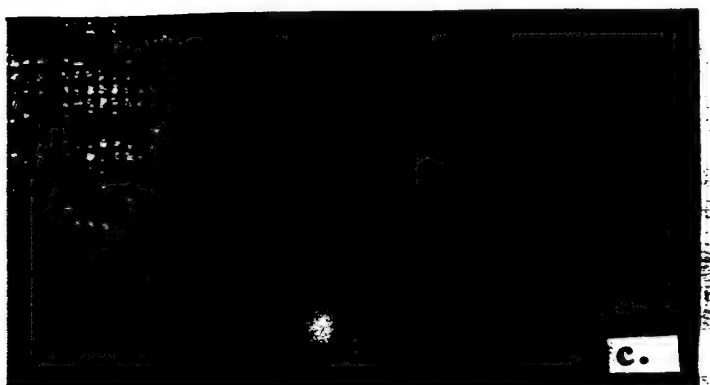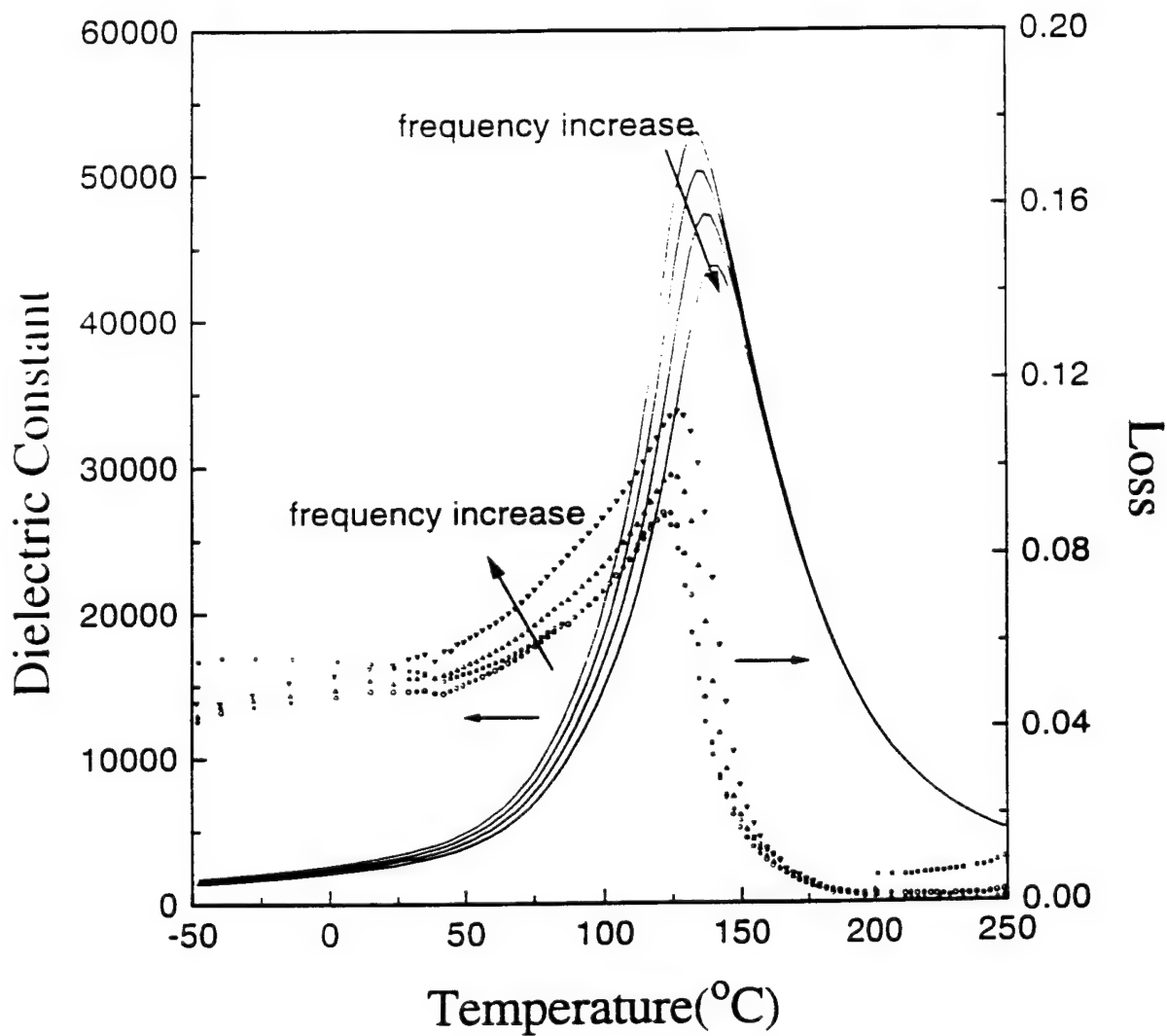Maureen Mulvihill, Seung Eek Park, George Risch, Zhuang Li, Kenji Uchino and Thomas Shrout

Fig. 4:
Maureen Mulvihill, Seung Eek Park, George Risch, Zhuang Li, Kenji Uchino and Thomas Shrout
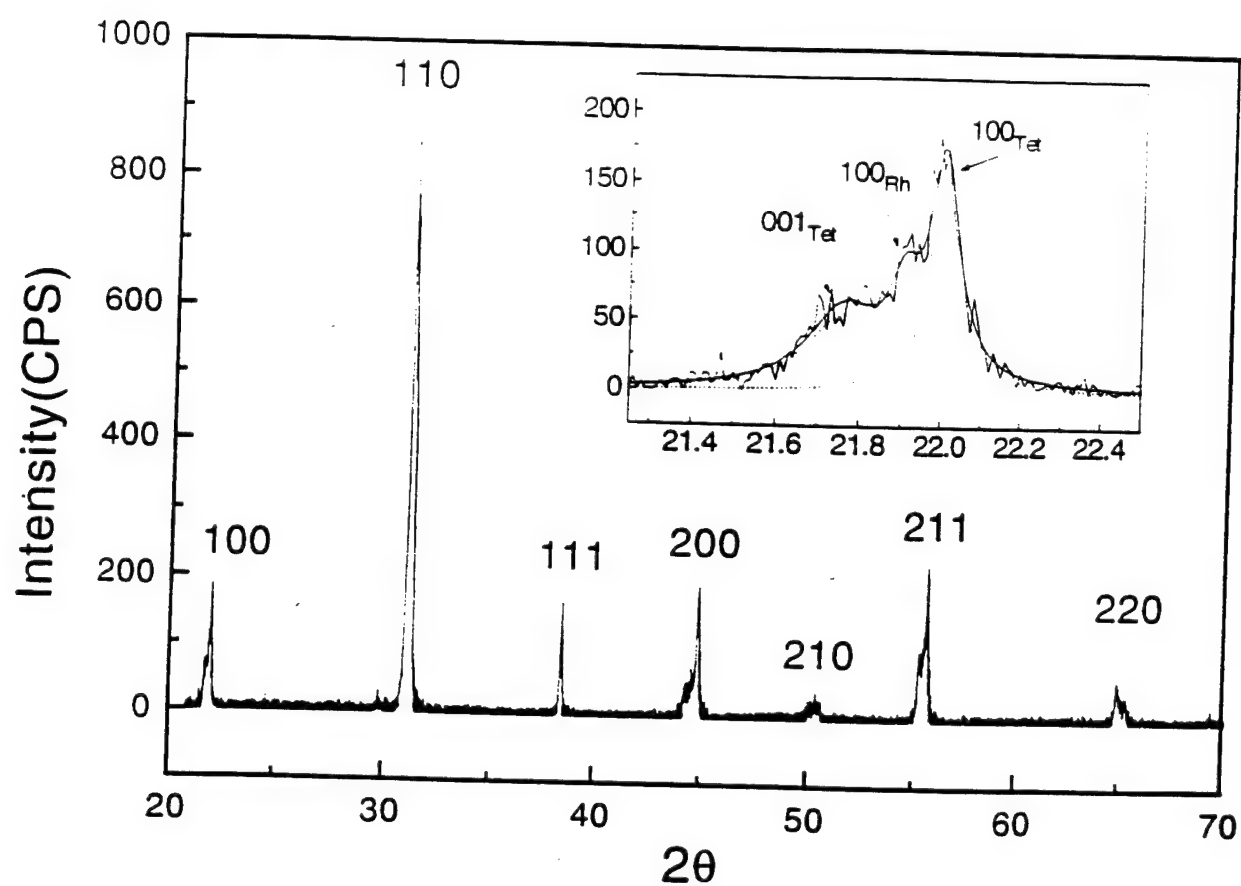Desired breadth undetermined, shrink so it fits and is clear to read.

Fig. 5:
Maureen Mulvihill, Seung Eek Park, George Risch, Zhuang Li, Kenji Uchino and Thomas Shrout
Desired breadth undetermined, shrink so it fits and is clear to read.

16

Fig. 6:
Maureen Mulvihill, Seung Eek Park, George Risch, Zhuang Li, Kenji Uchino and Thomas Shrout
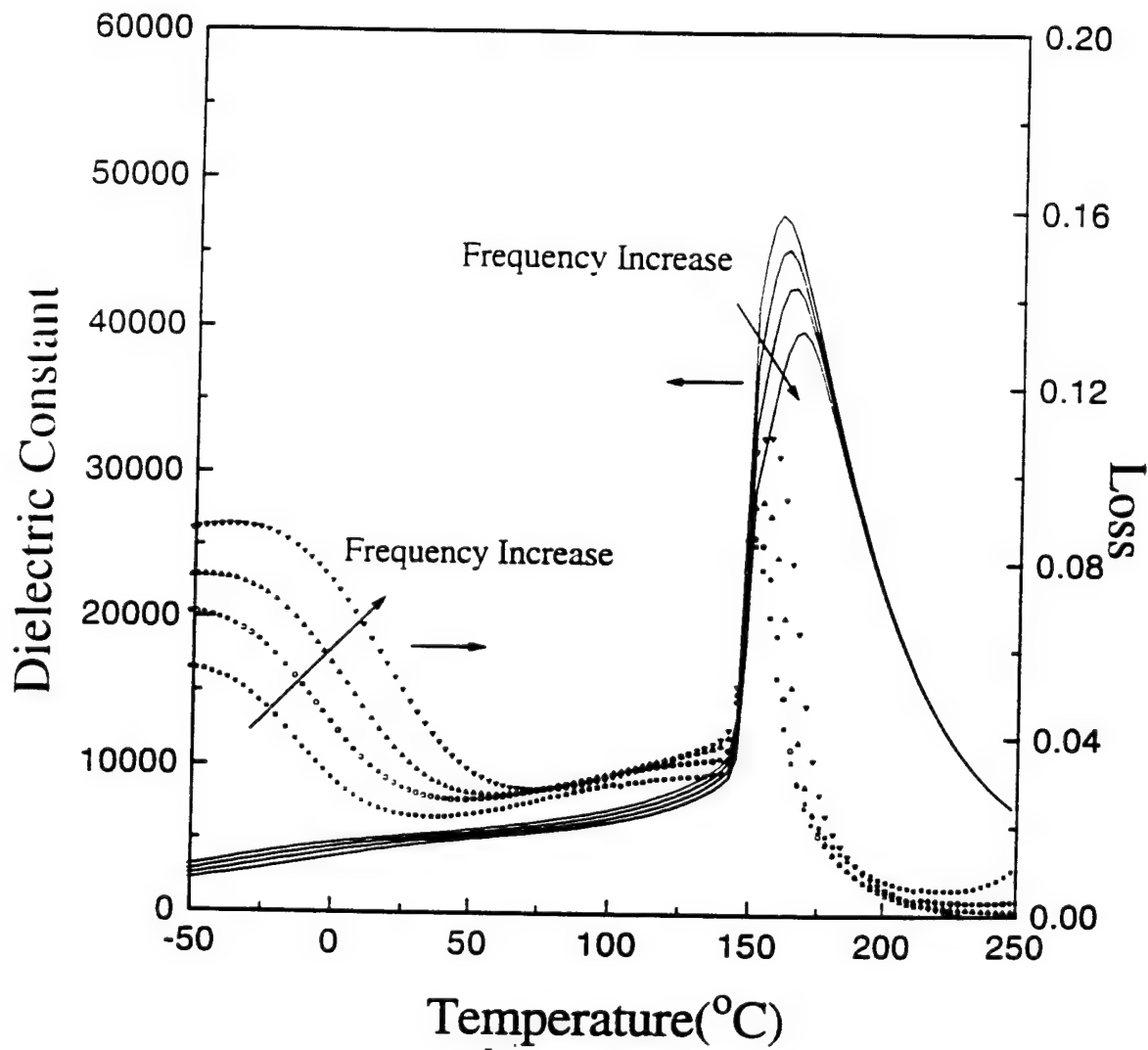Desired breadth undetermined, shrink so it fits and is clear to read.

17

Fig. 7:
Maureen Mulvihill, Seung Eek Park, George Risch, Zhuang Li, Kenji Uchino and Thomas Shrout
Desired breadth undetermined, shrink so it fits and is clear to read.

18

Fig. 8:
Maureen Mulvihill, Seung Eek Park, George Risch, Zhuang Li, Kenji Uchino and Thomas Shrout
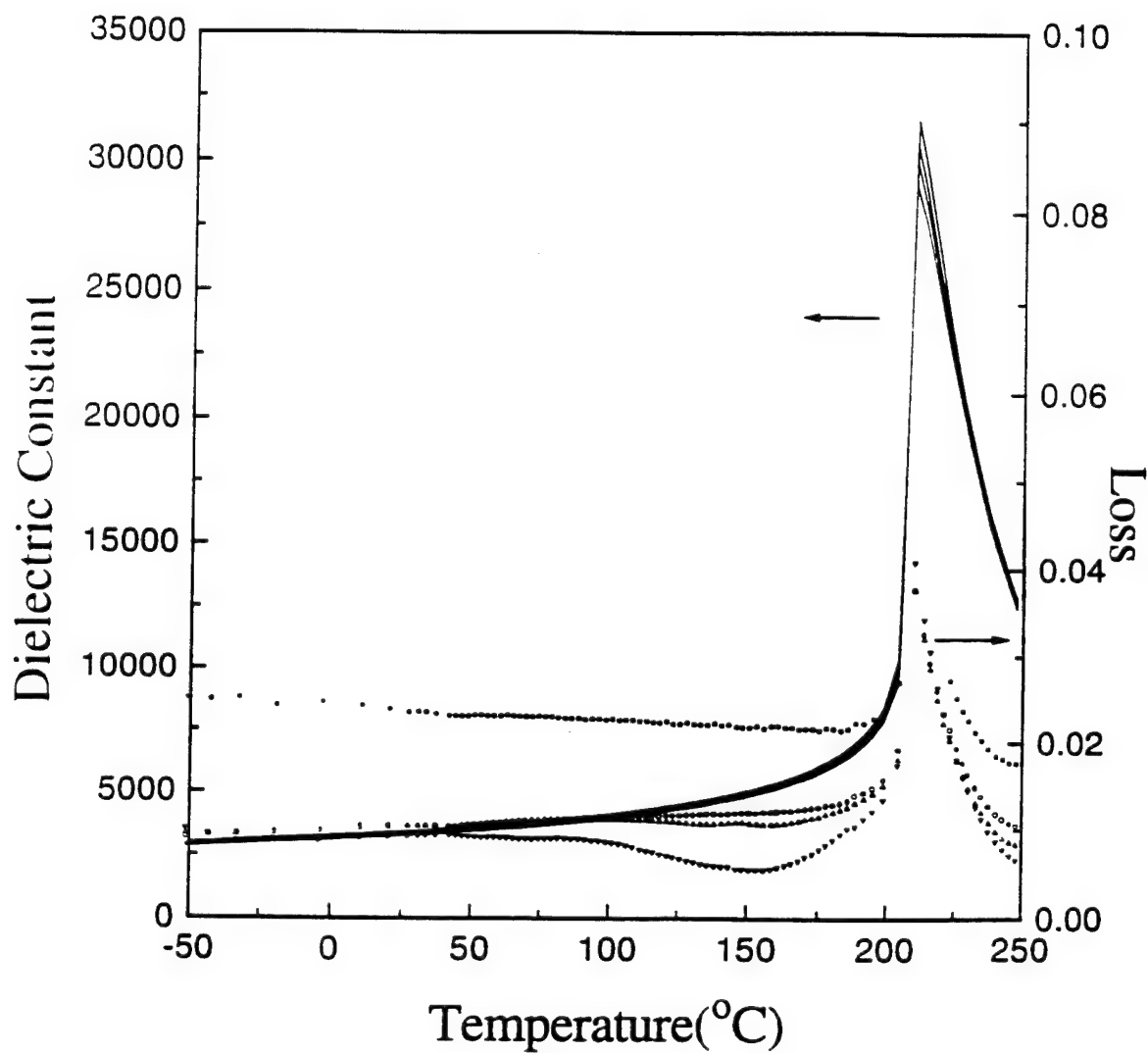Desired breadth undetermined, shrink so it fits and is clear to read.

Fig. 9:
Maureen Mulvihill, Seung Eek Park, George Risch, Zhuang Li, Kenji Uchino and Thomas Shrout
Desired breadth undetermined, shrink so it fits and is clear to read.

Table I: Study of the effect of the composition to flux (C:F) ratio on a PZN perovskite crystal formation.

Run Number	1	2	3
Crystal	PZN	PZN	PZN
C:F	**26:74**	**30:70**	**35:65**
Flux	PbO	PbO	PbO
t_{soak}	2	2	2
T_{soak}	1150°	1150°	1150°
C_S	2	2	2
T_{S-F}	900°	900°	900°
Color	NA	yellow	yellow
Size	NA	0.3 cm	0.5 cm
Percentage Perovskite	0%	85%	95%
Percentage Pyrochlore	100%	15%	5%

Maureen Mulvihill, Seung Eek Park, George Risch, Zhuang Li, Kenji Uchino and Thomas Shrout
Desired breadth undetermined, shrink so it fits and is clear to read.

Table II: Study of the effect of soaking time on a 90PZN-10PT perovskite crystal formation.

Run Number	1	2
Crystal	90PZN-10PT	90PZN-10PT
C:F	30:70	40:60
Flux	PbO	PbO
t_{soak}	2	10
T_{soak}	1150°	1150°
C_S	2	2
T_{S-F}	900°	900°
Color	yellow	yellow
Size	0.6 cm	0.6 cm

Maureen Mulvihill, Seung Eek Park, George Risch, Zhuang Li, Kenji Uchino and Thomas Shrout
Desired breadth undetermined, shrink so it fits and is clear to read.

Table III: Study of the effect of the soaking temperature on a PZN perovskite crystal formation.

Run Number	1	2
Crystal	PZN	PZN
C:F	40:60	40:60
Flux	PbO	PbO
t_{soak}	10	10
T_{soak}	**1150**	**1200**
C_S	1	1
T_{S-F}	900°	880°
Color	dark yellow	dark brown
Size	0.6 cm	1.5 cm

Maureen Mulvihill, Seung Eek Park, George Risch, Zhuang Li, Kenji Uchino and Thomas Shrout
Desired breadth undetermined. shrink so it fits and is clear to read.

Table IV: Study of the effect of the slow cooling rate on a PZN perovskite crystal formation.

Run Number	1	2	3
Crystal	PZN	PZN	PZN
C:F	30:70	30:70	30:70
Flux	PbO	PbO	PbO
t_{soak}	2	2	2
T_{soak}	1150	1150	1150
CS	0.5	2	5
T_{S-F}	900°	900°	900°C
Color	NA	yellow	white
Size	NA	0.5 cm	0.5 cm
Mechanical Integrity	NA	Strong	Weak
Percentage Pyrochlore	100%	15%	15%

Maureen Mulvihill, Seung Eek Park, George Risch, Zhuang Li, Kenji Uchino and Thomas Shrout
Desired breadth undetermined, shrink so it fits and is clear to read.

Table V: Study of the effect of the transition temperature on a PZN perovskite crystal formation.

Run Number	1	2
Crystal	PZN	PZN
C:F	40:60	40:60
Flux	PbO	PbO
t_{soak}	10	10
T_{soak}	1200	1200
C_S	1	1
T$_S$-F	**800°**	**880°**
Color	light brown	Dark Brown
Size	0.4 cm	1.5 cm
Percentage Perovskite	75%	95%
Percentage Pyrochlore	25%	5%

Maureen Mulvihill, Seung Eek Park, George Risch, Zhuang Li, Kenji Uchino and Thomas Shrout
Desired breadth undetermined, shrink so it fits and is clear to read.

25

Table VI: Dielectric constant, dielectric loss and transition behavior of PZN-PT crystals at 1 kHz.

Crystal	K_{RT}	Loss	T_{max}	K_{max}	Transition Type
PZN [111]	3200	0.05	~135°C	~50000	Relaxor
90PZN-10PT [111]	5000	0.03	~165°C	~45000	Mixed
85PZN-15PT [001]	2400	0.01	210°C	30000	First Order

Maureen Mulvihill, Seung Eek Park, George Risch, Zhuang Li, Kenji Uchino and Thomas Shrout
Desired breadth undetermined, shrink so it fits and is clear to read.

THIN FILM FERROELECTRICS

APPENDIX 62

Dielectric, ferroelectric, and piezoelectric properties of lead zirconate titanate thick films on silicon substrates

H. D. Chen, K. R. Udayakumar, and L. E. Cross
Materials Research Laboratory, The Pennsylvania State University, University Park, Pennsylvania 16802

J. J. Bernstein and L. C. Niles
The Charles Stark Draper Laboratory, 555 Technology Square, Cambridge, Massachusetts 02139

This article reports the fabrication of thick films of lead zirconate titanate (PZT) on platinum-buffered silicon substrates by screen printing. Crack-free films, up to 12 μm on a single pass, show a dielectric permittivity of 200, tangent losses of 0.05, remanent polarization of 2.5 μC/cm^2, and coercive field of 40 kV/cm. The field-induced longitudinal piezoelectric coefficient d_{33} at 40 kV/cm dc bias and 4 kV/cm alternating field corresponded to 50 pC/N. The magnitude of the piezoelectric voltage coefficient g_{33}, computed from the strain coefficient and dielectric permittivity, under the same conditions, was found to be 36×10^{-3} V m/N, higher than that of a poled PZT bulk ceramic in comparison. These results are promising for a broad variety of sensor applications. © *1995 American Institute of Physics.*

I. INTRODUCTION

The merits of using lead zirconate titanate (PZT) films in piezoelectric devices such as loudspeakers, couplers, strain gauges, and pressure sensors, by screen-printed thick film technology on 96% alumina and stainless steel substrates have been identified and discussed over the last several years.[1-4] While these are envisaged as stand-alone devices, the employment of silicon microstructures presents a great advantage of compatibility with today's integrated circuit (IC) manufacturing technology. In recent years, several processing techniques such as photolithography and three-dimensional anisotropic etching have been employed to create miniature mechanical structures with great precision. Silicon sensors or integrated sensors for radiant signals, mechanical signals, thermal signals, magnetic signals, and chemical signals are subjects of intense research; these sensors are fabricated using silicon-planar technology.[5]

The immediate application motivating this research is the need for two-dimensional arrays of high-frequency ultrasound detectors for medical and under water imaging. Currently, ultrasound detectors are fabricated by dicing of bulk PZT. Linear arrays are widely used in medical ultrasound imaging; however, two-dimensional arrays are not used. The large number of signal channels (e.g., 128×128) in a full two-dimensional array makes the array prohibitively expensive. Such an array (acoustic retina), in conjunction with an acoustic lens, could avoid the computational burden of beam forming.

Silicon micromachining techniques can be used to form arrays of small PZT on silicon transducers. Buffer amplifiers, switches, and data busses can all be fabricated on the transducer wafer or on adjacent chips electrically connected to the transducers by bump bonding. Figure 1 shows a diagram of PZT on silicon acoustic transducer. This transducer is the micromachined equivalent of a PZT bimorph bender disk. Analysis of submillimeter sized devices for its suitability for ultrasound applications is the subject of a separate study, and will be reported at a later time.

Piezoelectric PZT thick films are expected to exhibit high sensitivity as transducers, actuators or sensors. Fabricating such thick films is beyond the capabilities of current thin film physical and chemical vapor deposition techniques. Much of the research in integrating thin films on semiconductor devices has focused on memories in which the film thicknesses are typically in the 100–350 nm range. To fabricate advanced micromechanical transducers, actuators or sensors, this study has adopted screen printing of PZT on buffered silicon substrates, for which there existed, until now, no data on either its viability or its electrical characteristics. The results contained herein demonstrate the possibility of fabricating crack-free PZT thick films on buffered silicon substrates, and document the dielectric, ferroelectric, and piezoelectric properties.

II. EXPERIMENTAL PROCEDURE

Lead zirconate titanate powder, PZT 501A, obtained commercially from Ultrasonic Powders Inc., was of the morphotropic phase boundary composition, with a Zr/Ti mole ratio of 52/48, known to exhibit peak dielectric and piezoelectric properties in the bulk. Among a number of glass frits and sintering additives that were attempted, 4% by weight of Li_2CO_3 and Bi_2O_3 (at equimolar concentrations) provided the best electrical characteristics, and only these are reported here. The PZT powder was mixed with the additives in a vibratory mill for 24 h to reduce the average particle size of the powders, and then screened through a 200 mesh sieve. The dielectric paste was obtained by mixing the active powders with a proprietary DuPont organic vehicle, and modifying the viscosity and printability of the paste by dispersing with α-terpineol solvent. The homogeneity of the paste was enhanced by blending the mixture in a three-roll mill. The levels of the constitutents in the paste were 69% by weight of the primary functional component (PZT), 22% organic vehicle, and 9% α-terpineol. The viscous dielectric paste was screen printed through the apertures of a stencil screen to deposit the required pattern onto a 25-mm-square (100) sili-
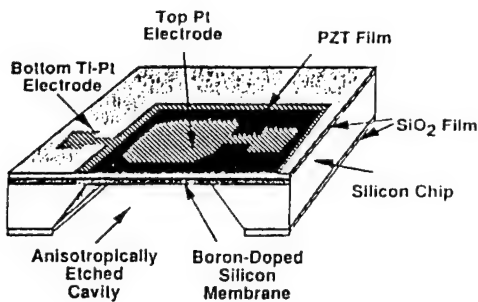
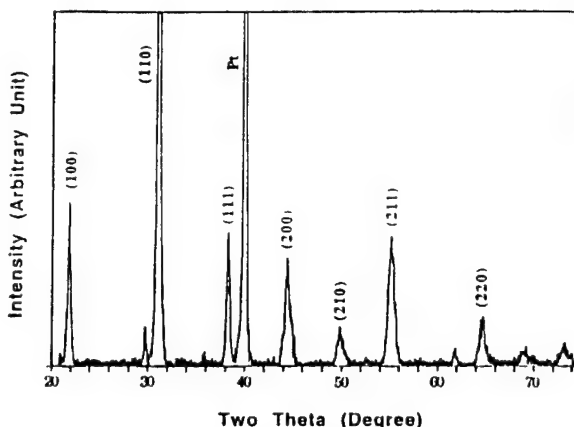FIG. 1. PZT on silicon micromachined ultrasonic transducer.

FIG. 2. X-ray diffraction pattern of PZT thick films fired at 850 °C for 15 min. The wafer structure consisted of 0.5-μm-thick thermally grown oxide on silicon, with 200 Å of titanium for adhesion and 1500 Å platinum as bottom electrode/diffusion barrier.

con wafer, with 500 nm thermally grown oxide, sputter coated with 150 nm platinum on a 20 nm titanium adhesion layer. After the screen-printed films were allowed to level, they were dried at 110 °C for 1 h to remove the solvent by evaporation, and fired for 15 min at a peak temperature of 850 °C. The organics are believed to burn out in the neighborhood of 550 °C during firing. The thickness of the film in a single pass was 12 μm. Multiple printings, dryings, and firings yielded thicker films. An Alpha-Step 100 profilometer from Tencor Instruments was used to record the film thickness profiles. The x-ray diffraction (XRD) patterns of the films were recorded with a Scintag DMC-105 diffractometer. A scanning electron microscope (SEM) was used to characterize the film microstructure.

Top contact electrodes of platinum, approximately 1200 Å thick, in varying sizes were sputter deposited to form a capacitor structure. Dielectric permittivity and loss tangents were measured on a Hewlett Packard 4274A multifrequency LCR meter. The temperature dependent behavior of the dielectric properties was obtained with the aid of a high-temperature oven, controlled through a Hewlett Packard 9121 computer. A dc bias source was used to investigate the field-dependent dielectric permittivity; the bias was stepped through 6 V increments, which correspond to 5 kV/cm for the 12-μm-thick films measured. The breakdown strength of the films was ascertained by measuring the current-voltage characteristics with the aid of a Keithley 237 high voltage source measure unit. Current was measured at increments of 6 V (5 kV/cm) up to a maximum of 800 V. At dielectric breakdown, the current typically rose by 6 orders of magnitude (from 10^{-8} to 10^{-2} A). The ferroelectric hysteresis behavior was examined with a modified Sawyer–Tower circuit, from which the remanent polarization and coercive field were determined.

The piezoelectric properties of the films were evaluated from the strain response to external driving forces. A modified double-beam laser interferometer, which is capable of resolving ac displacements of the order of 10^{-2} Å with a lock-in amplifier,[6] was adopted to measure the longitudinal strain. In this study, for the first time, the field induced piezoelectric coefficient d_{33} of the screen-printed PZT thick films was measured under several different driving fields. The piezoelectric voltage coefficient g_{33}, defined as the ratio

of open-circuit field to mechanical stress, was computed from the piezoelectric coefficient d_{33}, and the dielectric constant obtained earlier.

III. RESULTS AND DISCUSSION

The films were fired at a number of temperature-time regimens. It is apparent that high firing temperatures and long holding times are necessary to obtain a densified film. Zhang et al.[7] had to sinter PZT to a temperature of 1150 °C to reduce substantially the number of pores in their 10-μm-thick PZT films fabricated on alumina substrates. Firing, however, of the PZT films on buffered silicon at such high thermal budgets results in blistering of the titanium/platinum underlayer. Other barrier layers such as indium tin oxide and ruthenium oxide may permit higher sintering temperatures. These are currently under investigation. The films were, therefore, confined to firing at 850 °C for 15 min. The XRD pattern of the films with this firing protocol is shown in Fig. 2, indicating the formation of single phase perovskite. From the planar and cross-sectional microstructures of the PZT thick films fired at 850 °C for 15 min (Fig. 3), it is apparent that the films are not completely densified, revealed by the presence of residual porosity.

As in capacitor dielectrics made from bulk ceramics,[8] the presence of air voids reduces the measured permittivity. The room temperature weak signal permittivity of a 12-μm-thick film is 160–220, with a dissipation loss of 4% to 6% at 1 kHz. The dielectric permittivity of the PZT thick films exhibits a broad dispersion with temperature, as shown in Fig. 4. This phenomenon is similar to that observed in PZT thin films.[9] The dielectric permittivity at the Curie point is about twice its value at room temperature, in comparison to bulk ceramics which show an order of magnitude increase in permittivity at T_C. The Curie point of 360 °C is slightly lower than that of the bulk ceramics (385 °C). The dielectric response of the films on application of a dc bias is shown in Fig. 5; the maximum dielectric permittivity appears in the vicinity of 5 kV/cm, on both positive and negative electric
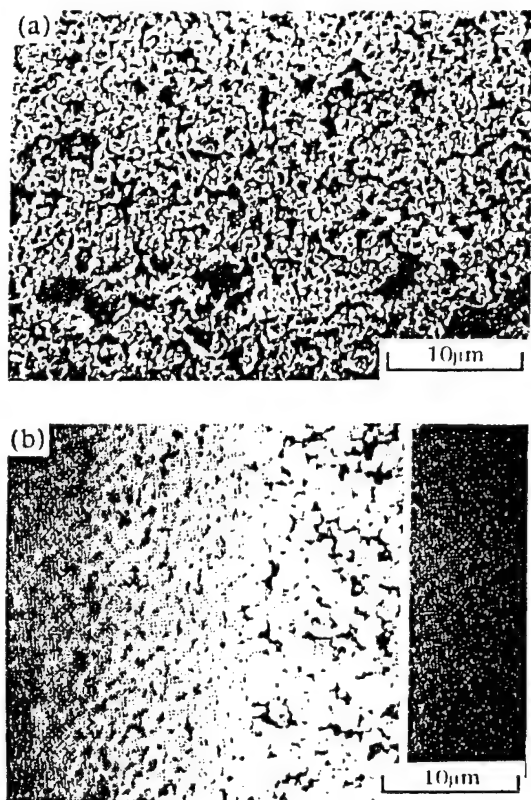
Chen *et al.*

FIG. 3. Scanning electron micrograph of the plan (a) and cross-section view (b) of the PZT films fired at 850 °C for 15 min.
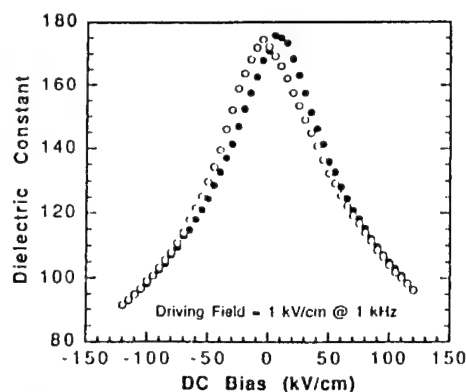

FIG. 5. Dielectric permittivity as a function of dc bias with slowly varying ac field for a 12-μm-thick PZT film. The dielectric response effectively corroborates the ferroelectric hysteretic nature of the films.

biases. Shown in Fig. 6 is the dielectric breakdown strength distribution of PZT thick films for 0.8-mm-diam top electrodes. Clearly, 70% of the test points hold up to an electric field of 400±50 kV/cm before breakdown. Complex factors including film defects, ink homogeneity, uniformity of the film thickness, quality of the sputtered platinum top electrodes, and air dust may add to the broadened breakdown

strength distribution. A discussion of the exact mechanism for the dielectric breakdown of the PZT thick films is outside the scope of this article.

The polarization-electric field hysteresis, which is the confirming evidence for ferroelectricity, is shown in Fig. 7 for the PZT thick films, with alternating fields varying between 100 and 175 kV/cm, at 25 kV/cm step increments. Without allowance for conduction compensation, a remanent polarization of 2.5 $\mu C/cm^2$ and a coercive field of 40 kV/cm have been observed under a 175 kV/cm peak driving field. The remanent polarization is higher than that reported for PZT films with PbO additions on alumina substrates,[4] and is comparable with that of PZT films with lead germanium silicate glass additive.[10]

Electric field induced longitudinal strain x_3 was measured with a double beam laser interferometer through direct measurement of changes in film thickness under external fields. Figure 8 represents the ac strain response of a 12-μm-thick PZT film at different dc bias fields; the longitudinal strain is found to increase in direct proportion to increasing ac and dc bias fields. Consequently, the field-induced longi-
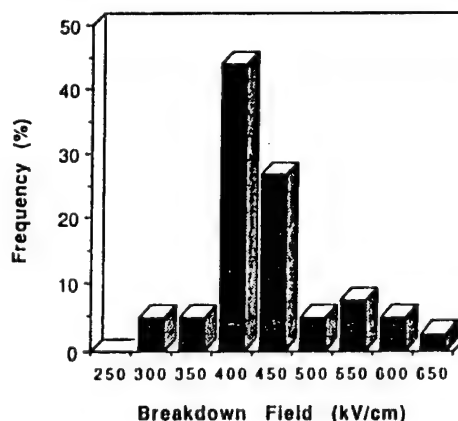

FIG. 4. Temperature dependence behavior of the dielectric permittivity and tangent loss factor for PZT thick films, measured at 1 kHz (A,A'), 10 kHz (B,B'), and 100 kHz (C,C'). The Curie point is at about 360 °C.

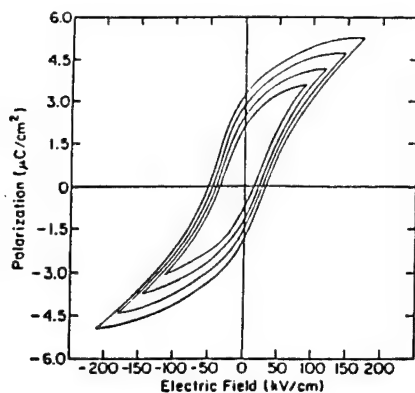FIG. 6. Dielectric breakdown strength distribution of the PZT thick films.

FIG. 7. Polarization-applied field hysteresis for a 12-μm-thick PZT film at 10 Hz. The polarization-electric traces are recorded at drive fields varying from 100 kV/cm (inner loop) to 175 kV/cm (outer loop) at 25 kV/cm intervals.

FIG. 9. Piezoelectric strain coefficient d_{33} as a function of applied field at a dc bias of 40 and 120 kV/cm. The maximum value of d_{33} is 50 pC/N.

tudinal piezoelectric coefficient d_{33} is calculated through the converse piezoelectric effect, defined by $x_3 = d_{33}E_3$, where E_3 is the applied field, and d_{33} is the longitudinal piezoelectric strain coefficient. Figure 9 is a plot of the piezoelectric coefficient as a function of the probing field and applied dc bias. The d_{33} maximum occurs at an external dc bias of 40 kV/cm. Figure 10 represents the effect of varying dc bias while maintaining a constant ac drive field; for the various alternating fields used, the turning point of the curves is located around 40 kV/cm of applied dc bias, beyond which the magnitude of d_{33} tends to drop. Recalling that d_{33} is directly related to the permittivity, polarization, and the electrostrictive coefficient, this fall in d_{33} is primarily a reflection of the weak signal dielectric response under cyclic bias (Fig. 5), the polarization charge having saturated at higher fields, and the electrostrictive coefficient being independent of field. The maximum value of the piezoelectric coefficient d_{33} is observed to be 50 pC/N in these films.

The piezoelectric voltage coefficient g_{33} is derived from the piezoelectric strain coefficient and dielectric constant

measured under the same ac field and dc biasing conditions ($g_{33} = d_{33}/\epsilon_0\epsilon_r$). This is plotted in Fig. 11 which shows g_{33} to increase with external dc bias. Although the piezoelectric strain coefficient and dielectric permittivity of the films are individually lower than that of the bulk ceramics, the piezoelectric voltage coefficient g_{33} of the PZT thick films is higher than that of the bulk ceramics.[11] At 40 kV/cm dc bias and 4 kV/cm drive field, g_{33} is calculated to be 36×10^{-3} V m/N. By comparison, g_{33} of an equivalent poled PZT bulk ceramic is 20×10^{-3} V m/N. This result should not be entirely surprising since the microstructure, as indicated earlier, is not completely dense, contributing to the reduced magnitude of permittivity, and consequently the high piezoelectric voltage coefficient.

IV. SUMMARY

Crack-free PZT thick films have been successfully deposited onto platinum buffered silicon substrates using the screen printing technique. The dielectric, ferroelectric, and piezoelectric properties of the films have been evaluated. The magnitude of the piezoelectric voltage coefficient g_{33} is in-
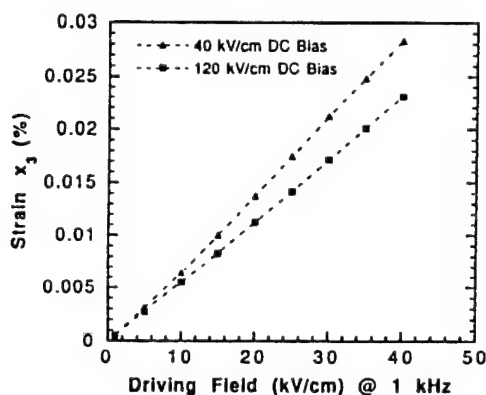

FIG. 8. Field-induced longitudinal strain vs applied field at different dc bias conditions. Notice the linear relationship between the strain and field; the slopes of these lines correspond to the piezoelectric strain coefficient d_{33}.
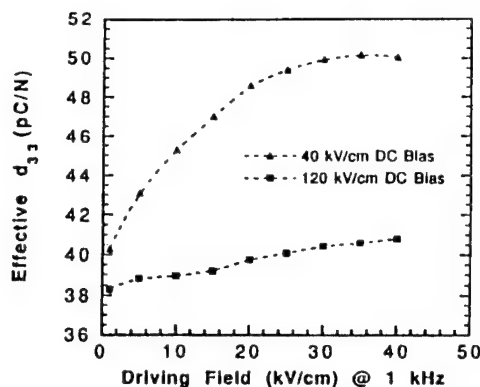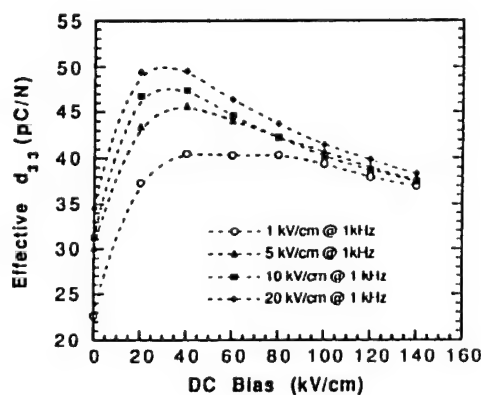

FIG. 10. d_{33} plotted as a function of dc bias at constantly held alternating fields from 1 to 20 kV/cm. Note the maximum in the piezoelectric strain coefficient occurs at around 40 kV/cm dc bias.
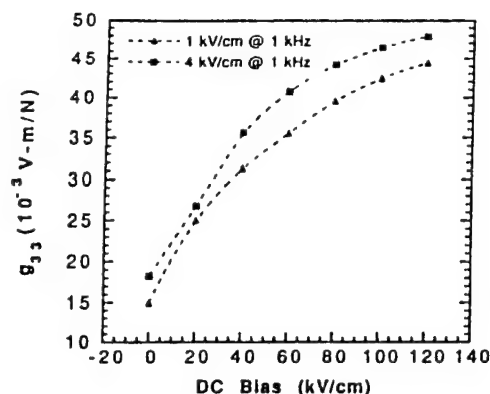
Chen *et al.*

FIG. 11. Piezoelectric voltage coefficient g_{11} plotted as a function of external fields. The positive side of the dielectric response with dc bias has been combined with the strain coefficient d_{11} variation with dc bias to obtain this plot.

dicative of its feasibility as a sensor in either the thickness or the hydrostatic mode. Efforts are continuing to densify the films so that they may be used in the flexural mode. These

results hold promise for the utility of PZT thick films in a wide range of sensor applications including vibration sensors and micromachined acoustic sensor arrays.

ACKNOWLEDGMENTS

[1] H. Baudry, Hybrid Circuits 14, 71 (1987).
[2] S.-L. Fu, J. K. Chung, and S. Y. Cheng, Jpn. J. Appl. Phys. 24 (Suppl. 24-2), 416 (1985).
[3] N. White and A. Cranny, Hybrid Circuits 12, 32 (1987).
[4] B. Morten, G. De Cicco, A. Gandolfi, and C. Tonelli, Hybrid Circuits 28, 25 (1992).
[5] S. Middelhoek and S. A. Audet, *Silicon Sensors* (Academic, San Diego, 1989).
[6] W. Y. Pan and L. E. Cross, Rev. Sci. Instrum. 60, 2701 (1989).
[7] H.-X. Zhang, S. Leppavuori, A. Uusimaki, P. Karjalainen, and R. Rautioaho, Ferroelectrics 154, 277 (1994).
[8] B. Walton, in "Hybrid Microelectronic Technology," edited by P. Moran, *Electro-component Science Monographs* (Gordon and Breach, New York, 1984), Vol. 4, p. 49.
[9] K. R. Udayakumar, J. Chen, S. B. Krupanidhi, and L. E. Cross, in *Proceedings of the 7th International Symposium on Applications of Ferroelectrics* (IEEE, New Jersey, 1991), p. 741.
[10] J. Collier, I. A. Cornejo, and M. J. Haun, Ferroelectrics 154, 47 (1994).
[11] D. P. Skinner, R. E. Newnham, and L. E. Cross, Mater. Res. Bull. 13, 599 (1978).

APPENDIX 63

Thickness-dependent electrical characteristics of lead zirconate titanate thin films

K. R. Udayakumar, P. J. Schuele,[a] J. Chen, S. B. Krupanidhi, and L. E. Cross
Materials Research Laboratory, The Pennsylvania State University, University Park, Pennsylvania 16802

Ferroelectric lead zirconate titanate thin films of morphotropic phase boundary composition were fabricated through the sol-gel spin-on technique to study the thickness dependence of electrical characteristics. At saturation, the films exhibited a dielectric constant of 1300, dissipation factor of 0.03, Curie temperature of 366 °C, remanent polarization of 36 $\mu C/cm^2$, coercivity of around 30 kV/cm, and dielectric breakdown strength of over 1 MV/cm. The temperature dependence of permittivity showed an anomalous behavior with annealing temperature. The high temperature dielectric behavior of the films were distinguished by smeared and stunted dielectric maximum. © *1995 American Institute of Physics.*

I. INTRODUCTION

Lead zirconate titanate (PZT) of the morphotropic phase boundary composition ($PbZr_{0.52}Ti_{0.48}O_3$) exhibits superior dielectric, ferroelectric, and piezoelectric properties in the bulk.[1] The morphotropic phase boundary (MPB) refers to the boundary between the tetragonal and rhombohedral forms which is nearly independent of temperature. Proximity to such a phase boundary between the ferroelectric phases is believed to favor enhanced physical properties in a ceramic due to the increased ease of orientation during poling. With six orientation states for the tetragonal phase, and eight for the rhombohedral, the MPB composition has the maximum number of orientation states available. Lead zirconate titanate of this composition is a candidate material for memory and logic devices, and in thin film form would be ideal for meeting the requirements of low drive voltage, optimization of storage density, and switching transients. Lead oxide-based ferroelectric films have been investigated for a variety of device applications including semiconductor nonvolatile memories, piezoelectric ultrasonic micromotors, pyroelectric detectors, and capacitors in dynamic RAMs which are based on the bulk characteristics of the ferroelectric.[2,3] For these applications, it is imperative, therefore, that the characteristics of the integrated ferroelectric film be investigated systematically to determine the thickness at which these match the bulk while ascertaining, in parallel, deviations from the bulk ceramic behavior. Consequently, PZT films up to a thickness of 6000 Å were fabricated in this study using the *sol-gel* chemical method to evaluate the thickness dependence of dielectric and ferroelectric properties. Thickness dependencies of relative permittivity, polarization reversal, and breakdown strength were explored through appropriate electrical measurements. Related studies included the effect of annealing temperature, dc bias, and temperature on permittivity.

II. EXPERIMENT

The procedure for preparing the solution and fabrication of thin films has been delineated in Ref. 4, and is based on the procedure reported in literature.[5,6] The substrate structure employed in this study consisted of 0.02 μm titanium/0.43 μm platinum layer atop a 0.5-μm-thick thermally oxidized layer on [100] silicon. The Pt layer serves as the bottom electrode in this configuration, and Ti ensures adhesion between the oxide layer and Pt.

Thin films were deposited on the platinized silicon substrates using a spin coater (model P-6000, Integrated Technologies Inc., Acushnet, MA), operated at 2500 rpm for 15 s. The films were pyrolyzed in air at 400 °C for 30 min to remove the organics, and the deposition-pyrolysis cycle was repeated until the desired thickness was obtained. The films were annealed in air for varying temperature-time combinations to produce the ferroelectric perovskite structure. In the annealing process, the films were first held at 400 °C for 30 min to ensure the complete pyrolysis of the organics, then the temperature was raised to the final anneal temperature at a heating rate of 20 °C/min; the final anneal temperature was maintained for 30 min. Sputtered gold electrodes, 660 μm in diameter, were used as top electrodes, which were connected to the measuring apparatus with air dry silver paste; the platinum bottom electrode served as the counter electrode.

Crystallization of the films into the perovskite phase was examined by a Scintag x-ray diffractometer using Cu $K\alpha$ radiation ($\lambda = 1.5418$ Å). The XRD patterns were recorded at a scan rate of 2°/min for phase and structure analysis. Microstructure of the films was studied using a scanning electron microscope (DS-130, ISI). The thickness of the films was determined by observing the fracture sections of the films with the scanning electron microscopy (SEM). The chemical composition of the film was determined by x-ray fluorescence analysis (XRF) with an analytical spectrometer (model 7000, μX).

The dielectric measurements were carried out on an automated system in which an oven (model 2300, Delta Design Inc.), an LCR meter (model 4274A, Hewlett Packard Inc.), and a digital multimeter were controlled by a desk top computer system (model 9816, Hewlett Packard Inc.). The capacitance and dissipation factor of the films were measured at frequencies below resonance over a temperature range of 25 to 450 °C, the high temperature measurements being car-

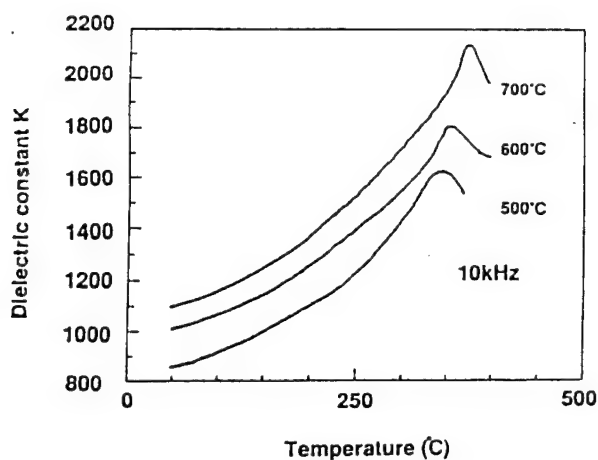[a]Micron Semiconductor, Inc., Boise, ID 83706.

FIG. 1. Effect of annealing temperature on the temperature dependence of permittivity. A shift in the Curie point is noticed with increasing annealing temperature.

FIG. 2. Relative permittivity and tangent losses as a function of temperature for a film annealed at 700 °C at different frequencies.

ried out in a vertical resistance tube furnace. A modified Sawyer–Tower circuit was used to record the P-E hysteresis behavior of the films. Typically, the room temperature P-E measurements were carried out at 60 Hz. Remanent polarization (P_r) and coercive voltage (V_C) were determined from room temperature hysteresis measurements carried out at 60 Hz with a load capacitor of 0.1 μF.

III. RESULTS AND DISCUSSION

The films were amorphous after the pyrolyzing step (400 °C for 30 min) while x-ray diffraction patterns of the PZT films on Si annealed in the temperature range of 500–800 °C for 30 min, all showed single phase perovskite peaks. Films annealed at 900 °C for 30 min showed the formation of TiO_2 (rutile), indicating the partial decomposition of PZT through the evaporation of PbO.

The room temperature small-signal dielectric constant of the film increases from 1000 for a film annealed at 500 °C to 1300 for a 700 °C anneal. In the same range of annealing temperatures, the temperature dependence of the dielectric constant shows an anomalous shift in the Curie point, T_C, which advances to higher values with increasing annealing temperature (the curves for the 700 and 800 °C anneal overlap). The Curie maximum displays a similar variation, being smaller for lower annealing temperatures (Fig. 1). This may be ascribed to the higher degree of crystalline orientation of the films with higher annealing temperature. The perovskite phase was detected for all films annealed in the temperature range of 500 to 800 °C, but the intensity of the (110) peak increased with rising annealing temperature, saturating at 800 °C. The area under the (110) peak for the films annealed at 800 °C for 30 min was about 20% higher than that of the films annealed at 500 °C.

From Fig. 2, which is the temperature dependence of the dielectric constant of a film annealed at 700 °C, it is evident that the Curie temperature is at 366 °C, a value roughly equal
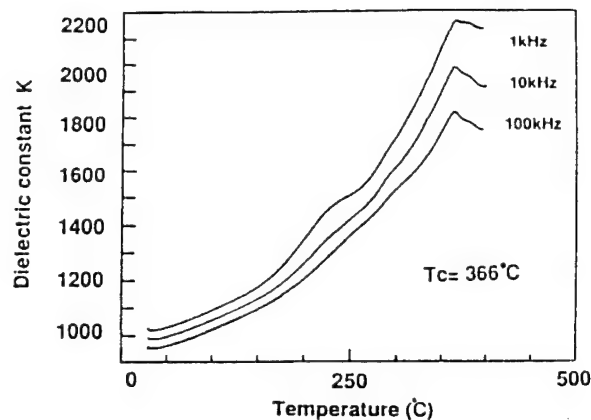
to that predicted by the bulk ceramic phase diagram.[1] The distinguishing features of the thin film dielectric response which differ from the behavior of the bulk ceramic are the lower peak dielectric constant and the highly rounded dielectric maxima. The peak dielectric constant of the film is only 2 to 3 times larger than the room temperature permittivity, in contrast to a value more than an order of magnitude larger in the bulk samples.

Lur'e et al.[7] have postulated an anomalous layer at the surface of ferroelectric films, associated with the presence of a space charge compensating the contact potential difference at the interface of the two phases. The oscillograms of the hysteresis loops, and the dielectric response at high fields with different electrodes (Au, Sb, Ag, Sn, Mg, and Cd) revealed a striking variation in the measured physical characteristics. The influence of the anomalous layer in the contact region was also evident in measurements of the switching time of the films. On the larger issue of contact phenomenon, the upper electrode (Au, Ag, Pt) had little effect on the maximum value of ϵ_r, and almost no effect on ϵ_r away from the phase transition in (Ba, Sr)TiO$_3$ films.[8] Slack and Burfoot[9] reported ϵ_r to be 1.3–1.5 times greater with a Au electrode than with Al on BaTiO$_3$ films.[10] Margolin et al.[10] ascribed the low increase in the permittivity maximum, typically by a factor of 1.2–2 over that of the room temperature permittivity, to the different degrees of tetragonality. The anomalous broadening of the XRD reflections in their study was assumed to originate from the films having regions with different degrees of tetragonality.

The influence of mechanical and thermal stresses on the $\epsilon_r(T)$ curves of barium titanate was illustrated by Dudkevich and Fesenko[11] by employing substrates of quartz, steel, and platinum. The shift in the Curie point and the more diffuse phase transition was related to a considerable extent to mechanical stresses, which, owing to the elastic anisotropy, are different for different grain orientations with respect to the substrate surface.
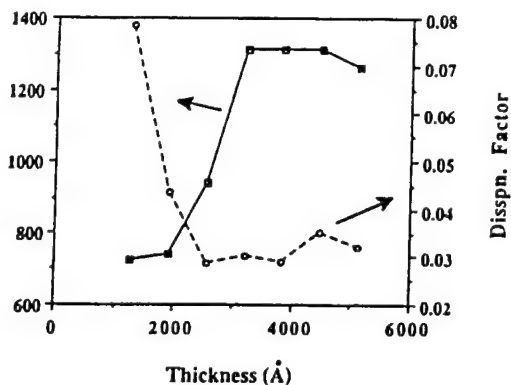
FIG. 3. Room temperature low field permittivity as a function of film thickness at 10 kHz. The permittivity levels off for thicknesses greater than 0.32 μm.

FIG. 4. Effect of film thickness on the temperature dependence of dielectric constant.

The smearing of the permittivity peaks may also be explained, in analogy with the bulk specimens,[12] using a model based on a Gaussian distribution of Curie temperatures due to the existence of microregions in the crystal with different transition temperatures. While this could not be verified directly in the present work, Huffman et al.[13] used nanoprobe EDS line scans on sputtered 48/52 PZT samples to observe a small compositional inhomogeneity between grains and grain boundaries and within the grains between dark matrix and lighter areas.

The dependence of the low field room temperature dielectric constant and dissipation factor on film thickness is shown in Fig. 3. The relative dielectric constant increases with thickness, saturating at 1300 for film thicknesses of 0.32 μm and above. A concomitant drop in dissipation factor is noted with increasing film thickness. Gitel'son et al.[8] have attributed a similar dependence in barium strontium titanate films to the presence of a transition layer between the film and the substrate, possibly to processes related to the initial stages of crystallization that can produce layers with increased defect concentration. The differences between the bulk properties of the substrate and the film lead to the presence of growth stresses and thermal stresses, with these stresses increasing with decreasing thickness, significantly so where ϵ_r decreases rapidly. In a more general sense, the presence of a very thin layer with a low ϵ_r will have a very large effect on the net ϵ_r, and this layer can be at the bottom electrode/film interface or at the top electrode/film interface or both.

Figure 4 is a trace of the high temperature film permittivity as a function of thickness. Although it is tempting to ascribe the diffuse phase transition characteristics to crystallite size, a systematic correlation could not be established, the grain size of the films generally being in the range of 0.05–0.15 μm (Fig. 5). In bulk ceramics, a decrease in the permittivity maximum at the Curie point and broadening of the peak has been associated with the reduction in the average grain size.[14] As a case in point, the diffuse phase transition observed in fine-grained BaTiO₃ based ceramics has
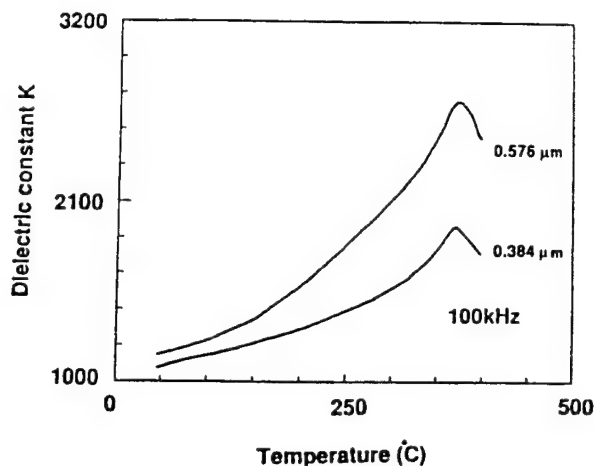
been explained in terms of a stress-induced coexistence of different ferroelectric and paraelectric phases. The smaller the grains, the broader and lower the permittivity maximum becomes at the Curie point; increasing the grain size, on the other hand, favors the formation of very high but narrow permittivity maxima.

The thin film literature on the blurring of the phase transition with thickness is replete with a number of inconsistencies. In (Ba,Sr)TiO₃ films,[8] and films made from the base composition of $Pb_{0.92}Bi_{0.07}La_{0.01}(Fe_{0.405}Ng_{0.325}Zr_{0.27})O_3$, PBLFNZ films,[15] the peak dielectric constant was found to be higher for thicker films which agrees with the result of Fig. 4. Loposzko et al.[16] detected a similar qualitative trend in $Ba(Ti_xSn_{1-x})O_3$ films 73–95 μm thick. Pratt and Firestone[17] failed to identify an unequivocal Curie maximum in rf-sputtered films of BaTiO₃, and furthermore, the high temperature capacitance behavior exhibited the opposite trend. Slack and Burfoot[9] have reported a mixed trend in
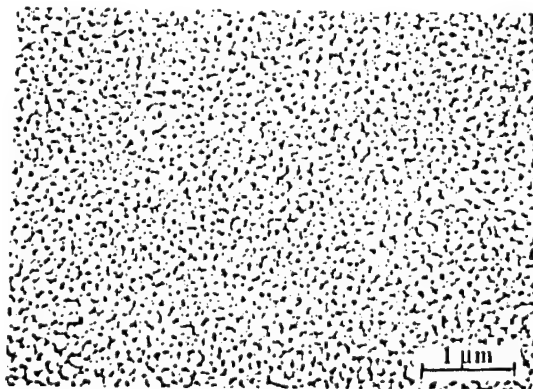

FIG. 5. SEM micrograph of a 0.63 μm PZT thin film annealed at 700 °C for 30 min.

J. Appl. Phys., Vol. 77, No. 8, 15 April 1995
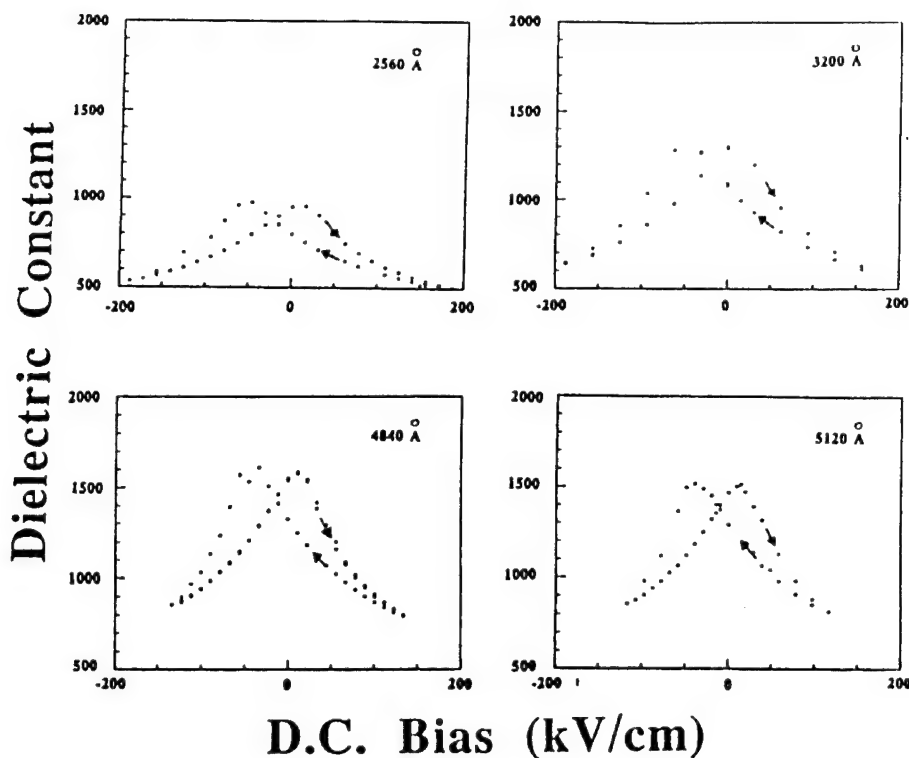
Udayakumar et al.   3983

FIG. 6. Dielectric permittivity as a function of dc bias for different film thicknesses.

flash evaporated $BaTiO_3$ films. At the other extreme, Tomashpol'skii and Sevost'yanov[18] reported a completely arbitrary thickness dependence of high temperature capacitance for vacuum evaporated $BaTiO_3$ films. It is noteworthy that this study reported a dielectric anomaly for films just 100 Å thick. Surowiak et al.[19] used the mean dimensions of areas of coherent scattering and of mean microdeformation as a measure of structural perfection of the films. These studies, along with that of Dudkevich et al.,[20] argue that size effects in polycrystalline ferroelectrics are determined by the size of the subcrystallites. High temperature capacitance measurements showed a distinct correlation between the size of the coherent scattering region and permittivity for sputtered $BaTiO_3$ films. In their investigation of the ferroelectric properties and switching characteristics of rf sputtered PZT films as a function of thickness, Desu et al.[21] measured switching down to a thickness of 30 nm. They argue that grain size is the determining factor in the study of size effects, and report that grain sizes of films at lower thicknesses appeared to be greater than the thickness of the film.

The dielectric response of the films on application of a dc bias is shown in Fig. 6. Figure 7 is a schematic illustration of the relationship between the P-E hysteresis loop and C-V data which demonstrates that the C-V curve is essentially the derivative of the hysteresis loop. As the measurement voltage increases from zero, switching occurs, and the apparent capacitance increases to a maximum at the coercive voltage. From an examination of Fig. 6, it is evident that PZT films in

the thickness range of 0.25–0.5 μm have a coercive field of 25–32 kV/cm. At a thickness of 0.1 μm, the coercive field rises to 80–100 kV/cm which is in agreement with an E_C of 100 kV/cm for films less than 0.05 μm thick reported by Sanchez et al.[22] This appears to be due to the same effect that causes the E_C of certain single crystal ferroelectrics to increase with decreasing thickness. Various explanations
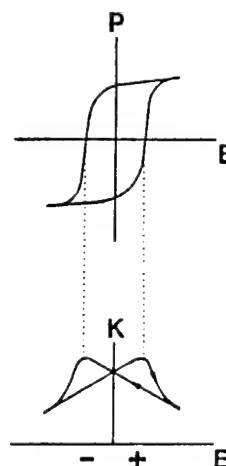

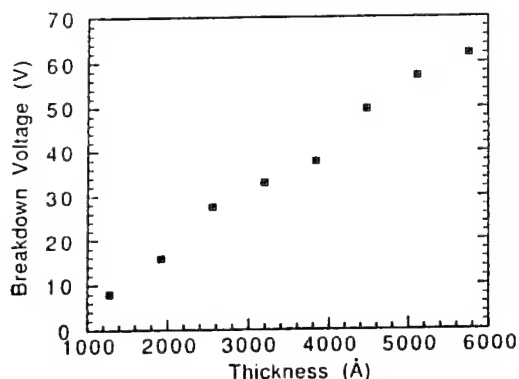FIG. 7. Relationship between P-E hysteresis loop and C-V loop.

APPENDIX 64

FIG. 8. Breakdown voltage of the films plotted as a function of thickness. Note the linear breakdown voltage dependence on thickness.

FIG. 10. P-E hysteresis loop of a 0.45 μm PZT film at 60 Hz. The polarization trace above is at an applied field of 120 kV/cm. The remanent polarization is 30 μC/cm^2 and the coercive field is 31 kV/cm.

have been offered for the single crystal case which include the concept of a thin surface layer having properties different from those of the bulk, and the distortion of the internal field by space charge.

The breakdown voltages bear an almost linear relationship with film thickness (Fig. 8). The normalized breakdown strength plotted in Fig. 9 shows a decrease in breakdown strength for films less than 0.25 μm thick. The exact mechanism responsible for the dielectric breakdown is difficult to ascertain due to the complex nature of the process. Various defects are believed to play a significant role in reducing the breakdown strength of ceramics. In ferroelectric thin films, defects include impurities, vacancies, grain boundary phases, pores, surface layers, and microcracks.

We believe that the breakdown in the films is electrically initiated at the grain boundary and thermally completed. The top electrode cusp produces a high field region at a grain boundary so that the smoother the surface, the higher the breakdown field. The low ϵ_r and high defectivity of the grain boundary should also lead to electrical breakdown. Strong
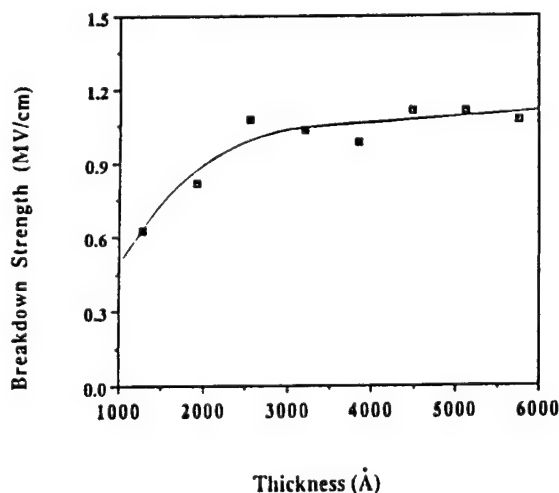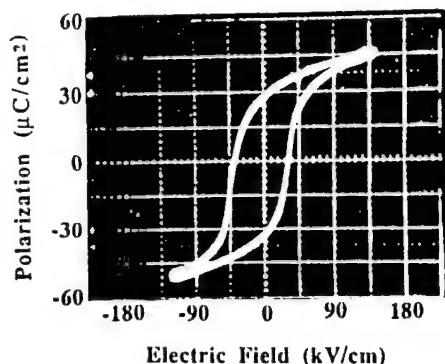
evidence for initiation of breakdown at the grain boundary comes from sputtered PZT films that are columnar and relatively coarse (5 μm), in which breakdown originates invariably at the triple points and propagates along the grain boundaries. The case is complicated in the case of *sol-gel* films considered here, though, because of the finer grain sizes, and the more tortuous path of the grain boundary.

The high breakdown strength of the PZT films (1 MV/cm), in comparison with 80 kV/cm of the bulk ceramic, might be attributed in part to the finer grain size of the thin film microstructure (Fig. 5). In their studies on the effect of microstructure on the breakdown strength of barium titanate ceramics, Yamashita et al.[23,24] found the breakdown strength of a large-grained sample to be lower than that of the small-grained ones. The behavior is consistent with the idea of the breakdown being initiated at the grain boundary. To produce the same local field in the grain boundary, the large grains require a smaller applied voltage than the small grains. It is indeed fascinating to note that the breakdown voltages of carefully prepared sputter deposited PZT thin films have shown a similar linear behavior with thickness as in the present study; the breakdown strength of the sputter deposited films has been reported to be 0.86 MV/cm.[25]

Figure 10 is the representative trace of the symmetric hysteresis loop of a film 0.38 μm thick. Figure 11 is a plot of the remanent polarization as a function of electric field for different film thicknesses. The polarization was found to saturate at 36 μC/cm^2 and the coercive field at 35 kV/cm for films thicker than 4500 Å. The literature on switching of ferroelectric films is characterized by major discordances even when the compositions and film fabrication techniques used are identical. Apparently, physical properties of thin films are extremely sensitive to processing. In the literature,[26,27] remanent polarization and coercive field for the MPB PZT films has been variously reported in the range 7–40 μC/cm^2 and 25 to 150 kV/cm, respectively.

IV. SUMMARY

This study of the thickness dependence of the electrical properties of the PZT films has demonstrated that reduction in film thickness leads to the following:
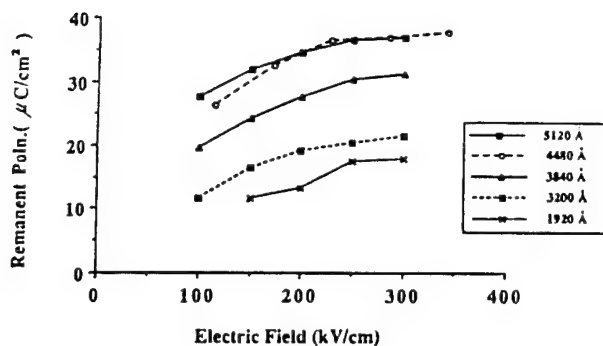

FIG. 9. Breakdown strength of the films plotted as a function of thickness.

FIG. 11. Remanent polarization plotted as a function of electric field at varying film thickness.

(1) reduction in the small signal permittivity and remanent polarization;

(2) increase in the loss tangent and coercive field;

(3) diffuseness of the phase transitions, and

(4) decrease in dielectric breakdown field.

As discussed in the preceding sections, these size-dependent properties are influenced by a number of factors. Foremost of these is the role of interface layers, arising in an as yet unclear fashion from interaction between the electrodes and the film, with properties that differ from the interior of the film, and which form part of a complex, composite structure. Mechanical and thermal stresses at the film-substrate interface, microstructural features, inhomogeneous distribution of the free charge carriers, and the influence of contact phenomena are but some of the other causes for the size effects.

[1] B. Jaffe, W. R. Cook, and H. Jaffe, *Piezoelectric Ceramics* (Academic, New York, 1971).

[2] C. A. Araujo, L. D. McMillan, B. M. Melnick, J. D. Cuchiaro, and J. F. Scott, Ferroelectrics 104, 241 (1990).

[3] W. A. Geideman, IEEE Trans. UFFC 38, 704 (1991).

[4] K. R. Udayakumar, J. Chen, S. B. Krupanidhi, and L. E. Cross, in *Seventh International Symposium Applied Ferroelectrics* (IEEE, New Jersey, 1991), pp. 741–42.

[5] K. D. Budd, S. K. Dey, and D. A. Payne, Brit. Cer. Proc. 36, 107 (1985).

[6] Y. Shimizu, K. R. Udayakumar, and L. E. Cross, J. Amer. Cer. Soc. 74, 3023 (1991).

[7] M. S. Lur'e, E. I. Vasil'eva, and I. V. Ignat'eva, Bull. Acad. Sci. USSR Physical Series 24, 1372 (1960).

[8] A. A. Gitel'son, A. M. Lerer, V. S. Mikhalevskii, V. M. Mukhortov, and S. V. Orlov, Sov. Phys. Solid State 19, 1121 (1977).

[9] J. R. Slack and J. C. Burfoot, J. Phys. C: Sol. State Phys. 4, 898 (1971).

[10] A. M. Margolin, L. A. Barabanova, V. S. Bondarenko, E. G. Fesenko, and V. P. Dudkevich, Bull. Acad. Sci. USSR Physical Series 24, 1768 (1971).

[11] V. P. Dudkevich and E. G. Fesenko, Ferroelectrics 22, 787 (1978).

[12] H. T. Martirena and J. C. Burfoot, J. Phys. C 7, 3182 (1974).

[13] M. Huffman, J. P. Goral, M. M. Al-Jassim, and C. Echer, J. Vac. Sci. Technol. A 10, 1584 (1992).

[14] D. Hennings, Inter. J. High Techn. Cer. 3, 91 (1987).

[15] B. S. Sharma, S. F. Vogel, and P. I. Prentky, Ferroelectrics 5, 69 (1973).

[16] M. Loposzko, M. Pawelczyk, M. Urbanska, and Z. Surowiak, Thin Solid Films 69, 339 (1980).

[17] I. H. Pratt and S. Firestone, J. Vac. Sci. Technol. 8, 256 (1972).

[18] Y. Y. Tomashpol'skii and M. A. Sevost'yanov, Sov. Phys. Solid State 14, 2319 (1973).

[19] Z. Surowiak, E. Nogas, A. M. Margolin, S. V. Biryukov, and I. N. Zakharchenko, Ferroelectrics 115, 21 (1991).

[20] V. P. Dudkevich, V. A. Bukreev, V. M. Mukhortov, Y. I. Golovko, Y. G. Sendeev, and E. G. Fesenko, Phys. Status Solidi A 65, 463 (1981).

[21] S. B. Desu, C. H. Peng, L. Kammerdiner, and P. J. Schuele, Mater. Res. Soc. Symp. Proc. 200, 319 (1990).

[22] L. E. Sanchez, S. Y. Wu, and I. K. Naik, Appl. Phys. Lett. 56, 2399 (1990).

[23] K. Yamashita, K. Kuomoto, M. Takata, and H. Yanagida, Jpn. J. Appl. Phys. 19, 867 (1980).

[24] K. Yamashita, K. Kuomoto, M. Takata, H. Yanagida, and T. Hamano, Commun. Amer. Cer. Soc. 67, C-31 (1984).

[25] P. J. Schuele and S. D. Traynor, Proc. 5th US-Japan Seminar on Dielectric and Piezoelectric Ceramics, Kyoto, Japan, 1990, pp. 286–289.

[26] A number of articles in the MRS Symp. Proc. Ferroelectric Thin Films 200 (1990); 243 (1992); 310 (1992).

[27] A number of articles in the Proceedings of 3rd International Symposium on Integrated Ferroelectrics (ISIF), held at Colorado Springs, April 3–5, 1991; Proceedings of the 4th International Symposium on Integrated Ferroelectrics (ISIF), Monterey, Mar 9–11, 1992.

Electrical properties' maxima in thin films of the lead zirconate–lead titanate solid solution system

H. D. Chen, K. R. Udayakumar, C. J. Gaskey, and L. E. Cross
Materials Research Laboratory, The Pennsylvania State University, University Park, Pennsylvania 16802

The piezoelectric strain coefficients have been measured as a function of composition for films in the $PbZrO_3$–$PbTiO_3$ (PZT) solid solution system, using a double-beam laser interferometry technique. This compositional dependence of piezoelectric, and the associated dielectric and ferroelectric properties for films 1 μm in thickness with varying Zr/Ti ratio, deposited on platinized silicon substrates using a modified sol-gel route, corresponds to data reported for undoped PZT ceramics with respect to the effective morphotropic phase boundary composition. Films with composition near the morphotropic phase boundary, $Pb(Zr_{0.52}Ti_{0.48})O_3$, show enhanced values of the longitudinal piezoelectric coefficient, 194 pC/N; dielectric permittivity, 1310; and remanent polarization, 36 μC/cm^2. © 1995 American Institute of Physics.

The compositional dependence of the structure and electrical properties of PZT bulk ceramics has been investigated extensively. Near the composition $Pb(Zr_{0.52}Ti_{0.48})O_3$, ferroelectric phases of tetragonal and rhombohedral modifications coexist metastably along a boundary which is a strong function of composition, but only a weak function of temperature, known as the morphotropic phase boundary, or MPB. Jaffe et al.[1,2] and Berlincourt et al.[3] have reported enhancements of the dielectric constant and induced piezoelectric effect in compositions near the MPB region. Carl and Härdtl[4] further observed that the maximum in the electromechanical activity is, in fact, caused by the maximum in the dielectric permittivity near the phase boundary composition, $Pb(Zr_{0.52}Ti_{0.48})O_3$; however, the increased poling efficiency due to the metastable coexistence of tetragonal and rhombohedral phases is also an important factor. PZT ceramic compositions near the MPB have been exploited in many transducer applications for their high electromechanical coupling efficiency.

While conventionally processed ceramics are not amenable to integration with microsized transduction devices, films of complex oxide materials, such as PZT, can be readily integrated into silicon device fabrication procedures through a number of deposition techniques, both chemical and physical. The feasibility of using a thin, chemically prepared PZT film as a piezoelectric transduction element in a silicon-based ultrasonic micromotor has been demonstrated by Flynn et al.[5] and Udayakumar et al.,[6] in which it was assumed that the MPB composition is not shifted due to either scaling effects imposed by the submicron thickness and grain size or the stress boundary conditions imposed on the film by the relatively massive silicon substrate. As the large electromechanical activity of the PZT compositions would be expected to couple a change in mechanical state to an electronic reconfiguration, it is not immediately obvious that this assumption is valid, and in this regard several groups have investigated the effect of the Zr/Ti ratio on the dielectric and ferroelectric properties of PZT thin films in the last few years,[7-17] though, perhaps due to the extreme sensitivity of film properties to even subtle variations in processing conditions, no consensus has been reached with respect

to the MPB composition. A major lacuna has been the virtual nonavailability of any data on piezoelectric properties as a function of composition. The investigation at hand is intent on elucidating the relationship between the Zr/Ti ratio and the effective longitudinal piezoelectric coefficients of PZT films, and, in a more general sense, further clarifying the relationship between the structure and properties of PZT films.

In this study, a number of $Pb(Zr_xTi_{1-x})O_3$ compositions, with x ranging from 0 to 0.8 were prepared by a sol-gel
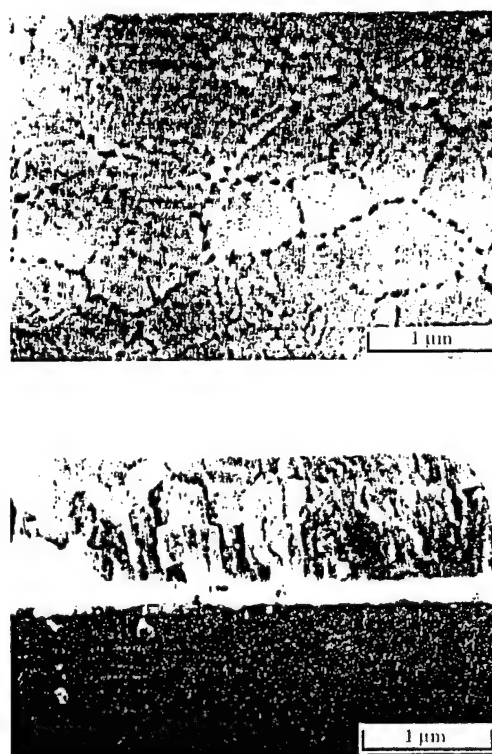

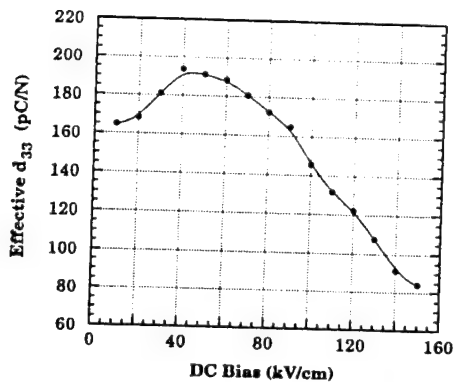FIG. 1. Planar and cross-sectional microstructures of 1 μm-thick PZT (52/48) film.

FIG. 2. The dc bias dependence of the effective d_{33} plotted for a 1 μm-thick PZT (52/48) film. The driving field applied corresponds to 1 kV/cm (rms) at 1 kHz. Note that the maximum value is 194 pC/N.

FIG. 4. The dielectric permittivity vs composition in the $PbZrO_3$-$PbTiO_3$ solid solution system. The top contact electrode is platinum 1.6 mm in diameter. Test signal is 0.1 kV/cm at 1 kHz. The data for bulk ceramics are referenced from Berlincourt et al. (Ref. 3).

technique similar to that used by Yi et al.[18] Lead acetate trihydrate was initially dissolved in acetic acid, and the water of hydrolysis was expelled during a brief distillation at 105 °C. Zirconium and titanium alkoxides were then added in the proportions dictated by the composition; excess lead, 10% by mole, was added to solutions throughout to compensate for lead loss during firing and to stabilize the perovskite phase. Ethylene glycol and water have been added to the final solution to adjust the viscosity and surface tension, reducing the likelihood of cracking during pyrolysis. The resulting solution, stable in air and relatively concentrated with a molarity of 0.9, is used to fabricate films through a multilayer spin-on procedure. After deposition on to (100) silicon wafers with a 0.15 μm-thick platinum electrode sputtered on a 0.5 μm-thick thermally grown SiO_2 buffer and a 0.02 μm-thick Ti adhesion layer, each layer was dried at 150 °C and pyrolyzed at 550 °C to preclude the entrapment of organics by subsequent layers. After four depositions in this manner, the multilayer structures were annealed at 700 °C for 1 h, resulting in perovskite films 1 μm in thickness. To facilitate electrical property measurements, platinum

top electrodes of 0.8 and 1.5 mm diameter were sputtered-deposited.

Whereas in the case of bulk ceramics, sample quality can be evaluated by routine, quantitative determinations of density and weight loss, film quality is more commonly determined from the microstructure in electron micrographs. The scanning electron micrographs of the surface and cross section of a representative PZT (52/48) film are presented in Fig. 1, from which a dense, layered structure with a bimodal grain distribution is revealed, indicating, in concert with x-ray diffractograms, the predominance of single phase, high quality film volume.

Following initial poling under 150 kV/cm dc field for 2 min at room temperature, each sample was characterized for field-induced strain in a highly sensitive double beam laser interferometer[19] by applying varying dc bias over a fixed, 1 kHz ac field of 1 kV/cm (rms value). The effective longitudinal piezoelectric coefficient d_{33} is calculated from the converse piezoelectric effect. The effect on d_{33} of a positive, increasing external dc bias is shown in Fig. 2 for a $Pb(Zr_{0.52}Ti_{0.48})O_3$ composition, from which a maximum ef-
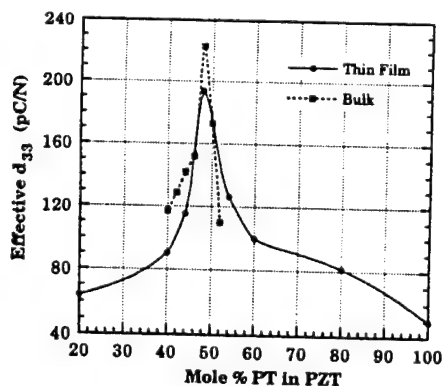

FIG. 3. The effective d_{33} as a function of composition in the PZ-PT solid solution system. The experimental points here correspond to the maximum in d_{33} obtained from plots generated for different compositions: notice that Fig. 2 is one such plot, for the PZT(52/48) composition. The dotted line represents the data reproduced from Berlincourt et al. (Ref. 3).
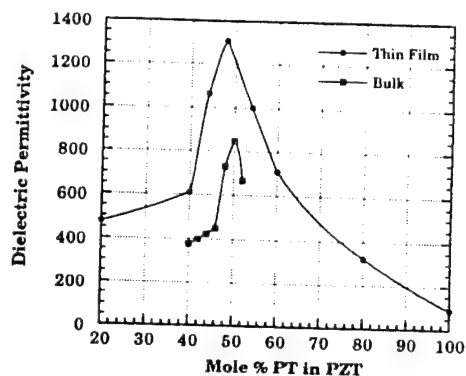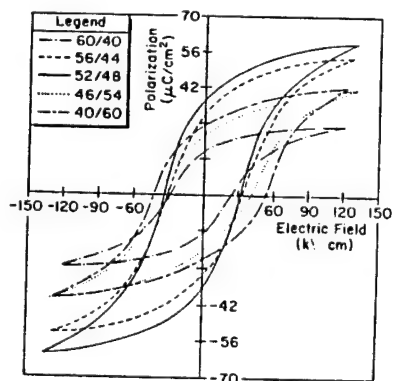

FIG. 5. A composite trace of ferroelectric P-E hysteresis loops for five neighboring compositions of 1 μm-thick film near the MPB of the PZT system. The top electrode size is 0.8 mm diam. The test signal is a triangular wave with a frequency of 10 Hz.
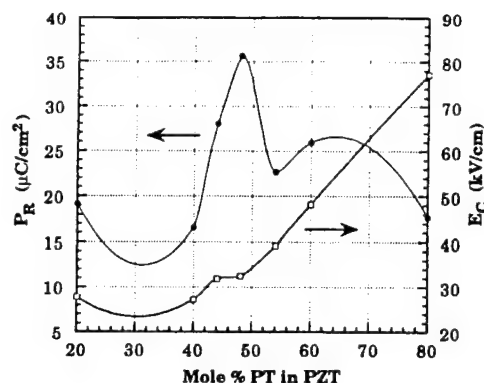
Chen et al.

FIG. 6. The remanent polarization and coercive field as a function of Zr/Ti ratio in the PZT system. Note that the maximum P_R is located at the PZT(52/48) composition. Ti-rich compositions show seemingly high coercive fields.

fective d_{33} of 194 pC/N is discerned, at an external bias field of 40 kV/cm. The reduction of d_{33} beyond a certain external bias value is due to the effective restraint of a domain wall movement, and hence the loss of significant extrinsic contributions.

It is important to establish that the definition herein of the "effective" d_{33}, plotted in Fig. 3 as a function of composition, is the maximum value of d_{33} observed as an increasing dc bias is imposed over a fixed ac driving field. The composition of maximum effective piezoelectric coefficient, (d_{33}=194 pC/N), perhaps referred to as the effective morphotropic phase boundary composition, and consequently the composition of highest electromechanical activity and transduction efficiency, contains 48% PbTiO$_3$ in solid solution, identical to the reported ceramic composition. Comparison between observed d_{33} values for PZT films and that of the bulk ceramics[3] shows similar trends, although the peak width of the films is larger and the peak value is lower than that of the bulk ceramics (d_{33}=233 pC/N). The slightly lower peak value of d_{33} in PZT films might be attributable to clamping from the stiff substrate and nonoptimal room temperature poling to which the films are limited.

While the primary objective of this undertaking, as stated earlier, has been the study of the variation of the piezoelectric properties as a function of composition in the PZT solid solution system, the inherent relationship[6] between the piezoelectric coefficients on the one hand, and the dielectric and ferroelectric properties on the other compels a further examination of the latter properties. The plot of dielectric permittivity as a function of composition for films in the PZT solid solution system suggests the similar occurrence of a morphotropic phase boundary near Pb(Zr$_{0.52}$Ti$_{0.48}$)O$_3$ (Fig. 4). Juxtaposition of this data with bulk ceramic data[3] reveals a fundamental similarity, albeit a

narrower peak distribution. Polarization-electric field hysteresis plots for several representative compositions near the MPB, shown in Fig. 5, indicate that the PZT(52/48) film has the largest value of remanent polarization. Compositional distribution of remanent polarization and coercive field, extracted from P–E traces is plotted in Fig. 6. While no simple relationships can be gleaned from the polarization profile, the maximum remanent polarization of 36 μC/cm^2 is located at 48% of PT in the PZT system. The coercive field, displayed as a function of the mole % of PbTiO$_3$, increases dramatically with the degree of tetragonality.

In summary, compositions in the lead zirconate–lead titanate solid solution system were prepared as films 1 μm in thickness, deposited by a sol-gel spin-on process on 1 in. platinized silicon substrates, and characterized with respect to piezoelectric, and the associated dielectric and ferroelectric properties. The position of the morphotropic phase boundary, as determined from significant enhancements in the effective longitudinal piezoelectric coefficient, dielectric permittivity and remanent polarization, coincides with the commonly quoted bulk ceramic composition, Pb(Zr$_{0.52}$Ti$_{0.48}$)O$_3$. Values of maximum piezoelectric coefficient, 194 pC/N; dielectric permittivity, 1310; and remanent polarization, 36 μC/cm^2, quoted for the phase boundary composition, compare favorably with values reported for undoped PZT ceramics.

[1] B. Jaffe, R. S. Roth, and S. Marzullo, J. Res. Natl. Bur. Stand. 55, 239 (1955).
[2] B. Jaffe, W. R. Cook, Jr., and H. Jaffe, Piezoelectric Ceramics (Academic, New York, 1971), pp. 135–148.
[3] D. A. Berlincourt, C. Cmolik, and H. Jaffe, Proc. IRE 48, 220 (1960).
[4] K. Carl and K. H. Härdtl, Phys. Status Solidi A 8, 87 (1971).
[5] A. M. Flynn, L. S. Tavrow, S. F. Bart, R. A. Brooks, D. J. Ehrlich, K. R. Udayakumar, and L. E. Cross, J. Microelectromechan. Sys. 1, 44 (1992).
[6] K. R. Udayakumar, J. Chen, A. M. Flynn, S. F. Bart, L. S. Tavrow, D. J. Ehrlich, L. E. Cross, and R. A. Brooks, Ferroelectrics 160, 347 (1994).
[7] K. Sreenivas, M. Sayer, and P. Garrett, Thin Solid Films 172, 251 (1989).
[8] N. Tohge, S. Takahashi, and T. Minami, J. Am. Ceram. Soc. 74, 67 (1991).
[9] H. Watanabe, T. Mihara, and C. A. Paz de Araujo, Proc. ISIF 1991, pp. 139–150.
[10] Y. Sakashita, T. Ono, H. Segawa, K. Tominaga, and M. Okada, J. Appl. Phys. 69, 8352 (1991).
[11] S. D. Bernstein, Y. Kisler, J. M. Wahl, S. E. Bernacki, and S. R. Collins, Mater. Res. Soc. Symp. Proc. 243, 373 (1992).
[12] M. Klee, R. Eusemann, R. Waser, W. Brand, and H. van Hal, J. Appl. Phys. 72, 1566 (1992).
[13] K. Iijima, I. Ueda, and K. Kugimiya, Ceram. Trans. 25, 33 (1992).
[14] C. K. Kwok, S. B. Desu, and D. P. Vijay, Ferroelect. Lett. Sec. 16, 143 (1993).
[15] M. de Keijser, P. J. van Veldhoven, and G. J. M. Dormans, Mater. Res. Soc. Symp. Proc. 310, 223 (1993).
[16] G. Teowee, J. M. Boulton, M. N. Orr, C. D. Baertlein, R. K. Wade, D. P. Birnie III, and D. R. Uhlmann, Mater. Res. Soc. Symp. Proc. 310, 423 (1993).
[17] H. N. Al-Shareef, K. R. Bellur, O. Auciello, X. Chen, and A. I. Kingon, Thin Solid Films 252, 38 (1994).
[18] G. Yi, Z. Wu, and M. Sayer, J. Appl. Phys. 64, 2717 (1988).
[19] W. Y. Pan and L. E. Cross, Rev. Sci. Instrum. 60, 2701 (1989).

APPENDIX 65

"Square" hysteresis loops in phase-switching Nb-doped lead zirconate stannate titanate thin films

C. J. Gaskey, K. R. Udayakumar, H. D. Chen, and L. E. Cross
Materials Research Laboratory, The Pennsylvania State University,
University Park, Pennsylvania 16802-4801

Niobium-doped lead zirconate stannate titanate thin films have been prepared by a modified sol-gel spin on technique, utilizing the hydrolysis-resistant precursor lead acetylacetonate. Films of compositions in the antiferroelectric tetragonal and antiferroelectric orthorhombic phases were prepared and phase-switched with the application of appropriate electric fields. A distinctly "square" hysteresis response was observed in a low titanium, low tin, orthorhombic composition, with a maximum polarization, P_{max}, of 40 μC/cm^2 and switching field values of $E_f = 175$ kV/cm and $E_a = 75$ kV/cm, while varying degrees of squareness, along with lower polarizations and switching fields, were observed in the higher tin, tetragonal compositions. Electric field-induced strains of up to 0.33% have been measured in the orthorhombic composition, with tunable electromechanical coefficients. Film properties showed only slight variation with electrode size over a range of diameters from 0.8 mm to 6.35 mm; large area electrodes are vital for practical actuator and sensor devices. With a capacitance density of 30–35 μF/cm^2, films of the orthorhombic composition are promising as power plane decoupling capacitors in multichip modules.

I. INTRODUCTION

The electric field forced antiferroelectric (AFE) to ferroelectric (FE) phase transition in ceramic PbZrO$_3$ was first demonstrated within a narrow region below its Néel temperature by Shirane et al.[1] Through a series of isovalent and A-site vacancy substitutions, Jaffe[2] and Berlincourt et al.[3,4] were able to broaden the phase-switchable temperature region, allowing for a number of practical applications of these electric field, pressure, and temperature switchable antiferroelectric ceramics. Because of the small free energy difference between the AFE and FE phases, switching from one phase to another is possible by the application of a reasonable electric field. Jaffe coined the term "soft" to describe an antiferroelectric that can be field-switched.[2]

Soft antiferroelectrics were proposed as high-energy-storage capacitors by Jaffe because they are free of remanence, like a linear capacitor, and also because the "energy area" traced out by the P-E hysteresis loop approaches a square rather than a triangle, as is the case with a linear element. When the poled FE phase is switched to the AFE phase, the polarization charge is released, supplying high currents.[2] Soft antiferroelectrics have also been investigated as transducer materials due to the large strains concurrent with AFE to FE switching. Strains of 0.1–0.5%, depending on the composition, result from transitions between the AFE tetragonal and FE rhombohedral phases, due to specific volume differences.

Transitions can be forced by temperature and pressure, as well as applied electric field, making these materials useful as pressure and temperature transducers.[3,4]

Berlincourt,[4] in a study of doped Pb(Zr,Sn,Ti)O$_3$ ceramics, has described two different types of AFE-FE transitions based on the character of the P-E hysteresis loops; the two types of loops have been termed "slanted" and "square". The "slanted" loop materials have much less hysteresis, lower transition fields, smaller volume differences between AFE and FE phases, and wider temperature ranges over which the transition can be forced by electric field. The "slanted" loop materials exhibit a small remanent polarization at zero field, while the "square" loop materials do not. Representative P-E hysteresis traces for slanted and square loop compositions are shown, with indications of switching field nomenclatures, in Fig. 1.

Because of the dramatic changes in polarization and strain accompanying the AFE-FE transition, these materials have been identified as promising candidates for use as high-energy-storage capacitors and electromechanical transducers. However, even at an early stage in their development, limitations inherent to the bulk ceramic form of these materials, namely low dielectric strength and a practical minimum thickness, were identified as deleterious to their extensive utility.[2] Thin ceramic films offer advantages of high dielectric strength (on the order of 1 MV/cm), low voltage operation, and the

$Pb_{.99}La_{.04}(Zr_{.42}Ti_{.18}Sn_{.4})O_3$

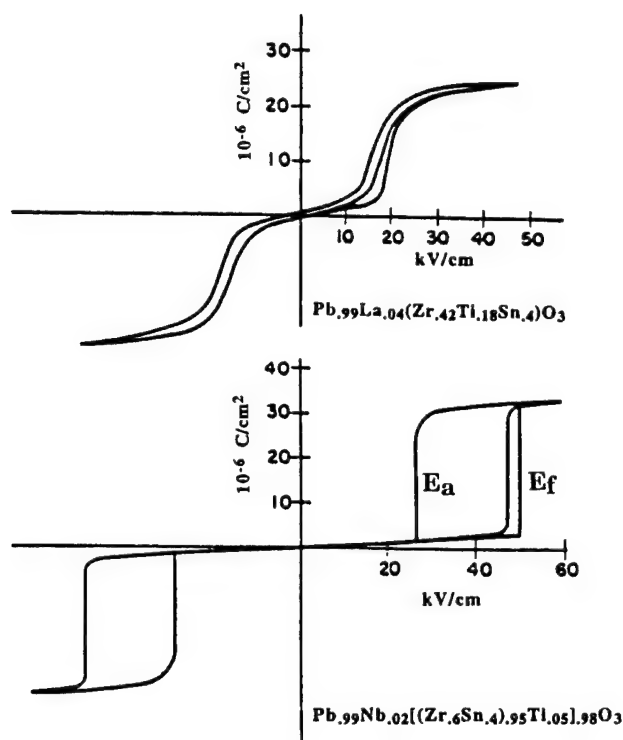$Pb_{.99}Nb_{.02}[(Zr_{.6}Sn_{.4})_{.95}Ti_{.05}]_{.98}O_3$

FIG. 1. Delineation of slanted and square switching behavior, reproduced from Berlincourt.[4] Also indicated are definitions of forward and backward switching fields, E_f and E_a.

possibility of integration into microtype device schemes. These advantages are especially useful in the study and application of phase-switching systems.

The phase-switching behavior of thin films in the La-doped PSZT system has been investigated by Brooks *et al.*[5,6] A number of compositions in varying proximity to the AFE-FE phase boundaries were prepared using a sol-gel spin coating method and characterized for electrical properties and strain. All of the thin film compositions studied (identical to those of Pan *et al.*[7] in bulk ceramics) showed remanent, "slanted" hysteresis loops.[5,6] The transition fields for the films were found to be larger than the bulk ceramics, while the maximum polarizations and strains measured in the films were lower. Residual tensile stresses due to substrate clamping and a metastable coexistence of FE and AFE phases were given as possible explanations for the observed remanence and lower strain.[5,6]

While the strains resulting from the field-forced AFE-FE transition make La-doped PSZT films useful for microactuator applications, the "slanted" loop hysteresis behavior is not desirable for the high-energy-storage capacitors mentioned by Jaffe.[2] The motivation for this work was to examine Nb-doped lead zirconate stannate titanate thin films in the hope of finding compositions that show "square" loop switching behavior with low remanence and large strains. In addition to an

orthorhombic composition, two AFE tetragonal compositions, similar to a composition studied by Berlincourt *et al.*,[3,4] were investigated to allow for a comparison of thin film and bulk ceramic properties.

For piezoelectric and phase-switching applications in micromechanical systems, large (several mm^2) electrode areas are required. A practical maximum electrode area is dictated by defects in the film, which can cause either shorting or high losses. In this study, lead acetylacetonate, which is less sensitive to hydrolysis,[8,9] has been used as a precursor in an effort to reduce the number of defects in the films, allowing for the use of larger electrodes.

II. EXPERIMENTAL PROCEDURE

The method used to prepare the solutions was a variant of the sol-gel procedure proposed by Selvaraj *et al.*,[8] using lead acetylacetonate as an alternative lead source to the more common lead acetate trihydrate. Other precursors used were titanium isopropoxide, zirconium *n*-propoxide, tin(IV) acetate, and niobium ethoxide. In a unique, one-step process, all of the precursors were initially combined with the solvent 2-methoxyethanol, and the mixture was refluxed at 130 °C for approximately 12 h. The solution was then allowed to cool to room temperature, the volume was adjusted for a 0.4 M concentration, and 4% formamide was added to promote proper drying.[10]

Thin films of the various compositions were prepared using a multiple layer spin-coating procedure. Each precursor solution was filtered through a 0.2 μm filter and deposited on a substrate, which was spun at 3000 rpm for approximately 30 s on a commercial resist spin-coater. The substrate structure consisted of a 0.5 μm-thick thermally grown SiO_2 buffer layer on (100) silicon wafers with a 0.15 μm-thick platinum bottom electrode sputtered on a 200 Å titanium adhesion layer.[11] After the application of each layer, the films were pyrolyzed at approximately 400 °C for 5 min to remove organics and allowed to cool to room temperature. Subsequent layers were applied until a thickness of greater than 0.4 μm was achieved. The films were then furnace annealed at 700 °C in air for 15 min to achieve crystallization into the perovskite structure.

Platinum top electrodes of diameters ranging from 0.8–6.35 mm were deposited by rf sputtering and then annealed at 550 °C for 1 h to improve electrical contact. The polarization-electric field (*P-E*) hysteresis loops were measured using a modified Sawyer–Tower circuit at room temperature. Samples were driven with a 5–20 V, 30 Hz signal. The low field dielectric permittivity and dielectric loss tangent of the films were measured at room temperature using a HP4274A impedance analyzer with an oscillating voltage of 1 mV and a

frequency of 1 kHz. Capacitance as a function of slowly varying dc bias field was collected with an HP4192A impedance analyzer. With the oscillating field and frequency set at 10 mV and 100 kHz, respectively, the dc bias was stepped through 0.5 V increments in a cyclic manner between -10 and $+10$ V. The thickness of the films was determined using a profilometer. The crystal phases were characterized by grazing angle x-ray diffraction, using a Scintag DMC-105 diffractometer. Field-induced strains were measured using a double beam laser interferometer, which has the capability of measuring displacements to a resolution of 10^{-2} Å.

III. RESULTS AND DISCUSSION

The thickness of the films ranged from 0.4–0.56 μm, as determined from the profilometer traces. X-ray diffraction patterns taken for films of the three compositions verified the presence of pseudo-cubic, perovskite phase reflections. The room temperature, low field relative dielectric constant, ϵ_r, the dielectric loss tangent, tan δ, and the phase-switching parameters of the three compositions are shown in Table I, for an electrode diameter of 2.36 mm. The dielectric constants of the two tetragonal compositions are considerably higher than that of the orthorhombic composition. It was noticed that annealing the top electrode lowered the loss considerably and the dielectric constant slightly.

The *P-E* hysteresis plot for composition (2) is shown in Fig. 2. Both tetragonal compositions, (1) and (2), showed this type of behavior, which can perhaps be described as a cross between the square and slanted types of loops, with slightly slanted transitions, high maximum polarization and near zero remanence. It should be noted that compositions (1) and (2) are very similar to a composition presented by Berlincourt *et al.*[3] as exemplary of the square loop type behavior, thus indicating a difference in the compositionally determined switching behavior in thin film form, although not as drastic a difference as previously suggested.[5,6] Magnitudes of the polarization and switching fields are similar to values found in Berlincourt *et al.*[3]

Figure 3(a) shows the *P-E* loop for orthorhombic composition (3), which demonstrates, for the first time, a thin film AFE exhibiting the "square" loop hysteresis. The forward and reverse switching fields are quite distinct, and the polarization is nearly zero at zero applied field, in contrast to the slanted loop phenomenon. Thin films of this antiferroelectric phase-switching, orthorhombic composition may be extremely valuable as dielectrics for power and ground plane decoupling in advanced multichip modules (MCM's). In an application where the available top surface area is severely limited and the clock rates are continuously on the rise, there is a need for off-chip capacitors that can generate ultrahigh capacitance density. Focusing on the FE $\rightarrow$ AFE arm of the double hysteresis loop in Fig. 3(a), a polarization charge of 16 μC/cm^2 may be released for a small voltage change of 0.5 V; this corresponds to a capacitance per unit area of 32 μF/cm^2, a magnitude larger than the 1 μF/cm^2 requirement projected for decoupling capacitors at microwave frequencies. While this magnitude of capacitance density clearly shows great promise the dielectric saturation function and the charge delivery speed are being examined at GHz frequencies to ascertain the applicability of the films in MCM's. Experiments are currently underway, involving the manipulation of film processing parameters and synthesis of related formulations in the Nb-doped PSZT ternary, to close the gap between the forward and backward switching arms of the loop so that the entire spontaneous polarization may be used to discharge current at a constant voltage; the dielectric would, then, essentially behave as a battery, ideally suited for the decoupling function.

The maximum polarizations and switching fields of the tetragonal compositions are lower than those of the orthorhombic (the switching fields given in Table I were determined from the *P-E* loops). In terms of applied voltages, the AFE-FE switching threshold correspond to 2.4 V, 3.4 V, and 7.0 V for a 0.4 μm film of compositions (1), (2), and (3), respectively. Film thickness can be adjusted to decrease the required switching voltage. It is interesting to note that while compositions in the orthorhombic phase field have not been considered in bulk ceramic studies, as their switching fields exceeded dielectric breakdown strengths, it is these compositions, field-switchable in thin film form, that have been identified herein to exhibit the desired "square" loop behavior at the submicron scale.

The square loop behavior of composition (3) is reproduced with a 5.94 mm diameter top electrode

TABLE I. Summary of dielectric and phase-switching characteristics of Nb-doped lead zirconate stannate titanate thin films.

Film composition	Thickness (μm)	ϵ_r at 1 kHz	tan δ	$E_{AFE \rightarrow FE}$ (kV/cm)	$E_{FE \rightarrow AFE}$ (kV/cm)	P_{max} (μC/cm^2)
(1) $Pb_{0.99}Nb_{0.02}(Zr_{0.57}Sn_{0.38}Ti_{0.05})_{0.98}O_3$	0.56	530	0.015	60	30	26
(2) $Pb_{0.99}Nb_{0.02}(Zr_{0.65}Sn_{0.31}Ti_{0.04})_{0.98}O_3$	0.44	530	0.016	85	45	35
(3) $Pb_{0.99}Nb_{0.02}(Zr_{0.85}Sn_{0.13}Ti_{0.02})_{0.98}O_3$	0.45	240	0.005	175	75	40

FIG. 2. *P-E* hysteresis trace for AFE tetragonal composition (2).

(a)

(b)

FIG. 3. "Square" *P-E* hysteresis behavior as seen in AFE orthorhombic composition (3) for electrode diameters of (a) 1.6 mm and (b) 5.94 mm, showing little degradation of maximum polarization.
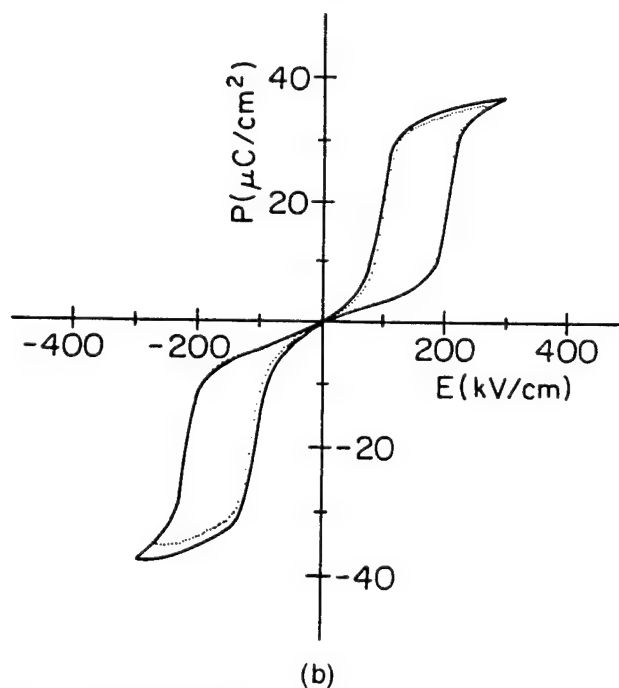
[Fig. 3(b)]. Note that the polarization has decreased slightly, while the switching fields remain constant. The same general trend was seen for all three compositions with increasing electrode area: slight decreases in polarization and dielectric permittivity, with no change in the switching fields. This type of deviation would be expected to arise from a random, spatial distribution of defects, possibly in the form of pores and grain boundaries, throughout the volume of the film.[12] The ability to use large area top electrodes facilitates the use of these films in devices involving sensing, actuating, and motor functions.

Plots of capacitance versus dc bias have been used to confirm the antiferroelectricity of thin films exhibiting "slanted" loops[5]; Figure 4 shows capacitance as a function of slowly varying bias field, taken from a virgin electrode, for composition (3). The presence of the "double butterfly" variation, a general characteristic of a soft antiferroelectric, corresponds to the forward and reverse switching fields of the phase transition. The magnitudes of the switching fields can be determined both from the peaks of the *C-V* curves, and from the intersections of the tangents drawn to the steepest portions of the *P-E* curves. The two differently determined values are in good agreement, as seen in the values for composition (3); the values of forward and reverse thresholds as determined from the *C-V* data are 150 and 78 kV/cm, while the corresponding values determined form the *P-E* curves are 175 and 75 kV/cm, respectively.

The electric field-induced longitudinal strain for a film of composition (3) is shown in Fig. 5 as a function of ac drive field at a dc bias of 100 kV/cm. The strain is low at ac fields below 40 kV/cm, but reaches a value of 0.33% at 100 kV/cm. There is no data available in the literature for bulk ceramics of equivalent composition with which this strain data may be compared. A strain of 0.16% for a La-doped film of composition $(Pb_{0.97}La_{0.02})(Zr_{0.60}Ti_{0.10}Sn_{0.30})O_3$ has been
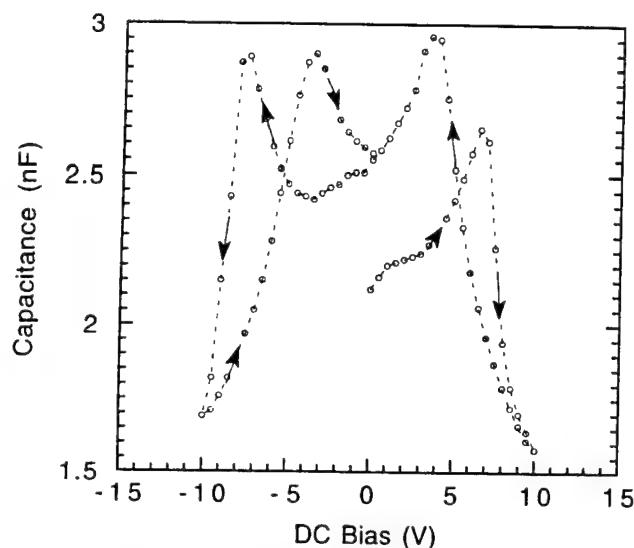
FIG. 4. Plot of capacitance as a function of varying dc bias for a film of AFE orthorhombic composition (3).
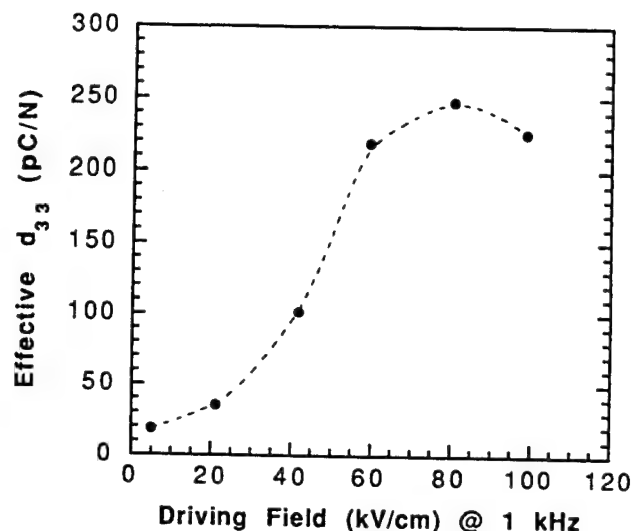

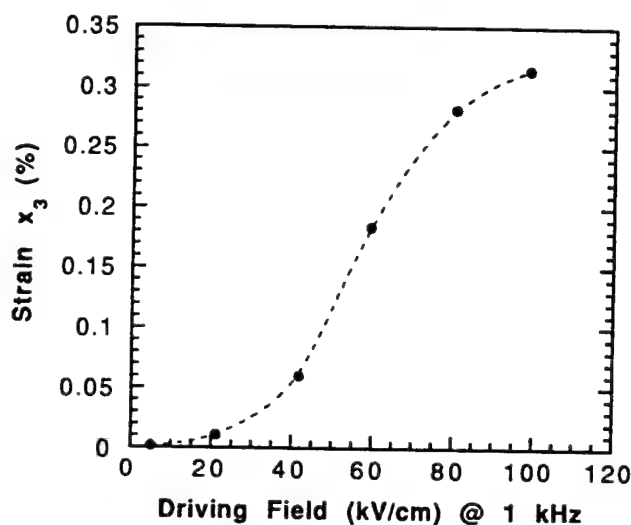FIG. 6. Effective d_{33} as a function of drive field for composition (3).

FIG. 5. Field-induced strain as a function of ac driving field at 1 kHz for composition (3). The film was maintained at a dc electric bias of 100 kV/cm.

field-induced strains of up to 0.3% have been optically determined for an AFE orthorhombic composition, representing the highest value for the phase-switching family of antiferroelectrics reported to date. Large area electrodes, up to 6.35 mm in diameter, have been successfully employed. Composition (3) shows a square, double *P-E* loop, and with a high capacitance density, is promising for applications as a decoupling capacitor in multichip modules. The low remanence observed in compositions (1) and (2) suggests that the Nb-doped $PbZrO_3$–'$PbSnO_3$'–$PbTiO_3$ ternary system provides a family of highly useful compositions, from which desired characteristics can be chosen, for applications as energy storage devices and in micromechanical systems. A closer, more detailed examination of the phase diagram is needed, specifically of the compositions that lie along the boundary of the AFE orthorhombic and FE rhombohedral regions, as the results of composition (3) are very promising.

ACKNOWLEDGMENT

reported.[5] An effective longitudinal piezoelectric coefficient, d_{33}, calculated through the converse piezoelectric effect (from the data presented in Fig. 5) is plotted in Fig. 6. It is apparent from the figure that the effective d_{33} can have a value as large as 250 pC/N, and is tunable with appropriate drive and dc bias conditions.

IV. SUMMARY

Sol-gel-derived thin films of antiferroelectric to ferroelectric phase-switching Nb-doped lead zirconate stannate titanate have been prepared, making use of an alternate lead precursor, lead acetylacetonate. Electric

REFERENCES

1. G. Shirane, E. Sawaguchi, and Y. Takagi, Phys. Rev. **84** (3), 476 (1957).
2. B. Jaffe, Proc. IRE **49**, 1264 (1961).
3. D. Berlincourt, H. H. A. Krueger, and B. Jaffe, J. Phys. Chem. Solids **23**, 659 (1964).
4. D. Berlincourt, IEEE Trans. Sonics Ultrason. Ind. Eng. Chem. SU-13 (4), 116 (1966).
5. K. G. Brooks, J. Chen, K. R. Udayakumar, and L. E. Cross, J. Appl. Phys. **75** (3), 1699 (1994).

6. K. G. Brooks, J. Chen, K. R. Udayakumar, and L. E. Cross, in *Ferroelectric Thin Films II*, edited by A. I. Kingon, E. R. Myers, and B. Tuttle (Mater. Res. Soc. Symp. Proc. **243**, Pittsburgh, PA, 1992), p. 443.

7. W. Y. Pan, Q. M. Zhang, A. S. Bhalla, and L. E. Cross, J. Am. Ceram. Soc. **72**, 571 (1989).

8. U. Selvaraj, K. G. Brooks, A. V. Prasad Rao, S. Komarneni, R. Roy, and L. E. Cross, J. Am. Ceram. Soc. **76** (6), 1441 (1993).

9. S. J. Milne and S. H. Pike, J. Am. Ceram. Soc. **74** (6), 1407 (1991).

10. K. R. Udayakumar, J. Chen, and L. E. Cross, Proc. 7th Int. Symp. Appl. Ferroelectrics, 741 (1990).

11. Y. Shimizu, K. R. Udayakumar, and L. E. Cross, J. Am. Ceram. Soc. **74** (12), 323 (1991).

12. R. Gerson and T. C. Marshall, J. Appl. Phys. **30** (11), 1650 (1959).

J. Mater. Res., Vol. 10, No. 11, Nov 1995

2769

APPENDIX 66

Reactive magnetron co-sputtered antiferroelectric lead zirconate thin films

K. Yamakawa,[a] S. Trolier-McKinstry, and J. P. Dougherty
Center for Dielectric Studies, Intercollege Materials Research Laboratory,
The Pennsylvania State University, University Park, Pennsylvania 16802

S. B. Krupanidhi
Indian Institute of Science, Bangalore, India

Antiferroelectric lead zirconate thin films were formed on platinum coated silicon substrates by a reactive magnetron co-sputtering method. The films showed (240) preferred orientation. The crystallization temperatures and the preferred orientation were affected by the lead content in the films. The electric field forced transformation from the antiferroelectric phase to the ferroelectric phase was observed at room temperature with a maximum polarization value of 36 $\mu C/cm^2$. The average field to excite the ferroelectric state and that for the reversion to the antiferroelectric state were 267 and 104 kV/cm respectively. © *1995 American Institute of Physics.*

In recent years, research activity in the area of ferroelectric thin films has grown due to their possible applications in the areas of microelectronic and microelectromechanical systems (MEMS). In particular, the prospect of integrating materials with exceptional charge storage ability or actuator capabilities directly with semiconductor device technology is attractive. The majority of this work has focused on Pb-based perovskite ferroelectrics and $Ba_{1-x}Sr_xTiO_3$ capacitor compositions.

In some of these applications, however, antiferroelectric compositions offer an alternative to the ferroelectric capacitors and transducers. Antiferroelectric (AFE) materials are characterized by rows of dipoles, with the dipole moment of adjacent rows equal but antiparallel so that in equilibrium there is no net spontaneous polarization. $PbZrO_3$ was the first compound to be identified as an antiferroelectric (Shirane et al.).[1] In $PbZrO_3$, the small free energy difference between the AFE phases and the ferroelectric (FE) phases makes it possible to force phase-switching from the AFE phase to the FE phase with an applied electric field. Thin films of these materials are interesting because the breakdown strength of thin films typically surpasses by an order of magnitude bulk ceramics of the same composition.[2] As a result, devices based on phase-switching may well be more robust and reliable in thin film form than in the bulk. In addition, recent work has shown that, in the case of $PbZrO_3$ thin films, it is possible to prepare materials which can be phase-switched at room temperature.[3-8]

The characteristic hysteresis loop resulting from the field-forced AFE–FE phase transition makes the materials interesting for charge storage applications. When the applied electric field is removed from the poled ferroelectric phase of $PbZrO_3$, the material reverts to the low-energy AFE phase, releasing all of the polarization charge at a fixed voltage. The AFE thus acts like a current source. Moreover, since this can be achieved free of remanent polarization at low fields, the material acts as a linear capacitor. Because the AFE phase typically differs from the field-forced FE phase in volume,

the phase transition is also accompanied by large strain changes typically on the order of 0.1%–0.5%. Again, since the low and high field states are extremely well-defined, this is attractive in actuator applications.

In this work, the preparation of $PbZrO_3$ thin films by reactive magnetron co-sputtering was pursued in order to investigate its applicability in developing Si-based microelectronic and MEMS devices. This is the first report of $PbZrO_3$ film preparation in which multimagnetron sputtering has been used. Films were characterized in terms of their structural and electrical properties.

The films were deposited from metal targets of lead and zirconium, placed in sputtering guns focused at an angle of 30° with respect to the normal. Each gun was powered by an independent dc magnetron power supply. Deposition was carried out in an environment of Ar/O_2 with ratios between 50%/50% and 90%/10%, while the total pressure was kept between 10 and 20 mTorr. This partial pressure of oxygen was sufficient to oxidize the metallic species during deposition. All films were deposited on unheated rotating platinum coated silicon substrates.

The thicknesses of $PbZrO_3$ films were kept between 0.2–0.5 microns. The Pt films showed preferred (111) orientation. In order to obtain the perovskite antiferroelectric phase, films were heat-treated in a rapid thermal annealer at temperatures between 400 and 750 °C. The annealing time was kept at 30 s.

The stoichiometry of the deposited films was analyzed by dc induction coupled plasma, and this data was used to optimize the deposition conditions for individual targets. Several runs were performed to establish the reproducibility.

Structural characterization of the films was performed by XRD and SEM. For electrical property measurements, gold top surface electrodes with 0.6 mm diameter were sputtered onto the film. Hysteresis loops and capacitance-voltage curves were measured using a Radient Technologies RT66A tester. The dielectric constant was measured using an impedance analyzer (HP4192A).

As expected, as-grown films were found to be amorphous. Crystallization of the perovskite phase was observed at temperatures above 550 °C. Figure 1 shows the XRD pat-
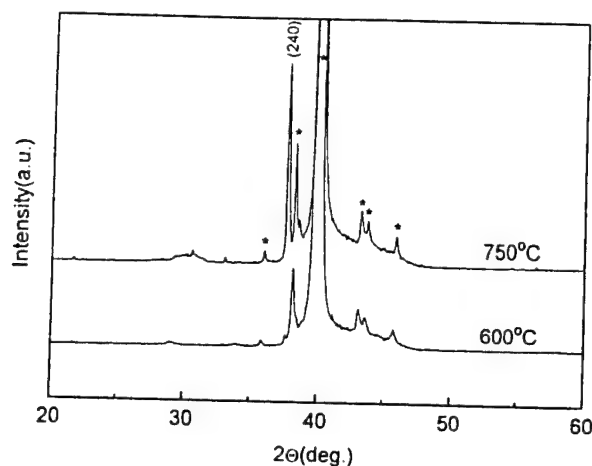
[a] Electronic mail: kxy4@psu.edu

FIG. 1. X-ray diffraction patterns for rapid-thermal annealed films at 600 and 750 °C. Substrate peaks are indicated by ⋆.

FIG. 3. Hysteresis loop for 750 °C annealed film as a function of applied voltage measured on an RT66A tester at 15 Hz.

terns for reactive magnetron co-sputtered PbZrO₃ thin films annealed at 600 and 750 °C respectively. Both temperatures offered well-crystallized perovskite films, however, annealing at temperatures of 750 °C imparted a preferred (240) orientation for the orthorhombic PbZrO₃. Based upon this observation, most films were annealed at 750 °C for 30 s.

The stoichiometry of the as-deposited films has often been reported to influence the final crystallinity in Pb based perovskites. Similar observations were also made in the present work as a function of deposition power ratio. The power for the Zr target was kept constant at 250 W while the power for the Pb target was varied between 10 and 20 W to vary the Pb content in the deposited films. At low powers such as 10 W for the Pb target, because the Pb content was well below the stoichiometric level, no perovskite phase was formed [Fig. 2(d)]. However, as the Pb content reached near the stoichiometric level, perovskite phase formation was regularly observed. The perovskite phase was observed with various Pb content with stoichiometric composition. At a specific ratio of 18/250 W for the Pb/Zr power, films attained preferred (240) orientation. In addition, the films with the
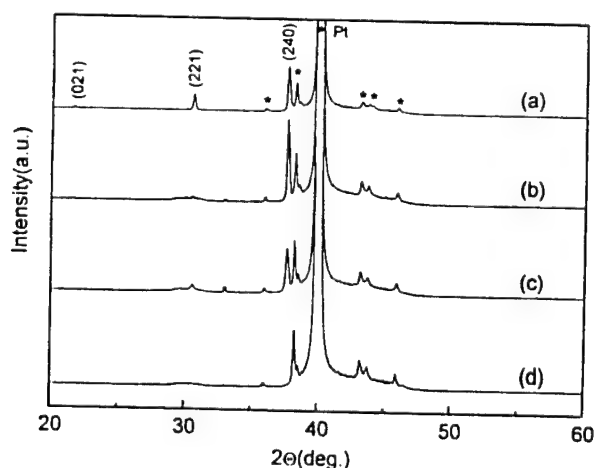

FIG. 2. X-ray diffraction patterns for annealed films at 750 °C deposited with Pb/Zr target power ratio of 20/250 W (a), 18/250 W (b), 16/250 W (c), and 10/250 W (d). Starred peaks are due to the substrate.
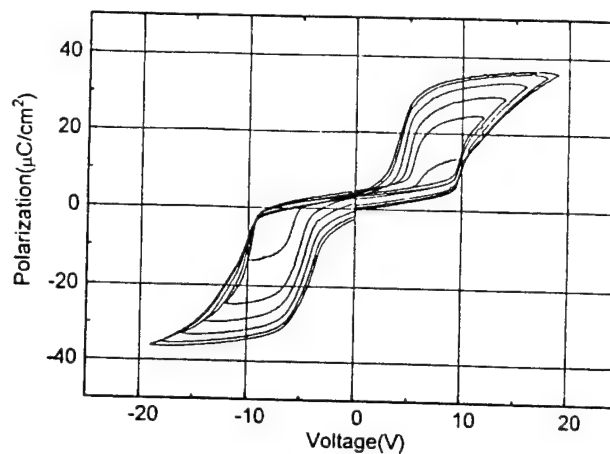
range of composition where the perovskite phase was observed, the films with relatively low Pb content (operation power for Pb target = 16 W) have to be annealed at higher temperatures than for higher Pb content films (operation power for Pb target = 22 W) to produce the perovskite phase. Thus, higher Pb content promotes lower crystallization temperatures.

The films consist of 0.2–0.5 micron grains, with a large number of small cracks at the grain boundaries. These cracks can be avoided by stacking the films several times or depositing ones at high temperatures.

The electrical behavior of the films was initially characterized in terms of the frequency dependence of the low field dielectric permittivity using an MIM (metal-insulator-metal) configuration. Films exhibited a dielectric constant of about 115 and a dissipation factor of 0.045 at room temperature, indicating the good quality of the present films. In addition, the frequency dependent response indicated no dispersion below 1 MHz.

It has been established that crystal or ceramic PbZrO₃ is capable of undergoing a field-induced phase transformation to the ferroelectric state when a strong electric field is applied below 232 °C, the Curie temperature for the material. In this field-forced change, the structure changes from a staggered orthorhombic arrangement to a polar arrangement, probably rhombohedral, whenever the applied field exceeds a certain threshold value.[9] This manifests itself by a double hysteresis loop with a linear central region and open areas on either end. Similar observations were made in the present magnetron co-sputtered PbZrO₃. Figure 3 illustrates the sequential evolution of the phase switching with increasing field until saturation is reached. The observed switching hysteresis loops are comparable to those reported for single crystals. The saturation polarization was found to be about 36 μC/cm². The switchable polarization is close to the polycrystalline value of ~30 μC/cm².[10] The linear polarization range extended from −10 to 10 V and indicates the good quality of present films. The film thickness was 0.38 microns.

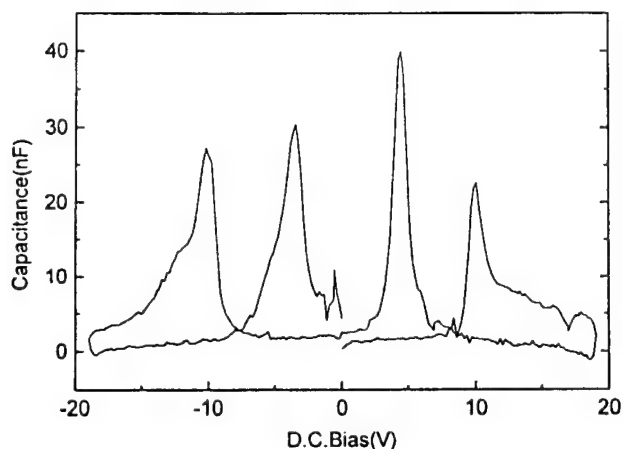Figure 4 also shows a capacitance–voltage curve for the

FIG. 4. Capacitance–voltage characteristics for 750 °C annealed films (capacitance derived from a derivative of hysteresis loop).

same film. Four peaks in capacitance which show the FE–AFE transition of PbZrO₃ can be seen. The average field to excite the ferroelectric state (E_f) and the average field for reversion to the antiferroelectric state (E_a) were calculated from the applied voltage of the maximum peaks of capacitance, and the values are 267 and 104 kV/cm, respectively.

This kind of soft antiferroelectricity has also been reported for Ti or Ba modified PbZrO₃ ceramics. The extremely large charge which is released on conversion from the ferroelectric state to the antiferroelectric state may be useful for alternate capacitor materials in dynamic random access memories (DRAMs). The hysteresis regions are well suited for either power storage or actuator applications.

In conclusion, antiferroelectric PbZrO₃ thin films were prepared by a reactive magnetron co-sputtering method. The film with stoichiometric composition showed (240) preferred orientation on a Pt(111)/Si substrate. The Pb content affects both the crystallinity and the degree of preferred orientation. The field-induced ferroelectric–antiferroelectric transition was observed at room temperature with a maximum polarization value of 36 μC/cm².

[1] G. Shirane, S. Sawaguchi, and Y. Takagi, Phys. Rev. 84, 476 (1951).
[2] K. R. Udayakumar, Ph.D thesis, The Pennsylvania State University, 1993.
[3] T. Tani, J. F. Li, D. Viehland, and D. A. Payne, J. Appl. Phys. 75, 3017 (1994).
[4] J. F. Li, D. D. Viehland, T. Tani, C. D. E. Lakeman, and D. A. Payne, J. Appl. Phys. 75, 442 (1994).
[5] I. Kanno, S. Hayashi, M. Kitagawa, R. Takayama, and T. Hirano, Appl. Phys. Lett. 66, 145 (1995).
[6] Y. Akiyama, S. Kimura, and I. Fujimura, Jpn. J. Appl. Phys. 32, 4154 (1993).
[7] K. G. Brooks, J. Chen, K. R. Udayakumar, and L. E. Cross, Mater. Res. Soc. Symp. Proc. 243, 443 (1992).
[8] C. J. Gaskey, B. thesis, The Pennsylvania State University, 1993.
[9] O. E. Fesenko, R. V. Kolesova, and Yu. G. Sindeyev, Ferroelectrics 20, 177 (1978).
[10] D. Berlincourt, H. H. Krueger, and B. Jaffe, J. Phys. Chem. Solids 25, 659 (1964).

APPENDIX 67

ALKOXIDE DERIVED SrBi$_2$Ta$_2$O$_9$ PHASE PURE POWDER AND THIN FILMS

D. Ravichandran, K. Yamakawa. A.S. Bhalla and R. Roy,
Materials Research Laboratory
The Pennsylvania State University
University Park, PA 16802, U.S.A.

Abstract

Novel ferroelectric materials SrBi$_2$Ta$_2$O$_9$ (SBT) phase pure powder and thin films have been prepared including the organic precursors. The xero-gel formed was dried and characterized using TGA and DTA to determine the organic burn out and crystallization temperatute of SBT phase. Powder X-ray diffraction was used systematically to crystallize SBT phase. Phase pure SBT powder was formed as low as 650°C and thin-films at 600°C in comparison to other earlier reported work. SEM micrographs show a grain size of ~0.5 μm and crack free fims with the film thickness of 2 μm.

Bismuth - layer oxides such as $SrBi_2Ta_2O_9$ or $SrBi_2Nb_2O_9$ were recently reported to have excellent ferroelectric properties [1, 2]. These compounds have a general form of $(Bi_2O_2)^{2+}$ $(A_{m-1}B_mO_{3n+1})^{2-}$ where "m" is the number of perovskite building blocks between (Bi_2O_2) layers[3]. A and B are the usual cations which enter the perovskite structure. B-site cation are ferroelectrically active and have strong interaction only on the two dimensional sheet perpendicular to the c- axis, as a result the ferroelectricity of layered perovskites are highly anisotropic.

SBT is a best material for a potential candidates to ferroelectric non- volatile memories[4]. Fig. (1) shows the layered structuer of SBT with even layer (m =2). SBT has $\{ (BiO_3)^{3-}\}_\alpha$ layers alternate with the perovskite like layers. The perovskite layers may have different thickness, depending on the m value. In the case of Bi_2MoO_6 compound corresponds to m=1, where as in the SBT corresponds to m=2, $Bi_4Ti_3O_{12}$ (m=3) and $BaBi_4Ti_4O_{15}$ (m=4). It is clear from fig.(1) SBT has two layers of octahedron (m=2). The compounds containing perovskite like layers consisting of octahedron (NbO_6, TaO_6 and TiO_6 octahedron) are present in the lattice of these materials, leads to spontaneous polarization can occur both in the planes and layers[5].

In this paper we report on prepartion of SBT phase pure powder and thin films synthesized via organic precursors incluging Sr - granules, $Ta (OC_2H_5)_5$ (Aldrich chemicals 99.99 % purity), Bi- 2, ethyl hexanoate (Johnson Matthey Chemicals 99.99 % purity) as the starting organic precursors.

At first Bi (2, ethyl hexanoate) in stoichiometric amounts was dissolved in 20 ml of 2-methoxyethanol in a three neck flask and refluxed at 125°C for 6 hours in an argon gas. Then required amount of $Ta((OC_2H_5)_5$ was dissolved in 15-20 ml of 2-methoxyethanol and 3-6 ml of CH_3COOH for complete solubility. The $Ta(OCH_2CH_2OCH_3)_5$ formed was reacted with Bi-sol to form the double alkoxide[6] at 125°C for 12 hours in an argon gas. Finally Sr- granules was dissolved in 2-methoxyethanol and 5-7 ml of acetic acid in order to have complete solubility and refluxed at 125°C between 6-7 hours. This clear solution was reacted with the double alkoxide Bi - Ta complex sol at 125°C for 12 hours. The reaction sequence for the formation of SBT gel is shown in fig. (2).

The resultant clear homogeneous solution was cooled to room temperature and hydrolysed by adding theoretical amount of de-ionized water diluted with 2-methoxyethanol in the volume ratio (1:4). The clear solution was placed in a 60°C oven for 4-8 hours to form the transparent xero-gel. The SBT xero-gel formed was dried, then crushed and analysed using Perkin Elmer Thermogravimetric analyser (TGA) to determine the drying and organic burn out behaviour of the

gel with a heating rate of 10°C/min. Diffrential thermal analyser (DTA) was used to determine the crystallization temperature of the SBT gel with a heating rate of 10°C/min. Phase identification was done using the Scintag powder X-ray diffractometer with Ni filtered $CuK_{\alpha 1}$ radiation. Another portion of the SBT solution was diluted to ~0.3 M and hydrolysed with de-ionized water and 2-methoxyethanol in the ratio (1:2). To deposit crack free films 4% (by volume) formamide was added into the solution. Prior to spin coating Pt- coated Si substrate was throughly washed with iso-propanol. Films were spun at 3000 rpm for 20 seconds using Integrated Technology P - 6000 spin coater.

The films were deposited and pyrolysed on a hot plate at 400 -450°C to remove the volatile organic and placed in a furnace pre set at 650°C for 6 hours. RTA (Rapid Thermal Annealing) was also done at 600, 700 and 800°C for 0.5 minutes. The films are characterized using Scintag X-ray diffractometer . Scanning electron microscopy (SEM model ISI-DS 130, Akashi Beam Tech. - Japan) was used to study the microstructure of the films and also to measure the film thickness. Hysterisis loop was also measured with the SBT fims by using the RT 66A tester (Radiant Technology). Gold electrodes with a diameter of 0.6 mm were sputter deposited to measure the ferroelectric behavior.

Fig.(3) shows the TGA curve for the xero-gel dried at 60°C. TGA curve shows there is steady weight loss upto 600°C and there after the weight change is negligible. The weight loss is mainly due to removal of water and organic matter from the organic gel to produce the inorganic phase. Fig.(4) shows the DTA curve for the xero-gel dried at 60°C. It shows two exothermic peak with an onset temperature at 203°C and at 595°C. The first exothermic peak at 203°C is attribuetd to decomposition of organic matter from the gel. The exothermic peak at 595°C indicates the crystallization of SBT phase.

Powder X-ray difraction pattern of the xero-gel shows glassy nature. However DTA curve shows crystallization temperatute at ~595°C. The xero-gel was crushed, later powder were calcined at 650°C - 6 hours and then analysed with X-ray diffractometer. Fig. (5) shows the powder X-ray diffraction patterns for the gel dried at 60°C and phase pure SBT phase. All the diffraction lines could be indexed without any seconday impurity phases on the basis of both tetragonal and orthorhombic crystal structure. It is essential to point out SBT phase crystallized as low as 650°C and thin films at 600°C (fig.6) in comparison to other reported work[7,8] wherein SBT thin films prepared at 700°C[7] and at 800°C[8,9]. The films annealed in RTA (Rapid Thermal annealing) in for 0.5 minutes crystallized at 700°C as shown in fig. (7).

The prepared films showed a ferroelctric charactersistics which was recogonized in hysterisis loop shown in figure (8). The SBT films annealed at 600°C for 6 hours shows a small polarization value in comparison to the bulk indicates a discrepency of Bi from stoichiometric composition. SEM micrograph shows the paritcle size are ~0.5 μm for the SBT fims annealed at 600°C for 6 hours. crack free films and with film thickness of 2 μm as shown in fig. 9 (a, b)

Acknowledgment

References :

1. C. A. Paz de Aranjo, J.D. Archiaro. M.C. Scott and L.D. McMillian. Pattent no : WO 93/12542 (24 June).

2. K. Amanuma, T. Hase and Y. Miyasaka, Appl. Phy. lett. 66, 221 (1995).

3. E. C. Subbarao, J. Phys. Chem. Solids, 23 665, (1962).

4. T. Mihara, H. Yoshimura, H. Watanabe, T. Itoh. C. Paz de Arauzo and L.D. Mcmillian, 7th Inter. Sym. on Integerated Ferroelectrics, March 20-22, 1995, Calorado.

5. I.G. Ismailzade, Proc. III conf. on Ferroelectricity (USSR) Acad. Sci. USSR, press, Moscow 1960.

6. D.C. Bradely, R.C. Mehrotra and D.O. Gaur, Metal alkoxides, Academic press, pp 303.

7. S.Y. Chen, X-F. Du and I-W. Chen, Mater. Res. Soc. sym, proc. vol. 361, pp. 15 - 1995.

8. K. Amanuma, T. Hase and Y. Mujaialha, maer. Res. Soc. Sym, proc vol. 361, pp 21- 1995.

9. D.P. Vijay, S.B. Desu, M. Nagata and X.Zhang and Tze. C. Chen. Mater. Res. Soc, sym. proc vol 361, pp. 3 - 1995.

Figure Captions

Fig (1). Pseudo tetrahedral unit cell of $SrBi_2Ta_2O_9$ structure.

Fig (2). Schematic reaction sequence for the formtaion of SBT gel.

Fig (3). TGA thermogram of SBT gel dried at 60°C with a heating rate of 10°C /min in air atm.

Fig (4). DTA thermogram of SBT gel dried at 60°C showing two exothermic peaks at 203°C and 595°C with a heating rate of 10°C/min ain air atm.

Fig (5). Powder X-ray diffraction patterns of SBT gel and SBT powder calcined at 650°C - 6hrs.

Fig (6). SBT thin films crystallized at various temperatures.

Fig.(7) RTA treatment of SBT films at various temperatures for 0.5 minutes.

Fig.(8). Hystersis loop of SBT thin films crystallized at 650°C - 6 hrs.

Fig.(9). a. SEM micrograph of SBT thin films showing grain size of ~ 0.5 µm.

b. Crack free SBT films with the film thickness of 2 µm.

Figure 1

Figure 2
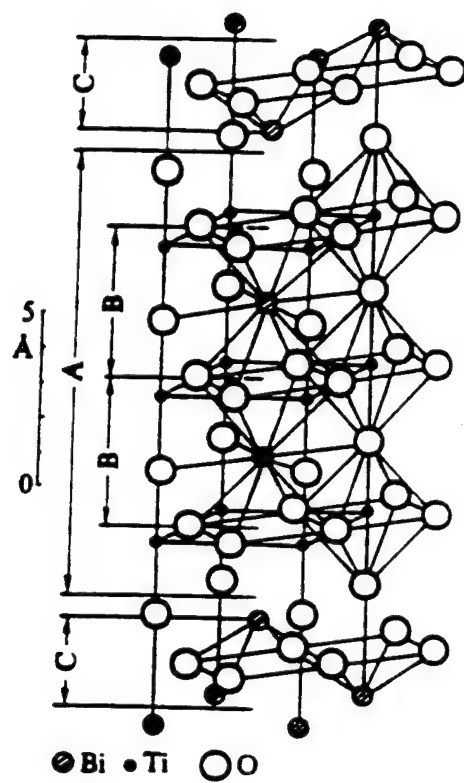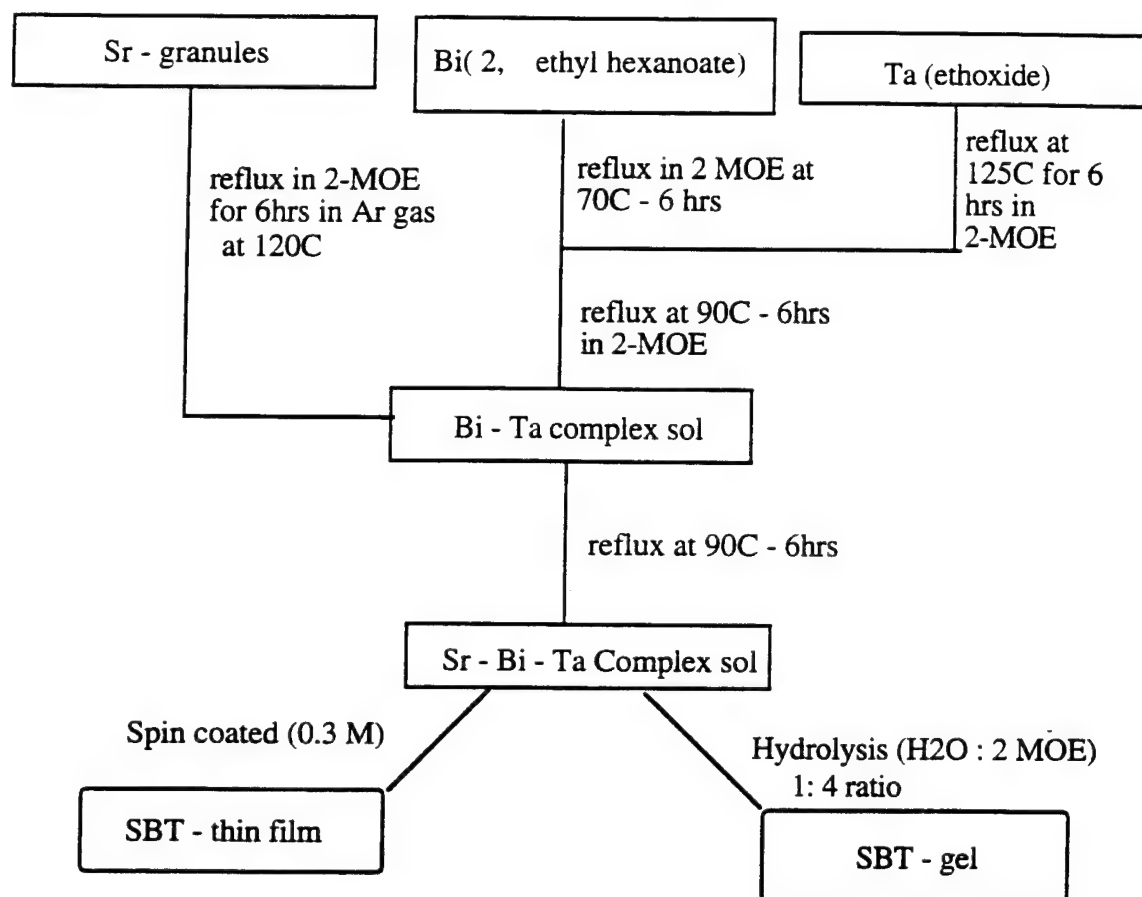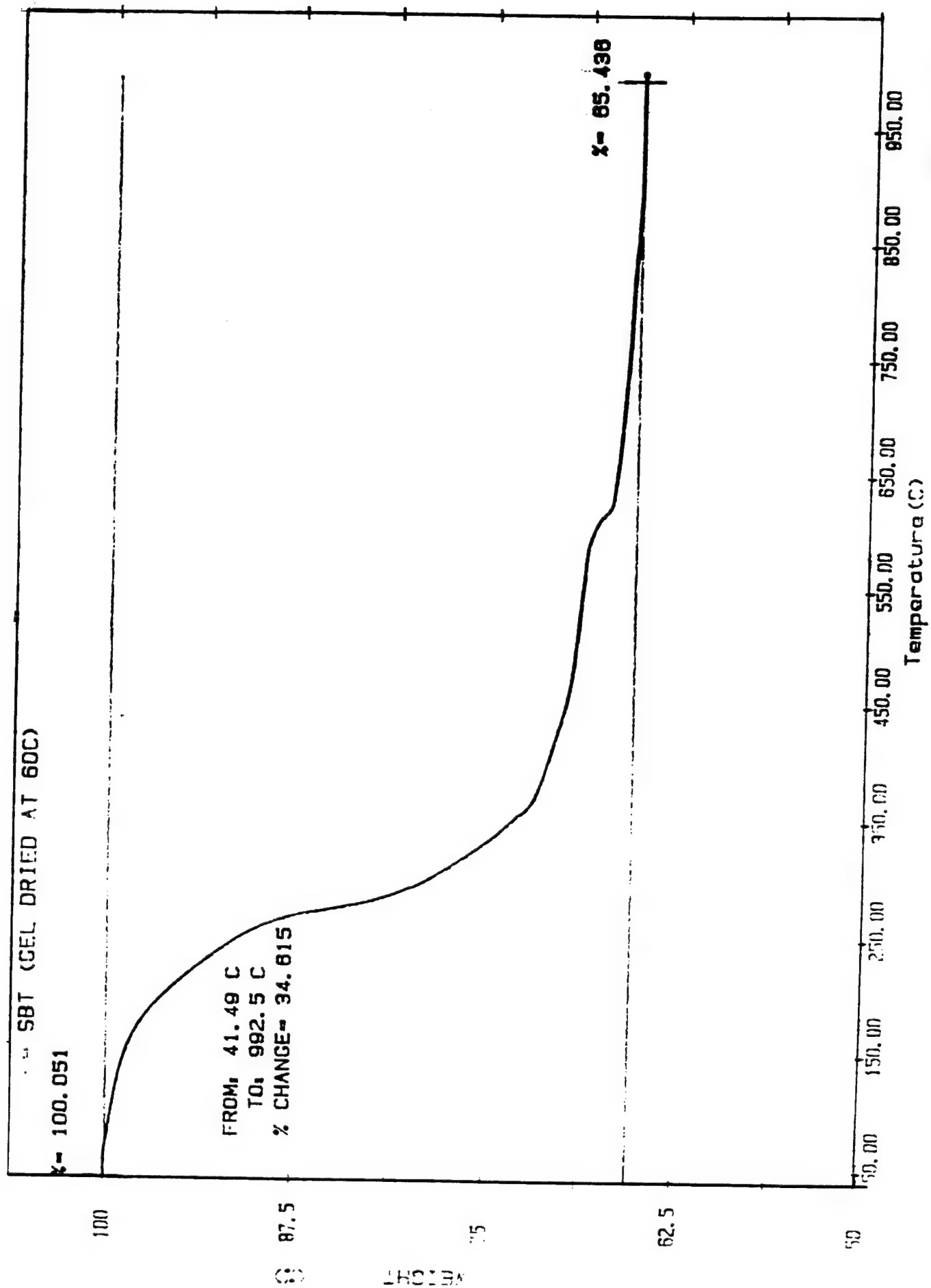
Figure 3

SBT (GEL DRIED AT 60C)

WT: 30.00 mg   SCAN RATE: 10.00 deg/min

ATMOSPHERE: AIR   40 cc/min

PEAK FROM: 190
      TO: 390
ONSET: 203.7
PEAK HEIGHT: 3.171
MAX: 286.3

<ENDO

DEGREES

TEMPERATURE (C)

Figure 4   DTA

Figure 5

Axis labels: Intensity(a.u.), 2Θ

Legend: O - Orthorhombic, T - Tetragonal

Curve labels: 650°C, Gel dried at 60°C

Peak labels:
- T(006)
- O(111), T(101)
- O(113), T(103)
- O(115), T(105)
- O(200), T(110)
- O(202), T(107)
- T(0010)
- O(208), T(118)
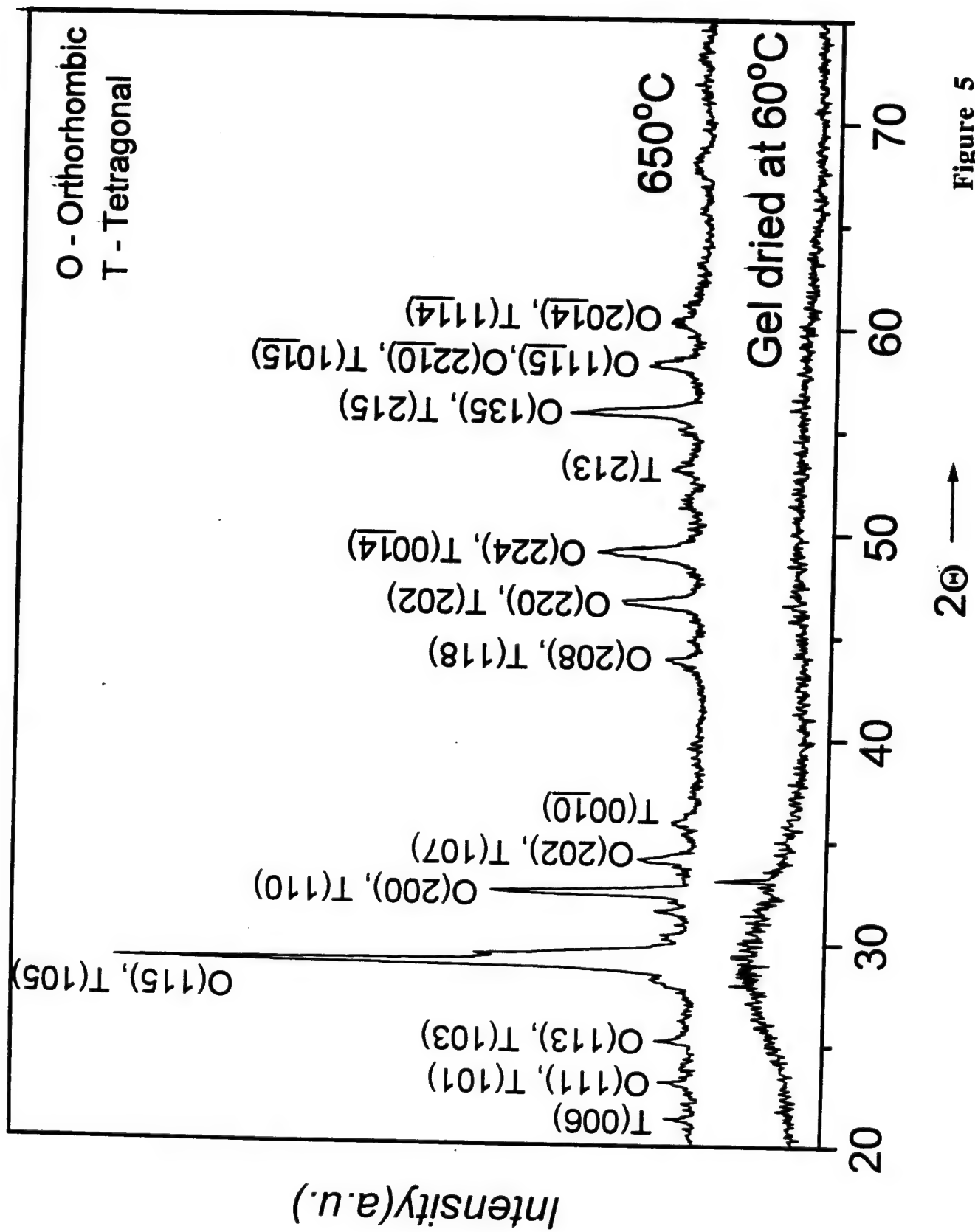- O(220), T(202)
- O(224), T(0014)
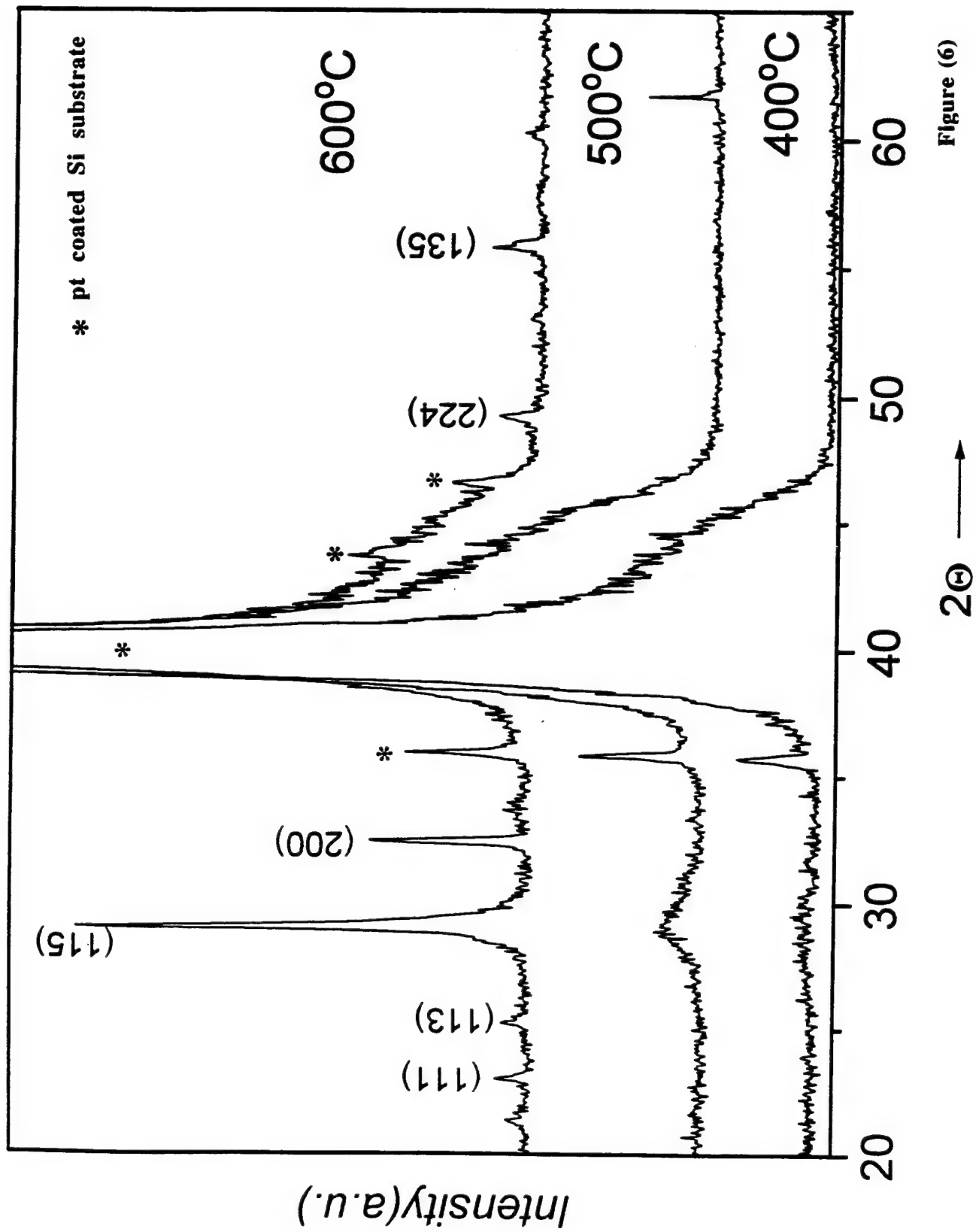- T(213)
- O(135), T(215)
- O(115), O(2210), T(1015)
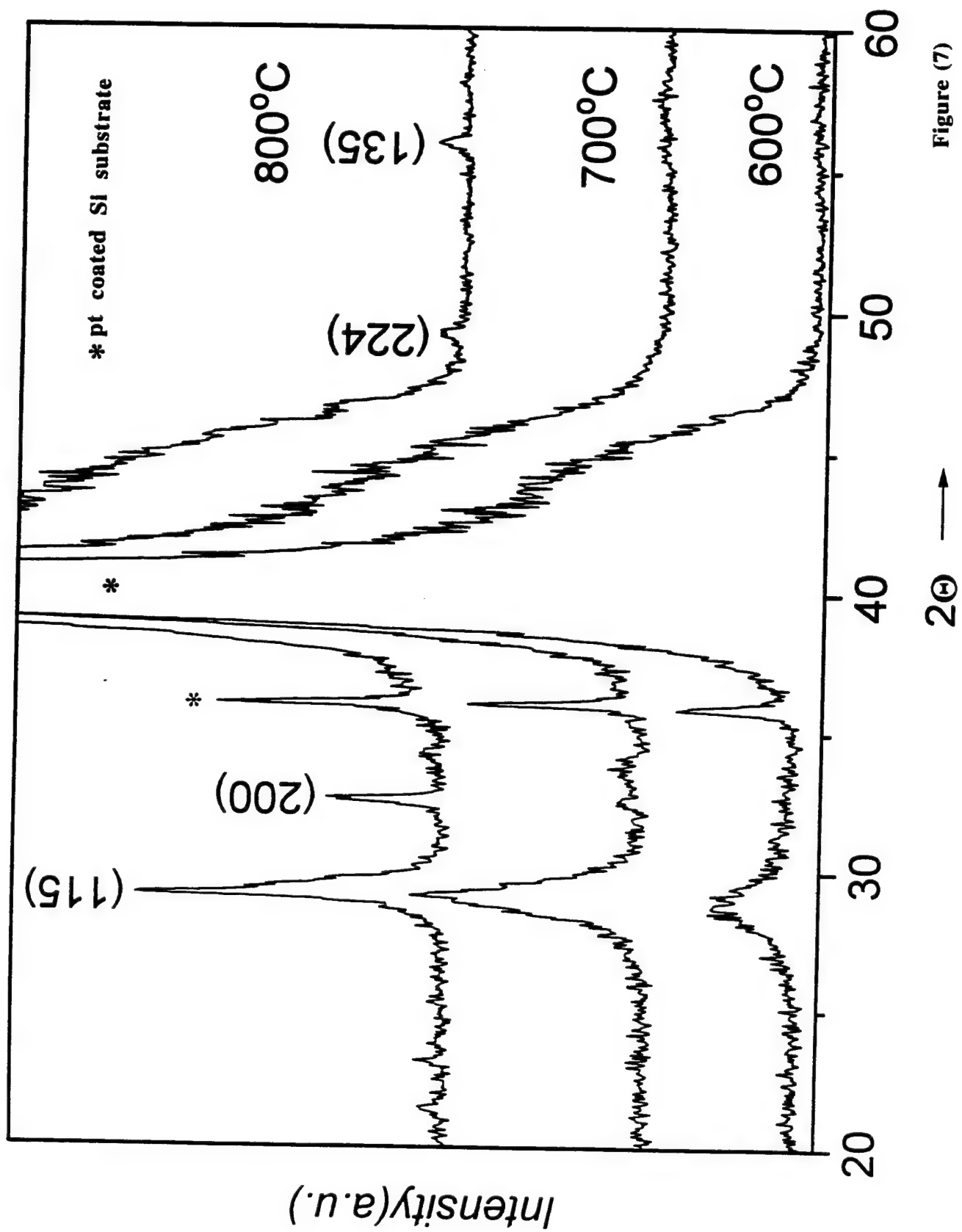- O(2014), T(1114)
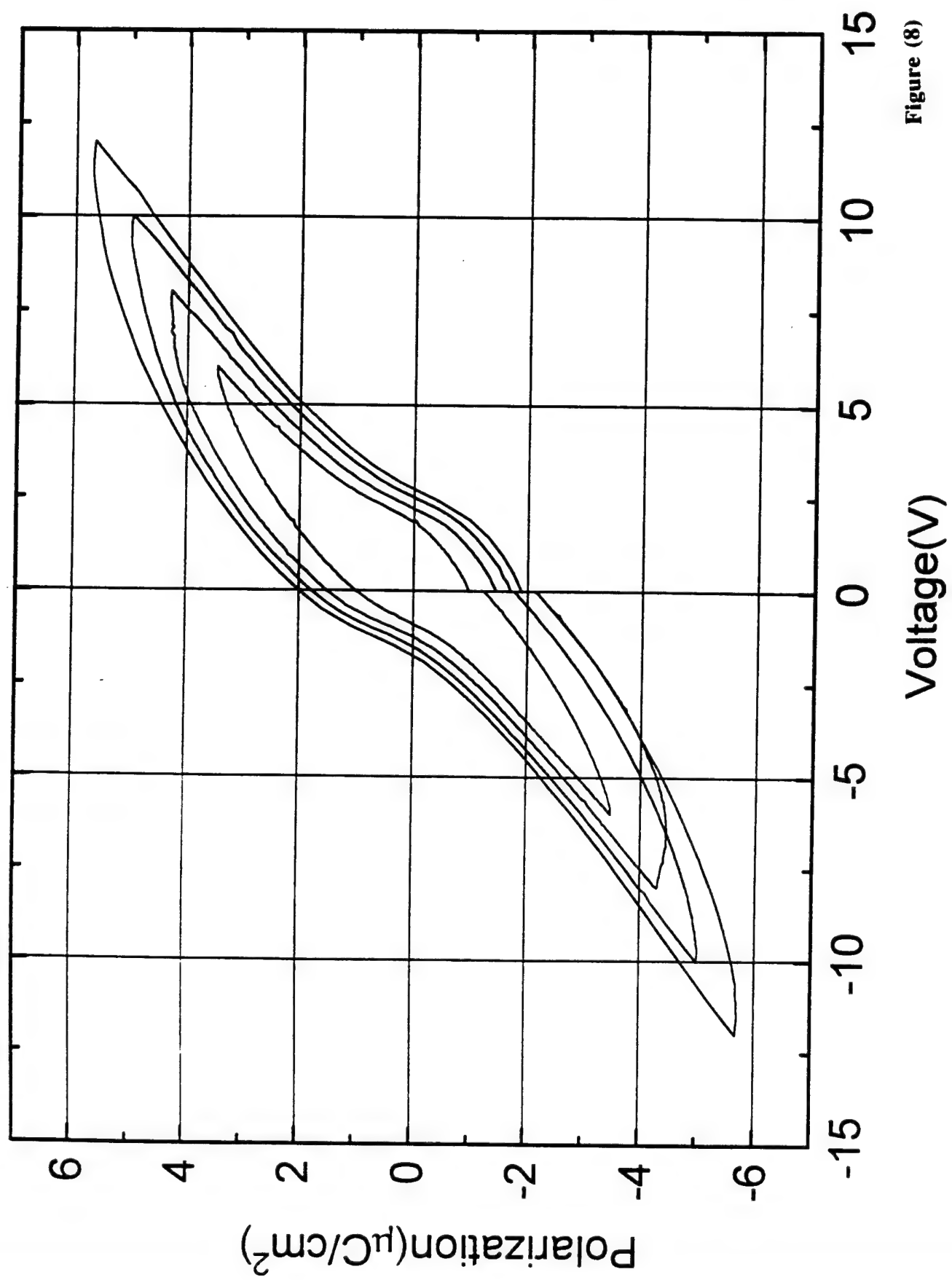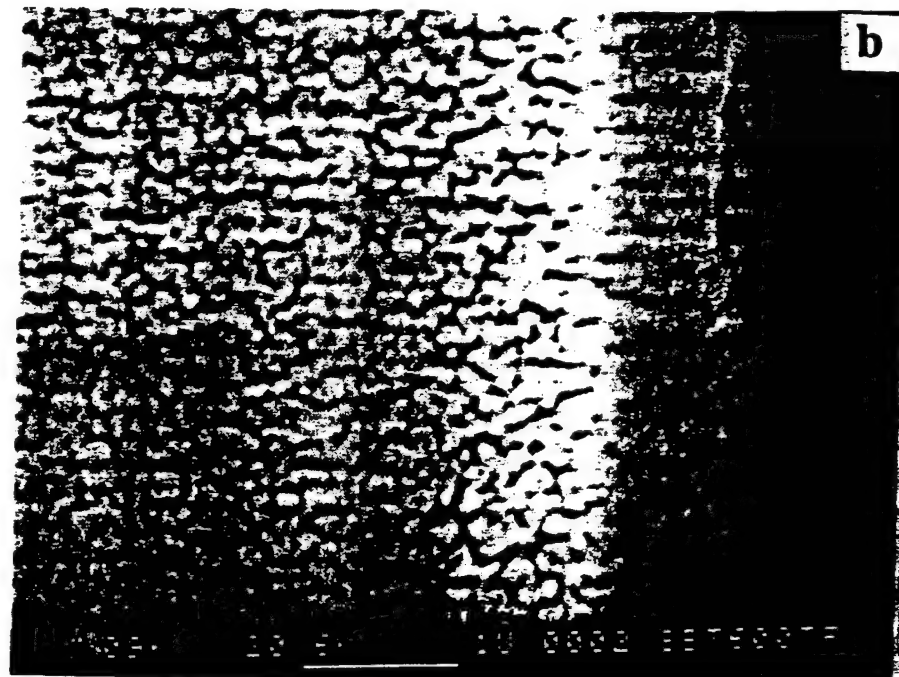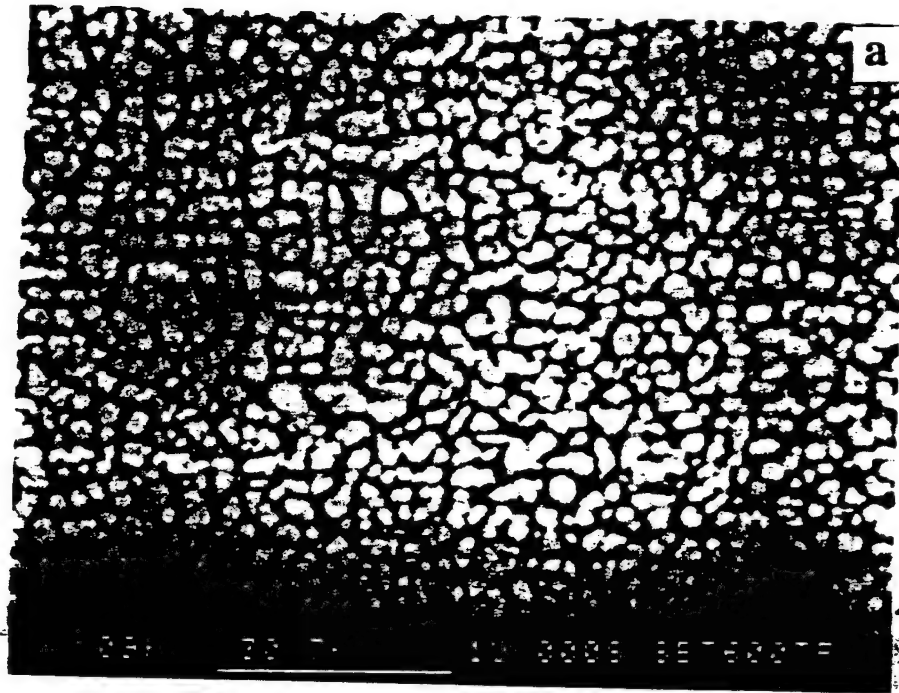
Figure (6)

Figure (7)

Figure (8)

Figure (9)

APPENDIX 68

OPTICAL NON-INVASIVE EVALUATION OF FERROELECTRIC FILMS/ MEMORY CAPACITORS

SARITA THAKOOR*, A. P. THAKOOR* AND L. ERIC CROSS**
*Jet Propulsion Laboratory, California Institute of Technology, Pasadena, CA 91109
**Pennsylvania State University, Materials Research Laboratory, University Park, PA

ABSTRACT

NON-INVASIVE photoresponse (photocurrent/voltage, reflectance and transmittance) from ferroelectric thin films and memory capacitors, with its strong dependence not only on the remanent polarization, but also on the film microstructure, crystal orientation, and nature of the interfaces (state of formation/degradation, etc.) offers an excellent "tool" for probing the ferroelectric capacitors at virtually any stage of fabrication, including on-line quality control. In fact, simultaneous measurement of spectral photoresponse and spectral reflectance, as a distinctive signature of the device probed, is an ideal, high speed, non-invasive means of evaluation for such thin films at high spatial resolution (~ 100 nm) using beam scanning. This paper discusses three aspects of such evaluation. First, the spectral transmittance of the film as a direct function of the microstructure, second, the use of band-gap illumination (365 nm) to condition a fatigued capacitor; and third, the optical E field interaction with the ferroelectric capacitor, yielding a high speed photoresponse which is related to the remanent polarization and the operational history (status of internal fields) of the ferroelectric capacitor. Combined, these different kinds of photoresponses provide a good signature of the device quality.

INTRODUCTION

Non-volatile ferroelectric memories are now in the advanced stages of development where issues such as high-yield manufacturability and long-term reliability are receiving increasing attention today. The leading implementation scheme[1-4] selected for the VLSI ferro-memories is based on remanent polarization within a ferroelectric capacitor, where the high speed switching of the polarization state provides a memory readout.

The performance characteristics (such as **fatigue**: loss of polarizability with read-write cycling, and **memory retention** issues-(a) aging: logarithmic decay of remanent polarization with storage time (b) imprint: the tendency of polarization to gradually return to a previously written state leading to a bit error) of ferroelectric memory capacitors are governed by parameters such as:

(a) stability of the electrode/ferroelectric interfaces,
(b) orientation/epitaxy/crystallization status of the ferroelectric film,
(c) microstructure of the film: compactness, void density, surface smoothness, grain size, etc. and
(d) operational history.

Although all such device parameters listed above are typically attempted to be well-controlled during the fabrication of the memories, there is no suitable "tool" to conveniently and non-destructively "probe" the memory cells (during or after fabrication), with high spatial resolution and at high speed, for their polarization behavior which in effect dictates their ultimate

performance with respect to fatigue, lifetime, imprint, etc. These problems are suspected to be originating due to the following causes:

(a)   charged mobile defects (such as oxygen vacancies),

(b)   existence of a-axis inclusions/90° domain walls,

(c)   charge injection from the electrodes into traps in the ferroelectric material, and

(d)   polarization of slow moving dipoles.

(e)   phase transformation from ferroelectric to non-ferroelectric phase

Particularly fatigue is suspected to occur because of the screening of the applied voltage/pinning of domains by the accumulated space charge/defects/traps. In the recent past[1,2,3], significant strides have been made to address the issue of fatigue with the advent[5,6] of new fatigue free, bismuth strontium tantalate thin films and oxide/perovskite electrodes that provide a more stable chemical/structural template for the growth of the ferroelectric thin film. Long term retention problems such as imprint, however, continue to be a major reliability impediment.

NON-INVASIVE photoresponse (photocurrent/voltage, reflectance and transmittance) from ferroelectric thin films and memory capacitors[7-15], with its strong dependence not only on the remanent polarization, but also on the film microstructure, crystal orientation and nature of the interfaces (state of formation/ degradation, etc.) offers[16] just such an ideal "tool" for probing the ferroelectric capacitors at virtually any stage of fabrication, including on-line quality control. In fact[16], simultaneous measurement of spectral photoresponse and spectral reflectance, as a distinct signature of the device probed, is an ideal, high speed, non-invasive means of evaluation at high spatial resolution (~ 100 nm) using beam scanning. This paper discusses three aspects of such evaluation of ferroelectric lead zirconate titanate (PZT) thin films. First, the spectral transmittance of the film as a direct function of the microstructure, second, the use of band gap illumination (365 nm) to condition a fatigued capacitor; and third, the optical E field interaction with the ferroelectric capacitor using pulsed lasers at 532 nm, yielding a high speed photoresponse which is directly related to the remanent polarization and the operational history (status of the internal fields) of the ferroelectric capacitor. This high speed photoresponse promises to be a unique non-invasive measure of the internal fields in the ferroelectric device as an evolving function of operation history, storage time and environmental history. Combined, these different kinds of photoresponses provide a good signature of the device quality.

EXPERIMENTAL DETAILS

PZT Sputter Deposition

The PZT films were deposited by multi-target dc-reactive sputtering of lead, zirconium and titanium sequentially on a substrate rotating about the central axis of the chamber. The details of the chamber and sputtering process are discussed elsewhere[17]. A variety of substrates, including borosilicate glass, quartz, indium tin oxide (ITO) coated glass, sapphire, and passivated silicon were used for the deposition. No intentional substrate heating was used. The temperature of the substrate during deposition was monitored using a thermocouple and was observed to stay below 60°C. The sputtering was carried out in a reactive gas mixture of high purity (99.999%) argon (inert gas) and oxygen (reactive gas). The flow rates of Ar and O_2 were independently controlled by their respective flowmeters. The deposition routine typically consisted of setting up the argon ambient and presputtering the targets to clean the surface. Next, oxygen was added and the ambient stabilized. The target powers were set and the targets conditioned. Following this, the shutter was removed and deposition initiated on the rotating

substrates. Typical deposition conditions in our chamber for obtaining PZT films at the morphotropic phase boundary are presented elsewhere[17].

As deposited, the films were amorphous. The composite film so obtained was baked in an open air furnace at 525°C for one half hour after attaining steady temperature to yield the Zr rich rhombohedral phase. The surface topography of these films was studied using a Cambridge S250 Scanning Electron Microscope. The transmission response of these films in the spectral range of 200 nm to 800 nm was observed using a Carey Model 5A Spectrophotometer.

Sol-Gel Deposition

The sol-gel lead zirconate titanate (PZT) thin films with a nominal composition of (Zr:52, Ti:48) were deposited by a modified Sayer's Technique[18,19] on oxidized silicon substrates covered with an evaporated Ti/Pt ($\sim$ 1000 Å/1000Å) base electrode. The lead zirconate titanate (PZT) film contained $\sim$ 18% excess lead and were $\sim$ 2000 Å thick. Crystallization of the as deposited PZT was accomplished by annealing the films at 550°C for 10 minutes in oxygen ambient. To complete a standard sandwich capacitor test structure[8], semitransparent thin films of platinum ($\sim$ 150Å thick) were sputter-deposited as the top electrode. The top electrodes were patterned by conventional lift-off techniques as dots of 125 μm and 250 μm diameter. Optical transmission through the semitransparent top electrode films (λ = 300 to 800 nm) was about 30%.

365 nm Illumination Set-up

Photonic probing at 365 nm was done using a short arc mercury lamp as the near UV/visible (300 nm to 600 nm) illumination source with the strongest line at 365 nm isolated using a filter. The choice of this light source to obtain maximum photoresponse was motivated by the bandgap value of PZT $\sim$ 3.5 eV [11]. A custom built liquid light guide was utilized to deliver a 5 mm divergent beam with an intensity of $\sim$ 0.1 watt/cm^2 onto the sample. A shutter controlled by a solenoid valve allowed a pulse illumination with a minimum pulse length of about 1 sec. The effect of this illumination on fatigued and unfatigued capacitors was observed. The details of the set-up utilized have been presented elsewhere[12,20]. The hysteresis loops were all recorded at a 500 Hz frequency.

High Speed Photoresponse Set-up

The high speed photoresponse measurements were done using an energetic laser pulse. The doubled output at 532 nm from a Nd-YAG pulsed laser utilizing accousto-optic switching was used for this experiment. The advantages of utilizing an accousto-optically switched laser over the electro-optically switched laser[7,9,10], in obtaining a low noise response signal free from electromagnetic pickup of the high voltages ($\sim$ KV) used for electro-optic switching, have been illustrated elsewhere[15]. The incident photon energy was lower than the PZT bandgap (3.5 eV)[11], and was therefore weakly (< 1%) absorbed by the PZT. The laser pulse, has a full width at half maximum (FWHM) of $\sim$ 10 ns and delivers power in the range of 2mW/μm^2 - 20 mW/μm^2 per pulse at 532 nm at a repeat frequency of 20 KHz. For the measurement of the photocurrent,

the top and bottom electrodes of the ferro-capacitor were connected across the 50 Ω internal impedance of an oscilloscope, which recorded the zero bias photoresponse from the capacitor on illumination with the laser pulse. The capacitor was poled positively by using a +4 V pulse for 1 msec or negatively by a -4 V pulse for the same duration.

RESULTS AND DISCUSSION

Surface Topography & Optical Transmission Correlation

The angle of incidence of the sputter deposit was a very critical parameter in determining the morphology and physical characteristics of the films. Fig. 1a shows the Scanning Electron Microscope (SEM) picture of the surface of a film deposited in an unrestricted manner, allowing all angles of deposition. This film (type A film) was rough, opaque, and of ceramic quality. Fig. 1b shows the surface micrograph of a film obtained using identical deposition parameters, except a collimator around each gun, restricting the deposition to a near-perpendicular incidence. Transparent electro-optic quality films (type B film) were obtained as a result of this restriction in the incidence angle of deposition. As expected, devices made from films of type B exhibited higher yield, unlike the type A films which suffered from frequent shorts.
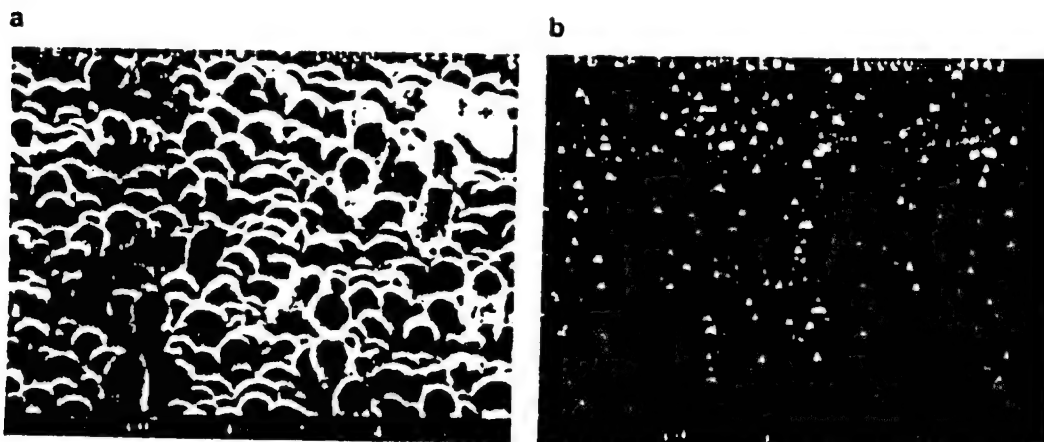

Figure 1: SEM photographs of (a) sputtered PZT film with surface roughness ~ 1 μm (Type A film) (b) PZT sputtered at near perpendicular incidence angle of deposit, lowering surface roughness to ~ 0.2 μm (Type B film).

Figs. 2(a) and 2(b) are the transmission spectra for PZT with surface topographies corresponding to Figs. 1(a) and 1(b) respectively. Therefore, as is well-known, the transmission spectra serve as a simple screening tool for films with high surface roughness and high optical scattering from the films with good optical transmission quality.
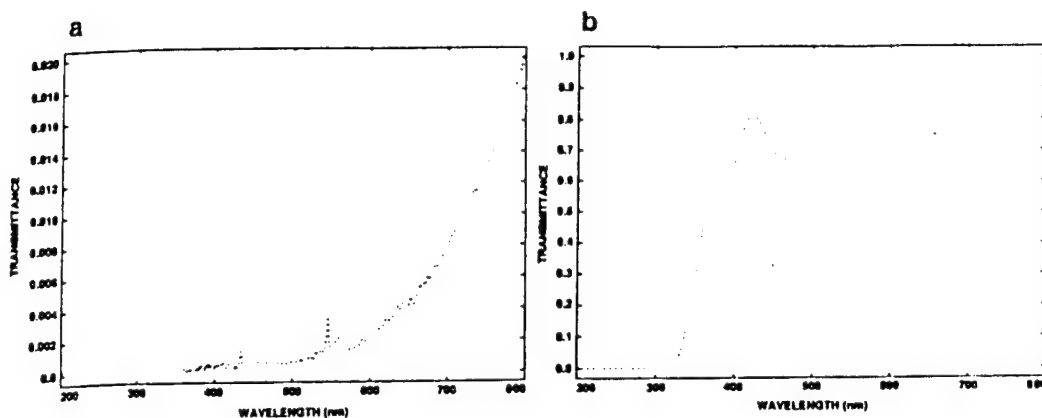
Figure 2: Comparison of Transmission Spectra of multimagnetron DC Sputtered PZT (a) Type A and (b) Type B films respectively
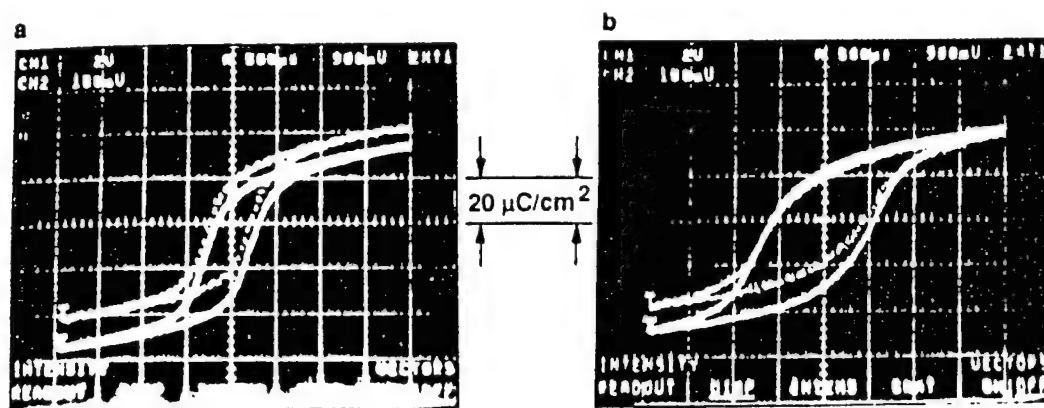

Figure 3: Comparison of (a) unfatigued and (b) fatigued state, 10^8 cycles, hysteresis loops without (dotted line) and with 365 nm illumination (full line)

Effect of 365 nm Illumination on Ferroelectric Memory Device:

Figure 3(a) shows the effect of band-gap light (365 nm) illumination on a fresh unfatigued ferroelectric memory capacitor. The dotted hysteresis loop is the one with no illumination and the solid line exhibits the hysteresis loop with illumination on (10 sec pulse of 365 nm). It clearly shows that the 365 nm illumination causes the hysteresis loop to shift along the Y-axis and also there is a marked blooming of the hysteresis loop. Earlier [1-12] we have reported on the generation of a photovoltage/photocurrent due to such illumination for the duration of the light pulse. The figure 3(b) shows a similar comparison of the "with" and
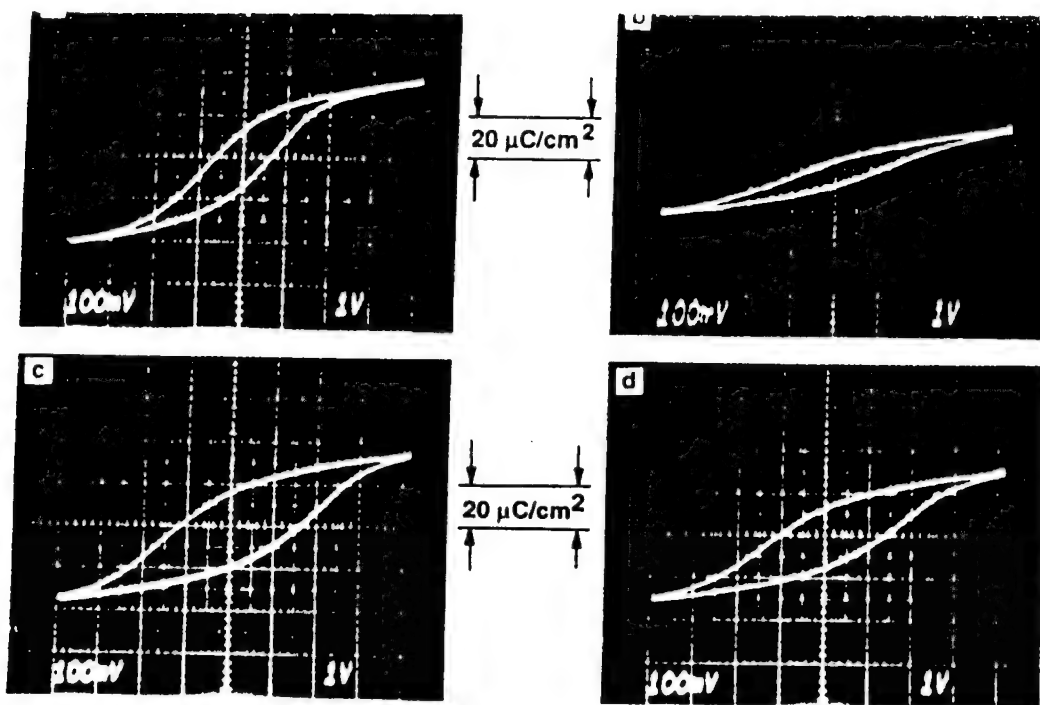
Figure 4: Comparison of hysteresis loops at 500 Hz, (a) unfatigued state (b) fatigued to 10^{10} cycles (c) fatigued state: first loop after illumination turn - off, (d) fatigued state: steady state loop - five hours after illumination turn off.

"without" illumination states of the hysteresis loop for this memory capacitor fatigued to $\sim 10^8$ cycles. However, in both these cases when the illumination was removed, the hysteresis loops reverted back to their original unilluminated status. This suggests that the unfatigued capacitors and mildly fatigued capacitors primarily show only a reversible photoinduced change. Also it is noteworthy that this mildly fatigued capacitor has changed its characteristics with respect to the fresh capacitor, only as a slight increase in its coercive voltage, however, its remanent polarization remains virtually unchanged. Figure 4 illustrates the effect of the 365 nm illumination on the ferroelectric capacitor fatigued to 10^{10} cycles. Figure 4(a) is the loop for the fresh unfatigued capacitor, Fig. 4(b) is the capacitor fatigued to 10^{10} cycles, Fig. 4(c) is the loop just after turn-off of illumination and figure 4(d) is the loop in the steady state 5 hours after turn-off of illumination. The illumination could thus be used as a quick indicator/estimator of the status of the fatigue.

Cycling has two effects: increase in coercive voltage, V_c, and reduction in remanent polarization, P_R. The increase in V_c appears to be due to the irreversible degradation in the ferroelectric film (possibly a phase transformation from ferroelectric to non-ferroelectric phase either within the film or at the ferroelectric/electrode interface). V. K. Chivikula[21] has also suggested the formation of a non-ferroelectric surface layer based on their dispersion data. The decrease in P_R on the other hand is due to local screening of the applied voltage. This could arise from presence of charged defects and /or traps that could pin the domains. As is observed,

162

the reduction in P_R is clearly recoverable (by 365nm illumination). The temporal nature of the enhancement of the hysteresis loop in terms of remanent polarization suggests the existence of traps with different time constants. Illumination induced charge pairs could either recombine with the free space charge and/or cause emptying of the filled traps. On one hand, the net result is to give rise to the observed[8,11] steady photocurrent for the duration of the illumination. On the other hand, this also leads to removal of the local screening fields due to the space charge and/or unpinning of domains pinned by the traps and hence, a recovery of the fatigued state by regaining the loss of polarization. Such a loss of polarization and its recovery (by 365 nm illumination) therefore appears to be predominantly electronic (trap mediated) in nature. Similar observation of recovery from fatigue by UV illumination has been made by Warren et al[22] and Lee et al[23]. However, in order to avoid confusion from the temporary photoeffects, the photoinduced recovery must be verified beyond just one switching cycle (or a single hysteresis loop). A temporary compensation/cancellation of the screening field by photoinduced charges would clearly not qualify as a photo-triggered recovery.

It is interesting to note that the bandgap illumination either has no effect on the coercive voltage, or in the fatigued cases, causes a slight increase in the coercive voltage suggesting that the re-distribution of the charges could lead to a net increase of the resistive layer. This further re-affirms the contention that this initial mode of fatigue (increase in V_c) is material degradation and is not easily recovered by illumination.

High Speed Photoresponse Results

A bipolar high speed photoresponse is obtained from freshly made capacitors and capacitors with bipolar cycling history for positive and negatively poled states respectively.
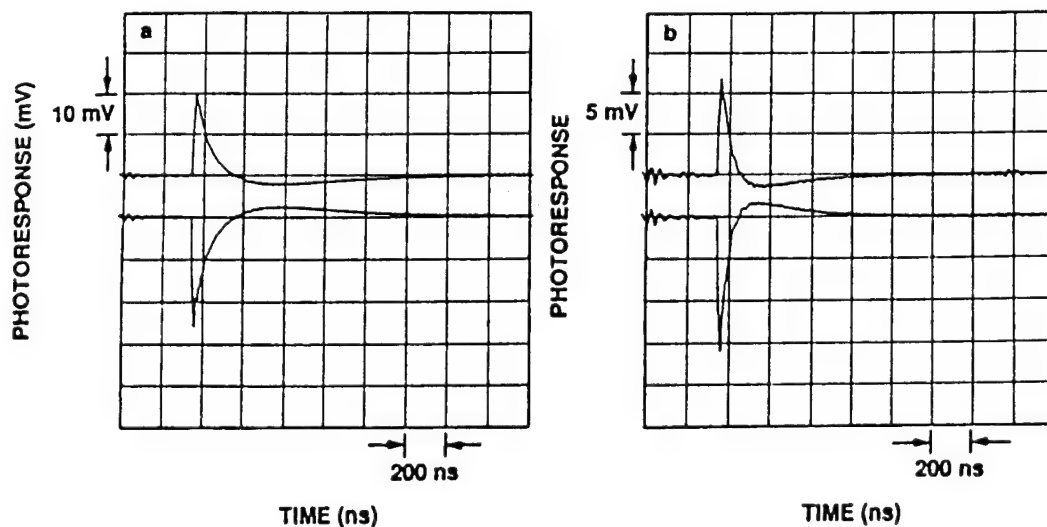

Figure 5: Comparison of High Speed Photoresponse (a) unfatigued state and (b) fatigued state.

Table 1. High speed photoresponse, ratio of area under the peak, and comparison with corresponding ratios of remanent polarization as obtained from conventional hysteresis loops, for unfatigued and fatigued capacitors respectively.

Polarity of Applied Voltage	$P_{R,\text{ unfatigued}}/P_{R,\text{ fatigued}}$ Determined By hysteresis loop	$A_{R,\text{ unfatigued}}/A_{R,\text{ fatigued}}$ Determined By Photoresponse
positive	2.57	2.57
negative	2.62	2.65

Figure 5 shows a comparison of the high speed photoresponse from the unfatigued and fatigued states of the memory capacitor (Pt/PZT/Pt). The capacitance of the unfatigued state was 2.4 nF and the capacitance of the fatigued state was 1.3 nF. This data was compared with the corresponding hysteresis loop data for the unfatigued and fatigued states of the memory, respectively. As shown in table 1, the ratio of the unfatigued remanent polarization ($P_{R,\text{ unfatigued}}$) to the fatigued remanent polarization ($P_{R,\text{ fatigued}}$) as determined from the hysteresis loops is identical to the ratio of the corresponding area under the peaks of the photoresponse signal for unfatigued ($A_{R,\text{ unfatigued}}$) and fatigued ($A_{R,\text{ fatigued}}$) case. This clearly shows that the area under the photoresponse signal is proportional to the remanent polarization of the memory capacitor. Also, the area under the photoresponse signal is interpreted[6,8-10] as being proportional to ΔP, the net shift in the dipole moment due to the incidence of energetic laser pulse onto the capacitor. The area under the photoresponse peak therefore provides an excellent non-invasive, quantitative measure of remanent polarization. Further, we observe that the speed of the photoresponse is directly dictated by the device capacitance and hence, the photoresponse is expected to become faster with reducing ferroelectric pixel size, allowing very high speed non-invasive measure of the memory state for the high density memories. The illumination pulse is non-invasive. The change ΔP is followed by an equivalent $-\Delta P$ so that there is no net change in the remanent polarization, P_R, as verified by cross checking using the conventional pulse switching measurement (DRO). Also, it was verified that the remanent polarization did not change for over 10^8 laser pulse readout cycles.

Measurement of the photoresponse as a function of frequency shows that the amplitude of the response saturates for frequencies lower than 10 KHz suggesting that this transient response attains its maximum value at $\sim 100\ \mu$sec. The rising edge of the response may contain higher speed(≤ 10 ns) contributions from the photovoltaic effect and/or photoresponse due to deep traps occurring at the incident wavelength of 532 nm. If isolated, identification of such deep traps and the ability to probe their evolution as a function of the process parameters /operation cycles/environmental stress cycling can be another useful aspect of this technique to provide feedback on the materials/device quality control.

The mechanism[6,8] by which the shift ΔP occurs could be pyroelectric (thermally triggered, associated with temperature change within the PZT), piezoelectric (due to propagation through PZT of an acoustic deformation wave, initiated by a sudden thermal expansion of the platinum top electrode), or optical rectification (due to interaction of the E-field associated with the incident photons and the internal fields within the ferroelectric.

Furthermore, the photoresponse has a dependence on the history of the memory capacitor. Fig. 6 illustrates how the high speed photoeffect sensitively reflects the polarization history of the ferroelectric capacitor. A history has been induced in an accelerated manner by applying a unidirectional voltage for extended duration of 10 sec. The figure shows that the conventional pulse polarization destructive read-out (DRO) merely exhibits a slight asymmetry

HISTORY	READOUT		
	POLING	PHOTORESPONSE MEASUREMENT	CONVENTIONAL DESTRUCTIVE READOUT

±4 V, 1 msec, BIPOLAR

+4 V, 1 msec
−4 V, 1 msec

−5 V, 10 sec

+4 V, 1 msec
−4 V, 1 msec

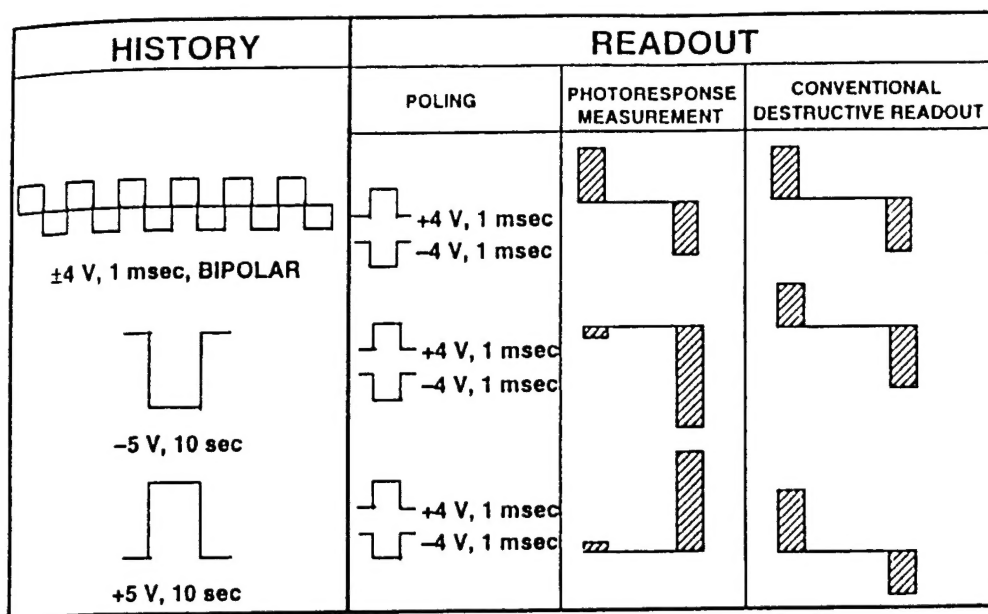+5 V, 10 sec

+4 V, 1 msec
−4 V, 1 msec

Figure 6: Photoresponse probing of "history" of the ferroelectric capacitors and comparison of photoresponse peak amplitude data with corresponding conventional destructive readout data of remanent polarization.

as a reflection of the history. In contrast, the high speed photoresponse shows an overall change from bipolar to unipolar response and therefore, is used directly for detecting the operational/environmental history of the ferroelectric memory **non-invasively**. This result may be of significant fundamental importance because it demonstrates that the photoresponse signal in addition to its dependence on remanent polarization is also dependent on the status of the evolving internal fields within the ferroelectric (i.e., is the optical rectification effect). Such measure of the internal screening fields within the ferroelectric is not available as sensitively and non-invasively by conventional electrical techniques.

CONCLUSIONS:

UV Illumination (365 nm) can be used to condition/recover the loss of polarization in fatigued ferroelectric memories and such photoresponse can also serve as a quick indicator/estimator of the status of fatigue in a ferroelectric capacitor.

The high speed photoeffect provides an excellant non-invasive, quantitative measure of remanent polarization and reflects sensitively the polarization history of the ferroelectric capacitor suggesting a unique measure of the internal fields within the ferroelectric. If the subtle reflections of the complex fatigue and retention characteristics of a device on its high speed photoresponse could be properly harnessed, it holds the potential for an effective quality control and reliability screening tool.

165

ACKNOWLEDGEMENTS

REFERENCES

1. W. Kinney, Integrated Ferroelectrics, 4(2), 131, (1994).

2. W. Kinney and F. D. Gealy, IEEE International Solid State Circuits Conference, p. 266, (1994).

3. J. T. Evans and R. Womack, An Experimental 512 bit Non-volatile Memory with Ferroelectric Storage Cell, IEEE Journal of Solid-State Circuits, 23, 1171-1176 (1988).

4. D. Bondurant and F. Gnandinger, Ferroelectric Non-volatile RAMs, IEEE Spectrum, 18, 30-33 (1989).

5. J. F. Scott and C. A. Paz De Araujo, Ferroelectric Memories, Science, 246, 1400-1405 (1989). Proceedings of the International Symposium on Integrated Ferroelectrics 1993 and 1994 - Integrated Ferroelectrics Volume 4 & 5. Ferroelectric Thin Films II (Vol. 243) and III (Vol. 310), Published by Materials Research Society.

6. M. Huffman, C. A. Paz De Aroujo, L. D. McMillan, M. C. Scott and C. Echer, Paper # I2-10.3, Proceedings MRS Symposium on Ferroelectric Thin Films IV, Vol 361, (Fall 1994).

7. S. Thakoor, Appl. Phy. Lett. 60, 3319, 1992.

8. S. Thakoor, A. P. Thakoor and S. E. Bernacki, Proc. Third International Symposium on Integrated Ferroelectrics, Pg. 262, April 3-5, 1991, Colorado Springs, Colorado.

9. S. Thakoor, Appl. Phy. Lett. 63, 3233, 1993.

10. S. Thakoor, Ferroelectrics,134, 355, 1992.

11. S. Thakoor and J. Maserjian, "Photoresponse Probe of the Space Charge Distribution in Ferroelectric PZT Thin Film Memory Capacitors" J. Vac. Sci. & Tech A, 12, 295, Mar/April (1994). C. E. Land, J. Am. Ceram. Soc., 72, 2059 (1989).

12. S. Thakoor, Journal of Appl. Physics, 75 (10), 5409, May 15 (1994). S.Thakoor, U.S. Patent # 5372859, December 13, 1994.

13. S. Thakoor, E. Olson and R. H. Nixon, "Optically Addressable Ferroelectric Memory and its Applications" Integrated Ferroelectrics", 4, 257 (1994).

14. S. Thakoor and A. P. Thakoor, "Optically Addressed Ferroelectric Memory with Non-Destructive Read Out", Applied Optics (in press, 1995).

15. S. Thakoor, J. M. Morookian, H. Hemmati and A. P. Thakoor, International Symposium of Applied Ferroelectrics held August 7-10, 1994 at Penn State Scanticon, State College, Pennsylvania (unpublished).

16. S. Thakoor, New Technology Report # NPO - 19393/8994. S. Thakoor, NASA TechBriefs, Vol. 17, p. 54 May (1993).

17. S.Thakoor, U. S. Patent # 5196101, March 23, 1993.

18. G. Yi, Z. Wu and M. Sayer, J. Appl. Phys. 64, 2717 (1988).

19. S. E. Bernstein et al., Proc. MRS Fall Meeting: Symposium on Ferroelectric Thin Films II, Vol 243, p 343, Published by Materials Research Society, Pittsburgh, Pennsylvania, Boston, Dec 2-4 (1991).

20. M. Lakata and S. Thakoor, "Automated Ferroelectric Capacitor Testing System", NASA Tech Briefs, 18, 30 (1994)15.

21. V. K. Chivikula, Proceedings MRS Symposium on Ferroelectric Thin Films IV, Vol 361, (Fall 1994).

22. W. L. Warren, D. Dimos, B. A. Tuttle, R. D. Nasby, and G. E. Pike, Proceedings MRS Symposium on Ferroelectric Thin Films IV, Vol 361, (Fall 1994).

23. J. Lee, S. Esayan, A. Safari and R. Ramesh, Appl. Phys. Lett. 64 3646 (1994).